

NASA Technical Memorandum 83235

**RAXJET: A Computer Program
for Predicting Transonic, Axisymmetric
Flow Over Nozzle Afterbodies
With Supersonic Jet Exhausts**

Richard G. Wilmot
*Langley Research Center
Hampton, Virginia*



National Aeronautics
and Space Administration

**Scientific and Technical
Information Branch**

1982

INTRODUCTION

The nozzle afterbody is one of the main drag-producing components of an aircraft propulsion system. Thus, considerable effort has been devoted to developing techniques for predicting the afterbody flow field and drag. Using methods ranging from empirical techniques based on experimental data (ref. 1) to solutions of the Navier-Stokes equations with turbulence closure (refs. 2 and 3), investigators have had some success for isolated axisymmetric nozzles. Patched viscous-inviscid interaction methods (refs. 4 to 6, for example) have had considerable success. The patched methods require considerably less computational time than the Navier-Stokes solutions and generally yield results of comparable (and in some cases greater) accuracy.

The present paper describes a viscous-inviscid method that has evolved over a number of years through the efforts of several researchers. Roubush and Putnam (ref. 4) combined a conventional integral boundary-layer technique (ref. 7) with a linearized potential flow computation to account for the boundary-layer displacement effect. For separated flows, they employed the discriminating streamline concept of Presz (ref. 8) to separate the reverse flow region from the outer flow. Wilmoth (ref. 5) extended the method to transonic speeds by replacing the linearized inviscid method with the relaxation procedure of South and Jameson (ref. 9) for solving the exact nonlinear potential flow equation. Abeyounis (ref. 10) conducted oil-flow studies to determine the separation location on a series of circular-arc boattails and used the results to evaluate several prediction techniques including the Presz model. Presz et al. (ref. 11) developed an improved analytical model of the separated region which accounts for axial pressure gradients, surface skin friction, and jet entrainment. Putnam (ref. 6) incorporated this improved model together with a simple one-dimensional model of the inviscid jet plume blockage into the linearized method. Wilmoth and Dash (ref. 12) developed a jet entrainment model that uses the overlaid mixing analysis of Dash and Pergament (ref. 13) to calculate a jet plume displacement. This entrainment model was incorporated into the transonic method by Wilmoth (ref. 14) together with the shock-capturing-shock-fitting inviscid plume model of Dash and Thorpe (ref. 15). The work described above has provided the basis for the present viscous-inviscid model.

The present model iteratively combines the South-Jameson relaxation procedure, the Reahotko-Tucker boundary-layer solution, the Presz separation model, the Dash-Pergament mixing model, and the Dash-Thorpe inviscid plume model. These computational models are combined into a single computer program called RAXJET. RAXJET predicts transonic axisymmetric flow over nozzle afterbodies with supersonic jet exhausts and accounts for boundary-layer displacement, separation, jet entrainment, and inviscid jet plume blockage. This paper describes the various components of the computational model, illustrates its capabilities by comparison with experimental data, and provides a user's guide to the computer program. The computer program may be obtained as program LAR-12957 from

COSMIC
Suite 112, Barrow Hall
University of Georgia
Athens, GA 30602

SYMBOLS

The symbols used in the computer printouts are given in the second column.

A	cross-sectional area of body of revolution
A_{ref}	SREF reference area for drag coefficients
BL	boundary layer
CDF,AFT	afterbody friction drag coefficient, $\frac{1}{A_{ref}} \int_{S(x_A)}^{S(x_M)} c_f ds$
CDF,BOD	body-of-revolution friction drag coefficient, $\frac{1}{A_{ref}} \int_0^{S(x_M)} c_f ds$
$c_{D,R}$	CDP,AFT afterbody pressure drag coefficient, $\frac{1}{A_{ref}} \int_{A(x_A)}^{A(x_M)} c_p dA$
CDP,BOD	body-of-revolution pressure drag coefficient, $\frac{1}{A_{ref}} \int_0^{A(x_M)} c_p dA$
CDT,AFT	afterbody total drag coefficient, CDP,AFT + CDF,AFT
CDT,BOD	body-of-revolution total drag coefficient, CDP,BOD + CDF,BOD
c_f	CF skin-friction coefficient, τ_w/q_∞
c_p	CP pressure coefficient, $\frac{p - p_\infty}{q}$
D_b	nozzle base diameter
D	nozzle maximum diameter
GAMMA	ratio of specific heats of gas mixture
H	boundary-layer shape factor, δ^*/ρ
I	longitudinal grid index
ke2	two-equation turbulence model
l	length of afterbody
2	

L	L or REFL	reference length
M	M	Mach number
	ML	local surface Mach number
M_∞	MO	free-stream Mach number
NPR		nozzle pressure ratio, ratio of jet total pressure to free-stream static pressure
p	P	static pressure
p_∞	PINF	free-stream static pressure
$p_{t,2}$	PT	total pressure measured by pitot tube; total pressure downstream of normal shock if $M > 1$
$p_{t,\infty}$	PTINF	free-stream total pressure
q_∞		free-stream dynamic pressure
r	R	radial coordinate of cylindrical coordinate system with orig. at nose of body of revolution
r_j		radius of jet at nozzle exit
RDS		body radius corrected for discriminating streamline and inviscid plume boundary
REFF		effective body radius used in inviscid external flow calculation
RPAVG		average residual in relaxation solution of potential equation
RPMAX		maximum residual in relaxation solution of potential equation
RVI		radius at outer edge of boundary layer or mixing layer
S		surface area
T	T	temperature
	TINF	free-stream temperature
u	U	axial velocity
	UINF	free-stream velocity
v	V	radial velocity
x	X	axial coordinate of cylindrical coordinate system with origin at nose o. body of revolution
x_A		axial location of start of afterbody

x_M	XM	axial length of body of revolution
x_{sep}		axial location of separation
X,Y		computational coordinates of body-fitted grid used in inviscid external flow solution
α	ALF	radial grid stretching parameter used in external flow solution
δ		boundary-layer or mixing-layer thickness
δ^*	DEL*	boundary-layer or mixing-layer displacement thickness
Δ		incremental value
θ	THETA	boundary-layer momentum thickness
ξ, η		body-fitted grid coordinates
τ_w		boundary-layer shear stress at body surface

DESCRIPTION OF METHOD

The viscous-inviscid interaction model is constructed by dividing the afterbody flow field shown in figure 1 into six separate computational regions (see fig. 2). The viscous interaction is taken into account by displacing the body-plume shape with an appropriate displacement thickness to yield an effective body geometry for the inviscid external flow calculation. The inviscid external flow solution and inviscid jet exhaust solution provide the necessary flow conditions to calculate conditions in the viscous regions by parabolized marching procedures. The viscous and inviscid flow fields are then iteratively solved.

Inviscid External Flow Solution

The inviscid external flow solution is based on the relaxation procedure of South and Jameson (ref. 9) for solving the exact nonlinear potential flow equation in nonconservative form. This technique is valid for subsonic, transonic, and supersonic irrotational flow over bodies of revolution. RAKJET uses the computer program RAXBOD developed by Keller and South (ref. 16) to implement this technique. RAXBOD uses a body-normal coordinate system from the nose up to the first horizontal tangent and a body-fitted sheared coordinate system aft of this point. The computational grid is stretched to infinity in both the normal and downstream axial directions to facilitate handling of the far-field boundary conditions. Since RAXBOD requires that a complete body of revolution be specified, special procedures have been incorporated into RAKJET to determine grid stretching parameters that provide optimal grid point distribution over the afterbody.

Inviscid Jet Exhaust Solution

RAKJET uses the computer program SCIPAC (ref. 17) to solve the flow field in the inviscid jet region. SCIPAC solves the flow field by explicit spatial marching of the conservative finite-difference form of the inviscid flow equations for a uniform

composition gas mixture. The nozzle exit flow is assumed to be supersonic, and the calculation is initiated at the exit with exhaust properties prescribed. A uniform distribution of grid points is used between the axis and the inviscid plume boundary. As the calculation proceeds downstream, oblique shocks are numerically captured while the triple point that occurs because of the formation of a Mach disk in an under-expanded jet is treated by a shock-fitting procedure. The Mach disk location is determined by the iterative procedure of Abbott (ref. 18) which treats the subsonic region downstream of the Mach disk as a one-dimensional isentropic streamtube. Generally, for mildly underexpanded jets (low nozzle pressure ratios), the Mach disk diameter is small, and the subsonic region is approximated by a constant area streamtube.

For low Mach number (near unity) jets, the supersonic marching procedure becomes inefficient since the marching step size of the explicit scheme approaches zero as the Mach number approaches one. Also, under such conditions, the shock-fitting procedure may yield poor results since shocks are weak and difficult to define from the numerical results. Thus, RAXJET includes a low Mach number solution procedure in which the flow properties are calculated based on an isentropic expansion to the local inviscid external pressure (refs. 15 and 17). This isentropic procedure may also be applied to the flow downstream of a Mach disk. The computer program provides tests based on exit pressure and Mach number to determine whether the low-Mach-number procedure should be applied.

Boundary-Layer Solution

The properties in the attached boundary-layer region are solved by a modified version of the Peshotko-Tucker integral method for turbulent flows (ref. 7). The computer algorithm is described in references 11 and 19. The integral solution is obtained by conventional boundary-layer marching procedures to yield the displacement-thickness distribution $\delta^*(x)$ over the body.

Knowledge of the internal boundary-layer thickness is needed only to initialize the jet wake and mixing analysis. Since the nozzle internal boundary layer is generally quite thin compared to the afterbody external boundary layer, an exit boundary-layer thickness is estimated from flat-plate theory.

Separated Flow Solution

The analysis of the separated region consists of predicting the separation location and calculating the discriminating streamline shape. The discriminating streamline analysis is further divided into two regions: the separation region from the separation point to the end of the body and the jet wake region from the end of the body to the reattachment point (see fig. 2).

Separation location prediction.- The location of separation on the afterbody is calculated by the control volume technique developed by Presz (ref. 8). The technique determines the separation point based on a calculated pressure rise to separation from the minimum pressure on the afterbody. Abeyounis (ref. 10) compared the results of the Presz model and several other prediction techniques with the results of oil-flow studies on a series of circular-arc boattail nozzles. While none of the methods examined was able to successfully reproduce the experimental results over all test conditions, the Presz method seemed to yield the most accurate predictions. The largest error in most cases occurred at transonic speeds where shock-induced separa-

tion was encountered. In view of the difficulty in making accurate separation location predictions, RAXJET allows the separation location to be specified by the user as an option.

Discriminating streamline for separation region.- The discriminating streamline concept is used to separate the reverse flow region from the outer boundary-layer flow. The streamline shape is calculated by the discrete control volume analysis developed by Presz et al. (ref. 11). The method solves integral forms of the continuity and streamwise momentum equations to account for streamwise pressure gradients and surface skin friction. An error-function-type velocity profile modified to allow reverse velocities is assumed. The solution is marched downstream from the separation point to the end of the afterbody.

Discriminating streamline for jet wake region.- Two methods are provided for calculating the discriminating streamline shape in the jet wake region shown in figure 2. The first is an integral method that accounts for entrainment effects based on the turbulent mixing analysis of Peters and Phares (ref. 20). The integral method assumes a three-parameter polynomial form for the velocity profile which is matched to the error-function profile of Presz at the end of the afterbody. Integral forms of the continuity, axial-momentum, and turbulent kinetic energy equations are solved by a marching technique from the end of the afterbody to the reattachment point (at which the reverse velocity vanishes). The turbulent kinetic energy profile is related to the velocity profile by a mixing-length model for the eddy viscosity as in reference 13.

The second method for treating the jet wake region is a simple extrapolation model. In this model, the slope of the discriminating streamline at the end of the afterbody (as calculated by the Presz method) is linearly extrapolated to intersect the inviscid plume boundary. While this model is ad hoc, its results do approximate the results of the original conical discriminating streamline model used in earlier work by Presz (ref. 8).

Mixing-Layer Solution

The displacement-thickness distribution arising from entrainment into the jet mixing layer is calculated by the overlaid mixing model of reference 13 and computer program BOATAC (ref. 17). BOATAC solves the parabolic mixing equations by a finite-difference marching procedure in cylindrical streamline coordinates. Turbulence is modeled by either a mixing-length or a two-equation ($k\epsilon$) transport model. A laminar viscosity option is also included. The calculation is initialized at the nozzle exit for attached flows or at the reattachment location for separated flows. A fixed number of grid points, evenly spaced in the stream function coordinate, span the mixing layer. This computational grid is overlaid onto the inviscid external and jet flow fields (also mapped into streamline coordinates) from which edge conditions and pressure gradients are determined. The solution is marched downstream a user-specified distance that is sufficient to account for the near-field interaction (typically 10 to 15 exit radii). An effective plume boundary which accounts for mass entrainment into the mixing layer and inviscid plume blockage is calculated as described in reference 14. Then the inviscid plume boundary is subtracted from this effective boundary to define a displacement thickness related only to entrainment. This displacement-thickness distribution is treated like an extension of the boundary-layer displacement distribution and is added to the inviscid plume boundary by underrelaxation in the iteration procedure described in the next section.

Viscous-Inviscid Iteration Procedure

The component solutions are combined into the following iterative procedure (presented in fig. 3):

1. Calculate the inviscid external flow field over the effective body of revolution.
2. Calculate the inviscid jet exhaust boundary and flow field. If the flow is separated, the inviscid jet exhaust solution is frozen after 10 iterations.
3. Calculate the boundary-layer displacement thickness.
4. Calculate the separation location if required. The predicted separation location may be frozen after a user-specified number of iterations.
5. Calculate the shape of the discriminating streamline if required. Note that this calculation is repeated for every iteration if separation occurs, even if the separation location is frozen.
6. Calculate the mixing-layer displacement thickness.
7. Correct the effective body geometry by adding the displacement thickness and discriminating streamline to the original body and inviscid plume boundary. The relaxation procedure given in reference 14 is used to add these corrections.
8. Repeat steps (1) to (7) for the desired number of iterations.

At the end of step (8), the user must manually check the solution for convergence (usually by monitoring surface pressure and displacement distributions). Note that the order of calculation above is different from that in reference 14, although a single iterative loop is still used.

COMPARISONS BETWEEN PREDICTIONS AND EXPERIMENT

Predictions of program RAXJET are compared in figures 4 to 6 with experimental afterbody pressures from references 21, 22, and 23. All predictions were made with 77 by 39 grid points in the inviscid external region, 41 grid points in the mixing layer, and 41 grid points in the inviscid jet exhaust. The two-equation turbulence model was used for all mixing-layer calculations. For the separated flow cases, the experimental separation location and extrapolated jet wake model were used.

The comparisons for attached boundary-layer flow on a circular-arc boattail nozzle with $\frac{l}{D} = 1.768$ and $\frac{D_b}{D} = 0.51$ are shown in figure 4 at several nozzle pressure ratios (NPR) and free-stream Mach numbers. Predicted and experimental pressure distributions agree very well in almost all cases. The only significant differences occur at $M_\infty = 0.96$ and $NPR = 2.0$ (fig. 4(c)) where shock-boundary-layer interactions are expected.

The comparisons for slightly separated flow on a circular-arc nozzle with $\frac{l}{D} = 1.0$ and for significantly separated flow on a nozzle with $\frac{l}{D} = 0.8$ are given in figures 5 and 6, respectively. Again the agreement between prediction and experiment is excellent except for the $\frac{l}{D} = 0.8$ nozzle at Mach numbers of 0.9 and

0.94 (fig. 6(c)). While converged solutions were obtained and reasonable levels for the separation plateau pressures were predicted, the results at Mach numbers of 0.9 and 0.94 are quite poor in the region of shocks and in the jet wake. Furthermore, calculations at these Mach numbers made with the Presz model gave poor predictions of the separation location, and attempts to improve the predictions by iterating on the separation location sometimes led to divergent solutions. Thus it appears that strong interaction modeling is needed to treat flows with shock-induced separation. Therefore, RAXJET is not recommended when separation Mach numbers are supersonic.

Calculations made with the Presz model to predict separation location are compared to those made with the experimentally determined location in figure 7 for the $\frac{l}{D} = 1.0$ and $\frac{l}{D} = 0.8$ nozzles. In both cases the integral wake model was used, and the predicted separation location was frozen after the first iteration. For the $\frac{l}{D} = 1.0$ nozzle, the separation was predicted at $\Delta x/D = 0.71$, well upstream of the experimental value of 0.84 which resulted in a significant underprediction of the pressures near the end of the afterbody. For the $\frac{l}{D} = 0.8$ nozzle the predicted separation was at $\Delta x/D = 0.54$, compared to an experimental value of 0.51, and much better agreement is seen. In principle, better predictions of separation location could be obtained by updating the predicted location for additional iterations since the inviscid pressure should be approaching a more correct solution. However, the Presz model was found to be so sensitive to the imposed pressure distribution that significant amounts of underrelaxation were required to achieve convergence, and the predicted separation locations were not found to be consistently improved over those obtained on the first iteration. This sensitivity of separation predictions is typical of separation criteria that are based on calculating a pressure rise to separation (see ref. 10).

Predicted results with the integral and extrapolated jet wake models are compared in figure 8. Both sets of calculations used the experimental separation location. Slight differences are noted between the results of the two methods, and the judgment as to which is the better method seems to depend on which aspect of the prediction is most important to a particular problem. From these and similar results at other flow conditions, the integral method seems to yield more accurate flow-field predictions, while the extrapolated method seems to yield more accurate drag predictions.

Predicted and experimental boattail pressure drag for the data of figures 4 and 6 are compared in figure 9. Predicted drag obtained with the Presz separation model and the integral wake model and with the experimental separation location and the extrapolated wake model are shown for the separated flow cases. The drag calculated with the experimental separation location and the integral wake model fell between these two curves. Predicted results from reference 6 which neglect entrainment effects downstream of reattachment are also included. Generally, the agreement between the present results and experiment is good with noticeable improvement over the results of reference 6. This improvement is primarily due to the inclusion of jet entrainment effects. Although there is an undesirable sensitivity of the present predictions to the separation and jet wake model used, the present method does correctly predict the qualitative behavior for a given model. Thus, for parametric drag studies it is recommended that a particular combination of separation and wake models be used consistently.

In figure 10, predicted pitot pressures across the jet and mixing layer are compared with the data of Mason and Putnam (ref. 24). Figure 10(a) gives the results for a nozzle with attached flow at a Mach number of 0.4 and a nearly fully expanded jet ($NPR = 2.0$). The agreement is reasonably good, except that the spread rate of

the mixing layer is underpredicted. Cline and Wilmoth (ref. 25), who used a Navier-Stokes solution method with essentially the same turbulence model, found a similar trend. The results of reference 14 suggest that at least some of the discrepancy may be due to deficiencies in the turbulence modeling. However, the overall afterbody flow-field predictions were found to be relatively insensitive to the turbulence model used in the mixing-layer calculation.

Figure 10(b) gives results for a nozzle with separated flow at a Mach number of 0.8 and a moderately underexpanded jet (NPR = 5.0). The prediction was made with the integral jet wake model. Note that the wake defect predicted by this model agrees with the experimental profile nearest the nozzle exit ($\Delta x/r_j = 0.1$). Also, the predicted structure of the inviscid plume flow field is in excellent agreement with the experimental structure. The location and strength of the barrel shock and Mach disk normal shock and the size of the Mach disk streamtube are all correctly predicted. Since this shock structure is known to be sensitive to the external pressure distribution imposed (see ref. 24), the present results suggest that the basic plume interaction model is reasonably correct.

DESCRIPTION OF COMPUTER PROGRAM

The organization of computer program RAXJET is presented in figure 11. The program is written in overlay form and consists of the main overlay (0,0) and six primary overlays (fig. 11(a)). The main overlay, RAXJET, controls the input and output of data and the viscous-inviscid iteration scheme. Primary overlay (1,0) contains the program RAXBOD which calculates the inviscid external flow. Primary overlay (2,0) contains the program SCIPAC which calculates the inviscid jet exhaust flow. Primary overlay (3,0) contains the program VISCOUS which calculates the boundary-layer growth and performs the separation analysis. Primary overlay (4,0) contains the program BOATAC which performs the overlaid mixing analysis. Primary overlay (5,0) contains the program INPT which reads the input data, and primary overlay (6,0) contains the program OUTPT which prints the computed results.

The program uses six disk files. Input data are obtained from file TAPE5 and the results are written to file TAPE6 which is equated to file OUTPUT. The remaining disk files are used internally by the program and are described later. RAXJET requires about 76 000 octal storage locations on the Control Data CYBER 175 computer and executes 20 viscous-inviscid iterations in approximately 12 minutes of CPU time for separated flow on an afterbody with a fully expanded jet. Attached flow computations generally require fewer iterations and therefore less computer time. Under-expanded or overexpanded jets generally require more computer time.

A brief description of each of the main routines is given in the following list:

1. Program RAXJET.- RAXJET initiates a run by calling program INPT to read the input data. Then an initial call is made to program RAXBOD to set up the inviscid external grid. This grid is used to define various grid indices used by other routines and to initialize various geometric arrays. RAXJET then starts the viscous-inviscid loop by calling RAXBOD, SCIPAC, VISCOUS, and BOATAC, successively. Then program OUTPT is called to print the results. Finally, RAXJET calculates the new effective body and repeats the viscous-inviscid iteration until the specified number of iterations is completed. RAXJET also calls subroutine AINTPL to interpolate the original body geometry onto the inviscid grid (which changes slightly during each iteration) and subroutine SMOOTH to smooth the effective body geometry for separated flows.

2. Program RAXBOD.- RAXBOD solves the exact nonlinear potential flow equation for the inviscid external flow and consists of the primary overlay (1,0) and four secondary overlays (see fig. 11(b)). RAXBOD first calls ONE1 (overlay (1,1)) to set up the tangential grid and ONE2 (overlay (1,2)) to set up the normal grid. Since the effective body shape may change with each iteration, these routines must be called before each inviscid calculation. For the first iteration only, subroutine ESTIM is called to initialize the perturbation potential to zero. For each succeeding iteration, potential values from the previous iteration are used as the initial estimate. Program ONE3 (overlay (1,3)) is then called to solve the exact potential equation by the South-Jameson relaxation scheme. The relaxation is continued until either the specified maximum number of relaxation iterations are performed or the specified convergence tolerance is reached. Finally, program ONE4 (overlay (1,4)) is called to calculate the flow quantities (velocity, pressure, etc.) from the perturbation potential and to transfer the results to disk file TAPE4.

3. Program SCIPAC.- SCIPAC solves the inviscid jet exhaust region by a shock-capturing-shock-fitting procedure and consists of the main program, 24 subroutines, and 6 function subroutines (see fig. 11(c)). SCIPAC initializes a jet calculation by calling SCIPPB which reads the external flow properties from TAPE4 and determines the pressure to be specified along the plume boundary. Then SCIPIN is called to generate the initial conditions at the nozzle exit from the input data and to discretize the initial flow conditions for the finite-difference marching procedure. Also, from nozzle exit conditions, SCIPIN estimates the length of the first inviscid cell which is used to terminate the marching procedure. Then SCIPCT is called to integrate the finite-difference flow equations and to perform the iterative Mach disk calculation. For the Mach disk calculation, disk files TAPE1 and TAPE2 store conditions upstream of the predicted Mach disk location while trial solutions downstream are attempted. Details of the Mach disk procedure are given in reference 17. Depending on certain input parameters and the predicted inviscid cell length, the marching procedure terminates either downstream of the Mach disk or at the end of the first or second inviscid cell. Properties downstream of this termination point are calculated by a simple isentropic expansion to local external pressure by calling subroutine SCIPDK. Jet exhaust properties at axial locations corresponding to the external inviscid grid are transferred to disk file TAPE3 by calling SCIPOT. Finally, SCIPPL is called to determine the coordinates of the inviscid plume boundary and to store them for later use.

4. Program VISCOUS.- Program VISCOUS calculates the boundary-layer growth, separation location, and discriminating streamline shape by calls to subroutines ONE, TWO, and THREE (see fig. 11(d)). Subroutine ONE calculates the boundary-layer displacement thickness, skin friction, and power-law exponent by a modified Reshotko-Tucker integral procedure with the inviscid pressure gradient imposed by the external flow solution. Subroutine TWO calculates the separation location by the Presz control volume method. Subroutine THREE calls B834 which calculates the discriminating streamline shape by the modified discrete control volume method of Presz et al. If the integral wake model is specified, B834 calls JET to calculate the discriminating streamline from the end of the body to the end of the recirculation region. If the integral wake model is not specified, B834 linearly extrapolates the discriminating streamline until it intersects the inviscid plume boundary.

5. Program BOATAC.- Program BOATAC calculates the turbulent mixing layer and the plume displacement thickness and consists of the primary overlay (4,0) and two secondary overlays (see fig. 11(e)). BOATAC first calls BOATSA (overlay (4,1)) which in turn calls (1) BOATIF to read the inviscid flow field from TAPE3 and TAPE4, (2) BOATIP and BOATKE to generate the initial velocity, temperature, and turbulence

profiles, and (3) BOATSB to map the profiles into equally spaced streamline coordinates. BOATAC then calls BOATM1 (overlay (4,2)) which in turns calls (1) BOATS3 to integrate the parabolized flow equations, (2) BOATDS to calculate the plume displacement thickness, (3) BOATEN to estimate the necessary computational boundary growth rate, (4) BOATM2 to reset the discretized profile to begin the next marching step, and (5) BOATOT to transfer the results to disk file TAPE2 at axial locations corresponding to the external grid. BOATAC starts at the nozzle exit for attached flows or at the reattachment location for separated flows and marches downstream the user-specified number of jet radii. Mixing-layer properties downstream of this axial location are not calculated.

6. Program INPT.- INPT reads the input data from TAPE5, checks for possible input errors, and prints the appropriate warning messages (fig. 11(f)). If certain RAXBOD grid parameters are not input, INPT calls subroutine OPTIM which attempts to optimize those parameters not given so that a maximum number of grid points are located on the afterbody consistent with an accurate solution of the total flow field. Finally, INPT calls subroutine IOUTPT to print the input data.

7. Program OUTPT.- OUTPT prints the surface quantities, drag coefficients, and convergence history (fig. 11(f)). If requested, OUTPT calls subroutine OFFOUT to generate and print a composite viscous-inviscid flow field.

Description of Input Data

The program input data are entered by a title card followed by eight namelists. A sample input data deck is given in the appendix. Some of the geometric input quantities are defined in figure 12, and certain input parameters for the off-body flow-field output are given in figure 13.

1. Title card.- The first card of each data deck consists of 80 alphanumeric characters that identify the case. The eight namelists must then appear in the following order.

2. Namelist CNTRLN.- CNTRLN contains the input parameters that control the main logic of the program:

IMAX	Integer that specifies the number of grid points in the streamwise direction for the inviscid external flow solution (81 maximum). The default value is 81.
JMAX	Integer that specifies the number of grid points in the body normal or radial direction for the inviscid external flow solution (41 maximum). The default value is 41.
MIT	Integer that specifies the number of relaxation cycles used per viscous-inviscid iteration for the inviscid external flow solution. The default value is 20.
MVI	Integer that specifies the number of viscous-inviscid iterations (30 maximum). The default value is 1.
ISEP	Integer that specifies the separation model used: If ISEP = 0, no separation model is used. If ISEP = 1, the Presz control volume method is used.

If ISEP = 2, the separation location is specified by the user.
The default value is 0.

NSEP Integer that specifies the number of viscous-inviscid iterations after which the separation location is held fixed (needed only if ISEP = 1).
The default value is 1.

IWAKE Integer that specifies the jet wake model (needed for ISEP = 1 or 2):
If IWAKE = 0, the integral wake model is used.
If IWAKE = 1, the extrapolated wake model is used.
The default value is 0.

XSEP Axial coordinate of the separation location nondimensionalized by REFL (needed only if ISEP = 2). The default value is XM.

IUI Integer that specifies the type of units used for input quantities:
If IUI = 0, lengths are input in feet, temperatures in Rankine, and pressures in pounds per square foot (psf).
If IUI = 1, lengths are input in meters, temperatures in kelvin, and pressures in atmospheres (1 atm = 101.325 kPa).
The default value is 0.

IUO Same as IUI except it applies to output quantities.

3. Namelist FSC.- FSC contains the free-stream conditions and reference quantities:

GAM Ratio of specific heats. The default value is 1.4.

AMINF Free-stream Mach number. No default value is specified.

PT Free-stream total pressure in pounds per square foot or atmospheres.
The default value is 2116 psf or 1 atm, depending on IUI.

TT Free-stream total temperature in °R or K. The default value is 530°R or 294 K, depending on IUI.

REFL Reference length used to convert input coordinates to feet (IUI = 0) or meters (IUI = 1). All other inputs having dimensions of lengths are assumed to be nondimensionalized by REFL. The default value is 1.0.

SREF Reference area in square feet or square meters used to calculate drag coefficients. The default value is $(\pi/4)(REFL)^2$.

ALPHAE Array containing the mole fractions of the six species in the following order: N₂, O₂, CO₂, H₂O, CO, and CH₄. The default values are the nominal values for air: ALPHA(1) = 0.79, ALPHA(2) = 0.21, ALPHA(3) = ALPHA(4) = ALPHA(5) = ALPHA(6) = 0.0

4. Namelist JETDAT.- JETDAT contains the nozzle exit conditions and control parameters for the inviscid jet exhaust solution:

XNPR Nozzle pressure ratio, ratio of jet total pressure to free-stream static pressure. No default value is specified.

EMJET Nozzle exit Mach number (EMJET > 1.05). The default value is 1.05.
 TTJET Nozzle exit total temperature in °R or K. The default value is 530°R or 294 K, depending on IUI.
 RJET Nozzle exit radius nondimensionalized by REFL. No default value is specified. (See fig. 12.)
 THLIP Nozzle exit lip angle in degrees. The default value is 0.0. (See fig. 12.)
 NMAXJ Integer that specifies the number of radial grid points used in the inviscid jet solution (81 maximum). The default value is 81.
 IGAS Integer that specifies the thermodynamic option for the inviscid jet solution:
 If IGAS = 0, a perfect gas is assumed and GAMJ = 1.4.
 If IGAS = 1, a perfect gas is assumed and GAMJ must be input.
 If IGAS = 2, a calorically imperfect gas is assumed and GAMJ will be calculated.
 If IGAS = 3, a perfect gas is assumed but GAMJ will be calculated based on nozzle exit conditions and held constant downstream.
 The default value is 0.
 GAMJ Ratio of specific heats for inviscid jet exhaust. See IGAS for defaults.
 IDK Integer that controls the solution method downstream of a Mach disk:
 If IDK = 0, an isentropic decay is imposed.
 If IDK = 1, a finite-difference shock-capturing solution will be attempted.
 The default value is 0.
 ALPHAJ Array containing the mole fractions of the six jet species. Same as ALPHAE (namelist FSC) except it applies to the inviscid jet.

5. Namelist MIXDAT.- MIXDAT contains the input quantities that control the overlaid mixing-layer calculation:

IVIS Integer that specifies the turbulence model.
 If IVIS = -2, the $k\epsilon^2$ model is used.
 If IVIS = 0, the Prandtl mixing-length model is used.
 If IVIS = 2, a laminar model is used.
 The default value is -2.
 MPSI Integer that specifies the number of radial grid points used in the mixing-layer calculation (50 maximum). The default value is 31.
 FDL Factor that multiplies the marching step size (FDL < 1.0). The default value is 1.0.
 FFF Mixing-length scale used in the Prandtl mixing model in the near-field region. The default value is 0.065.
 GGG Mixing-length scale used in the Prandtl mixing model in the fully developed region. The default value is 0.080.

SIGMA	Turbulent Prandtl number. The default value is 1.0.
TCONT	Maximum allowable temperature change in one marching step in °R or K, depending on IUI. The default value is 400/(MPSI - 1) K.
XJENT	Axial distance in jet radii from the nozzle exit where the mixing calculation will be terminated. The default value is 15.
KMAXJ	Integer that specifies the number of mapped radial grid points in the inviscid jet solution that are used in the overlaid mixing calculation (25 maximum). The default value is 25.
KMAXE	Same as KMAXJ except it applies to the inviscid external flow solution.
TKEJ	Factor that multiplies the initial turbulent kinetic energy in the jet at the nozzle exit. The default value is 1.0.
TKEX	Same as TKEJ except it applies to the external flow side of the initial profile.

6. Namelist RELAX.- RELAX contains various relaxation parameters used in the inviscid external flow solution and viscous-inviscid interaction:

RF1	Relaxation factor for subsonic points in the inviscid external flow solution ($0 < RF1 < 2$). The default value is 1.4.
QF3	Supersonic damping factor for improving iterative stability in the inviscid external flow solution ($QF3 > 0$). The default value is 0.1.
COVERG	Convergence criterion for inviscid external flow solution. Inviscid relaxation cycles stop for a given iteration when the average residual is less than $COVERG/(IMAX - 1)^2$ or MIT cycles are completed, whichever occurs first. The default value is 1.0.
WB and WBF	Underrelaxation parameters for adding the displacement thickness and discriminating streamline to the body. WB is the value for the first iteration and WBF is the value for the final iteration. For intermediate iterations, the underrelaxation factor is varied linearly from WB to WBF. (WB and WBF must be in the range from 0 to 1.) The default values are 0.5. Larger values of WB or WBF give more underrelaxation.

7. Namelist GRID.- GRID contains the parameters that control the body-fitted grid used in the inviscid external flow solution:

XBT	Axial location of the start of the afterbody nondimensionalized by REFL. No default value is specified. (See fig. 12.)
XM	Axial location of the end of the body nondimensionalized by REFL. No default value is specified. (See fig. 12.)
DXIDXO	Derivative of the tangential coordinate stretching function at the nose, $(dF/dX)_{X=0}$. A reasonable value can be estimated from $DXIDXO = (IMAX - 1)\Delta F_0$ where ΔF_0 is the desired grid size at the

nose. If no input value is given, the program will attempt to calculate an optimum value.

DXIDXM Derivative of the tangential stretching function at the end of the body, $(dF/dX)_{X=X_M}$. A reasonable value can be estimated from $DXIDXM = (IMAX - 1)\Delta x_M$ where Δx_M is the desired grid size at the end of the body. If no input value is given, the program will attempt to calculate an optimum value.

CXM Fraction of streamwise grid points that lie on the body ($0 < X < XM$). (CXM must be in the range from 0 to 1.) The default value is 0.75. Note that if no input value of $DXIDXM$ is given, CXM may be changed in an attempt to find an optimum value for $DXIDXM$.

DNDYO Derivative of normal coordinate stretching function at the body surface, $(dn/dY)_{Y=0}$. A reasonable value may be estimated from $DNDYO = (1 - \Delta Y)^\alpha \Delta n_0 / \Delta Y$ where Δn_0 is the desired grid size at the surface, α is the stretching exponent, and $\Delta Y = 1/(JMAX - 1)$. If no input value is given, the program will attempt to calculate an optimum value.

ALF Exponent in the normal coordinate stretching function. ($ALF > 0$.) The default value is 1.3. Larger values of ALF move the last finite value of n farther away from the body and smaller values move it closer.

8. Namelist OUTPTC.- OUTPTC contains parameters which control the printing of results. Some of the parameters used to generate the composite flow-field output are defined graphically in figure 13. Figure 14 shows how the composite flow field is constructed.

IOUT Integer that specifies the iteration number at which the printing of results will begin. All iterations from IOUT to MVI will be printed. The default value is 0.

IAFT Integer that controls the amount of results printed:
If IAFT = 0, results will be printed starting at the nose.
If IAFT = 1, results will be printed starting at the first grid point ahead of the afterbody.
The default value is 0.

IOFF Integer that controls the printing of the off-body flow-field results:
If IOFF = 0, no off-body results will be printed.
If IOFF = 1, off-body results will be printed.
The default value is 0.

XSTART Axial location (nondimensionalized by REFL) at which the printing of off-body results will begin. No default value is specified.

XEND Axial location (nondimensionalized by REFL) at which the printing of off-body results will end. No default value is specified.

ROB Radial outer boundary (nondimensionalized by REFL) for printing off-body results. No default value is specified.

IMAP	Integer that specifies the number of mapped output points between the body (or inviscid plume boundary) and $r = ROB$ (see fig. 13). ($IMAP < 100 - JMAP$.) The default value is 25.
JMAP	Integer that specifies the number of mapped output points across the jet exhaust ($0 < r <$ Inviscid plume boundary). ($JMAP < 100 - IMAP$.) The default value is 25.
ALFO	Exponent in radial stretching function used to distribute output points in off-body results. $ALFO > 1$ will pack points in the boundary layer and mixing layer. $ALFO = 1$ will give equally spaced points. The default value is 1.
9. <u>Namelist GEOMN</u> .-- GEOMN contains the body geometry data. Note that a finite-length forebody geometry must be input even if only afterbody results are desired. The forebody nose may be blunt or pointed, and the input coordinates are assumed to be referenced to the nose ($x = 0$, $r = 0$ in fig. 12).	
IXY	Integer that specifies the number of body input coordinates (140 maximum). No default value is specified.
IORDER	Integer that specifies the type of interpolation used to determine the geometry at the inviscid grid points: If $IORDER = 1$, first order will be used. If $IORDER = 2$, second order will be used. The default value is 1.
XO	Array of IXY axial body coordinates (nondimensionalized by REFL) with origin at the nose of the body of revolution. No default values are specified.
YO	Array of IXY radial body coordinates (nondimensionalized by REFL) with origin at the nose of the body of revolution. No default values are specified. Note that the first point of the XO and YO arrays must correspond to the nose, $XO(1) = 0$, and the last point to the end of the body, $XO(IXY) = XM$.

Description of Output

An example of the printed output is given in the appendix for the sample input data also presented there. The first two pages are duplicate output with RAXJET bannerized followed by the case title, date, and time of run. Warning messages generated by the input data are printed on the third page and diagnostic messages from the grid optimization routine are printed on the fourth page. The fifth page contains the program title and abstract, case title, and free-stream and jet exhaust conditions. On the sixth page, the gas composition and remaining input parameters are printed. The next two pages list the input geometry. The tabular input geometry has been augmented with points that define a cylindrical sting starting at the end of the body as an initial guess for the plume shape.

The following pages list the results. For each iteration starting with IOUT the case title, iteration number, free-stream Mach number MO, jet pressure ratio, and reference length L are given. If boundary-layer separation is predicted, the separation and reattachment locations are also printed. A tabulation is given of

Axial grid point number I

Body axial coordinate X/L

Body radial coordinate R/L

Pressure coefficient CP

Local Mach number ML

Skin-friction coefficient CF

Body radius corrected for the discriminating streamline and inviscid plume shape RDS/L

Effective body radius REFF/L

Radial location of the outer edge of the viscous layer RVI/L

Displacement thickness DEL*/L

Boundary-layer momentum thickness THETA/L

Compressible shape factor H

Note that REFF/L is the effective body obtained by underrelaxation, while RDS/L + DEL*/L is the calculated displacement body for a given iteration. Note also that the definition of DEL*/L for the plume mixing layer used here differs from that presented in reference 14. Here, values of DEL*/L for X/L downstream of the nozzle exit include only the contribution due to jet entrainment and do not include the inviscid plume blockage. However, the effective body definition used here is the same as in reference 14. After the final iteration is printed, the following drag coefficients for each iteration are tabulated:

Afterbody pressure drag CDP,AFT

Afterbody friction drag CDT,AFT

Total (pressure and friction) afterbody drag CDT,AFT

External pressure drag for the complete body of revolution (forebody and afterbody) CDP,BOD

Body friction drag CDF,BOD

Total body drag CDT,BOD

Next, the maximum residual RPMAX and average residual RP AVG for the RAXBOD calculation are listed as an indication of the convergence history.

If off-body flow-field results are requested, the remaining pages tabulate

Axial location X/L

Radial location R/L

Nondimensionalized pressure P/PINF

Nondimensionalized temperature T/TINF

Nondimensionalized axial velocity U/UINF

Nondimensionalized radial velocity V/UINF

Mach number M

Ratio of specific heats GAMMA

Nondimensionalized pitot pressure PT/PTINF

Pressures, temperatures, and velocities are determined by linear interpolation directly from the appropriate flow solution as indicated in figure 14 except for points in the boundary layer (denoted by BL). For the BL points, edge conditions and pressures are determined by interpolation from the inviscid solution, streamwise velocities are calculated from a power-law profile, and temperatures are calculated by assuming a constant total temperature across the layer. Axial and radial velocity components are determined from the streamwise values by assuming a linear variation in streamline slope across the layer from the local body slope at the surface to the inviscid streamline slope at the outer BL edge. For all points, local Mach number and pitot pressure are computed from these interpolated and calculated quantities. Note that for supersonic points, the pitot pressure is obtained by normal shock relations for an adiabatic, perfect gas. Points in the inviscid jet region that are computed from isentropic theory are denoted by (*) and points in the mixing layer downstream of where the mixing solution terminates are denoted by (**). Note that the axial location of points in the inviscid jet and mixing layer may not correspond exactly to the grid location in the external flow. These points correspond to actual marching step locations that are nearest the external grid location. No attempt was made to interpolate these points in the axial direction since the discrepancy is usually quite small. Also note that flow-field results are not given within the separated region.

Instructions to the User

The following special instructions are provided to assist the user in applications of program RAXJET. These instructions do not cover all possible user problems but are intended to assist the user in anticipating cases where the physical and computational models may not give accurate results. Many of the problems associated with inappropriate input data are flagged by the program followed by explanatory warning messages, and these are not discussed here.

Grid generation.- The user has input control over the streamwise and normal grid used by RAXBOD, and the radial grid used by SCIPAC and BOATAC. The streamwise grid used by VISCOUS for the boundary-layer calculation is the same as that for RAXBOD. For most problems, the built-in procedures for optimizing the RAXBOD grid parameters give satisfactory results as long as the afterbody length comprises approximately 10 to 25 percent of the total body length. For shorter afterbodies, other unusual geometries, or much fewer than the maximum allowable number of grid points (IMAX,JMAX), the user should verify that the grid is adequate. For the SCIPAC calculation, accurate shock-capturing may require nearly the maximum allowable number of

points ($NMAXJ = 81$). If fewer points are used, SCIPAC gives less accurately defined shocks and may encounter problems when computing cases with small Mach disks or regular barrel shock reflections or when attempting to extend the computation beyond the first Mach disk or reflection ($IDK = 1$). If such problems are encountered, the user should try increasing $NMAXJ$. For the BOATAC calculation, the default value of $MPSI = 31$ may be adequate for the basic entrainment interaction; however, larger values of $MPSI$ are recommended if accurate mixing-layer profiles are desired.

Convergence.- The convergence history of the RAXBOD calculation is given as part of the output. If convergence is not achieved by the final iteration, the number of global iterations MVI, the number of relaxation cycles MIT, or both should be increased. An indication of the global convergence of the viscous-inviscid calculation can be obtained by monitoring the afterbody pressure drag (CDP,AFT) or selected pressures and, for separated flows, the separation location (if $ISEP = 1$, $NSEP > 1$).

Attached flows ($ISEP = 0$).- Calculations in which attached flow is anticipated generally converge in 5 to 10 iterations with most input parameters set at their default values. Flows with incipient separation may also be run as attached flows but may require greater amounts of underrelaxation (increased WB and WBF) and more iterations to converge.

Separated flows ($ISEP > 0$).- Separated flows require considerably more user intervention in selecting appropriate control parameters than attached flows. The greatest source of error generally lies in prediction of the separation location. More accurate flow predictions can be made if the separation location is known and is input by the user ($ISEP = 2$). If the separation location is not known, it is recommended that a solution first be attempted as for attached flow ($ISEP = 0$). If the solution diverges or if the boundary-layer shape factor exceeds a value of 2, then assume that the flow is separated and attempt a solution with $ISEP = 1$. A value of $NSEP = 1$ (the default value) is recommended which bases the separation location prediction on the initial inviscid solution. This procedure yields reasonable results except where the flow is approaching shock-induced separation. RAXJET is not recommended for strong shock-induced separation. More accurate predictions of the separation location can sometimes be obtained by allowing the predicted location to be updated over several iterations ($NSEP > 1$), but larger amounts of underrelaxation are usually necessary ($WB = 0.75$, $0.5 < WBF < 0.75$, typically). The choice of the wake model depends on the type of result that is of primary interest. If aft-body pressures and drag are the main interest, $IWAKE = 1$ is recommended. If mixing-layer profile results are important, $IWAKE = 0$ is recommended.

Real gas thermodynamics.- The real gas thermodynamics used in SCIPAC and BOATAC contain built-in data for the six species, N_2 , O_2 , CO_2 , H_2O , CO , and CH_4 . Alternate species may be used by replacing the appropriate polynomial coefficient data in subroutines SCIPC and BOATSD with that for the alternate species. Detailed definition of these coefficients is given in reference 17.

CONCLUDING REMARKS

A viscous-inviscid interaction method has been developed to compute the subsonic and transonic flow over nozzle afterbodies with supersonic jet exhausts. The method accounts for the interaction between the inviscid external flow, an underexpanded jet exhaust, an attached or separated boundary layer, and the turbulent jet mixing layer. A computer algorithm called RAXJET has been written which iteratively combines

solutions for the various flow regions by a relaxation procedure. The results of the method are in good agreement with experiment for afterbodies with attached flow up to moderately high transonic speeds. For afterbodies with separated flow, the agreement is good except when shock-induced separation is encountered. The results indicate a need for improved modeling of separated flows where strong interactions occur. The method correctly predicts the effects of jet entrainment and plume blockage on nozzle drag. Good agreement is obtained with flow-field data for moderately underexpanded jet exhausts.

Langley Research Center
National Aeronautics and Space Administration
Hampton, VA 23665
January 4, 1982

APPENDIX

SAMPLE INPUT AND OUTPUT FOR PROGRAM RAXJET

Sample Input Data

```
L/D=0.8, DB/D=0.51 CIRCULAR ARC RADTAIL = " = 0.8, NPK = 5,0  
$CNTRLN IMAX=77, JMAX=39, MVI=20, MIT=40, ISEP=1, IUD=1 $  
$FSC GAM=1.4, AMINF=0.8, PT=7110., TI=560., REFL=0.5 $  
$JETDAT XNPHE=5.0, TTJFT=530., RJET=0.25, NMAGJ=41, IGAS=2, IDK=0,  
EMJET=1.05 $  
$MIXDAT MPSI=41 $  
$RELAX WB=0.75, KRF=0.5 $  
$GRID CXR=75, XBT=8.0, XM=8.0 $  
$UITHTC IOU1=20, IAFT=1, IUFT=1, XSTRT=8.0, XEND=9.4, RUH=0.75 $  
$GEOMN IXY=89,  
X0(1)=0.0,.1,.2,.3,.4,.5,.6,.7,.8,.9,1.0,1.1,1.2,1.3,1.4,1.5,1.6,1.7,  
1.8,1.9,2.0,2.1,2.2,2.3,2.4,2.5,2.6,2.7,2.8,2.9,3.0,3.1,3.2,3.3,3.4,  
3.5,3.6,3.7,3.8,3.9,4.0,4.1,4.2,4.3,4.4,4.5,4.6,4.7,4.8,4.9,5.0,5.1,  
5.2,5.3,5.4,5.5,5.6,5.7,5.8,5.9,6.0,6.1,6.2,6.3,6.4,6.5,6.6,6.7,6.8,  
6.9,7.0,7.1,7.2,7.3,7.4,7.5,7.6,7.7,7.8,7.9,8.0,8.1,8.2,8.3,8.4,8.5,  
8.6,8.7,8.8,  
Y0(1)=0.0,.025013,.050026,.075038,.100051,.125064,.150077,.175090,  
.200102,.225115,.250128,.275141,.300154,.325166,.350179,.375192,  
.400205,.425218,.450230,.475050,.489760,.498360,59*.5,.496490,  
.485932,.466146,.442860,.409646,.367897,.316754,.255 $
```

APPENDIX

Sample Output

CASE - L/D = 0.8, D/H/D = 0.51 CIRCULAR ARC BOATTAIL = H = 0.8, NPR = 5.0

DATE = 01/07/16,
TIME = 08:57:57.

Pages 1 and 2. (Note that page 2 is a duplicate of page 1.)

APPENDIX

---WARNING MESSAGES---

INPUT VALUE OF DXDUXU NOT GIVEN OR < 0, WILL TRY TO CALCULATE AN OPTIMUM VALUE
INPUT VALUE OF DXIDAM NOT GIVEN OR < 0, WILL TRY TO CALCULATE AN OPTIMUM VALUE
INPUT VALUE OF DNUYU NOT GIVEN OR < 0, WILL TRY TO CALCULATE AN OPTIMUM VALUE
NOZZLE GEOMETRY GIVEN HAS A BASE THICKNESS OF .005000, TOO LARGE A BASE MAY GIVE UNRELIABLE RESULTS

APPENDIX

==.TYPE 8 GRID OPTIMIZATION REQUESTED

CXM	CHANGED FROM	.75 TO	.82
DX1DX0	CHANGED FROM	0.0000 TO	5.5488
NX1DXM	CHANGED FROM	0.0000 TO	5.5488
DNVDO	CHANGED FROM	0.0000 TO	2.6799

**RAXJET --- A VISCOUS/INVISCID PROGRAM FOR TRANSONIC, AXISYMMETRIC FLOW
OVER NOZZLE AFTERBODIES WITH SUPERSONIC JET EXHAUSTS**

BY RICHARD G. WILMOTH, NASA, LANGLEY RESEARCH CENTER

PROGRAM ABSTRACT -

THE VISCOUS/INVISCID SOLUTION IS OBTAINED USING THE FULL POTENTIAL,
RELAXATION METHOD OF SOUTH AND JAMESON FOR THE TRANSONIC, EXTERNAL FLOW
COMBINED WITH (1) THE SHOCK-CAPTURING/SHOCK-FITTING INVISCID PLUME MODEL
OF DASH, PERGAMENT AND THORPE; (2) A MODIFIED RESHOTKO-TUCKER INTEGRAL
BOUNDARY-LAYER SOLUTION; AND (3) THE OVERLAID, NEARFIELD MIXING MODEL OF
DASH AND PERGAMENT. FOR SEPARATED FLOWS, PLESZ'S SEPARATION CRITERIA AND
MODIFIED DISCRIMINATING STREAMLINE SOLUTION ARE USED. THE VISCOUS/INVISCID
INTERACTION IS TAKEN INTO ACCOUNT BY AN ITERATIVE UNDERRELAXATION PROCEDURE.

CASE TITLE -

L/D=0.6, DH/D=0.51 CIRCULAR ARC BOATTAIL - M = 0.8, NPR = 5.0

FREE STREAM CONDITIONS -

MACH NUMBER	=	8.00
GAMMA	=	1.400
TOTAL PRESSURE	=	1.000 ATM
TOTAL TEMPERATURE	=	311.111 KELVIN
REYNOLDS NUMBER	=	12.9E+7 MILLION METER

JET EXHAUST CONDITIONS -

MACH NUMBER	=	1.050
PRESSURE RATIO	=	5.000
TOTAL TEMPERATURE	=	294.444 KELVIN
NOZZLE EXIT RADIUS	=	.038 METERS
NOZZLE LIP ANGLE	=	0.000 DEGREES

APPENDIX

APPENDIX

COMPOSITION = SPECIES	JET	FREESTREAM
N2	•790E+00	•790E+00
U2	•2.0E+00	•210E+00
CO2	0.	0.
H2O	0.	0.
CO	0.	0.
CH4	0.	0.

CONTROL PARAMETERS =

I MAX = 77	R F1 = 1.40
J MAX = 39	QF3 = .10
M I = 40	C OVERG = 1.00
M V1 = 20	WB = .75
J SEP = 1	WBF = .50
N STEP = 1	
I WAKE = 0	

RELAXATION PARAMETERS =

R F1 = 1.40	C XH = .62
QF3 = .10	D XIDX0 = 5.548830
C OVERG = 1.00	D XIDXM = 5.548830
WB = .75	D NDY0 = 2.679878
WBF = .50	ALF = 1.30

MIXING CONTROL PARAMETERS =

I VIS = 72	F DL = 1.00	T CONT = 10.00
M PSI = 41	FFF = .065	X JENT = 15.00
K MAXJ = 25	GGG = .080	T KEJ = 1.00
K MAXE = 25	SIGMA = 1.000	T KEX = 1.00

JET CONTROL PARAMETERS = NMAXJ = 41, IGAS = 2, IDK = 0

OUTPUT CONTROL = IOUT = 20, IAF1 = 1, IUFF = 1, IUD0 = 1

INPUT GEOMETRY - 1ST-ORDER INTERPOLATION WILL BE USED TO FIT THE INVISCID GRID
 TIME AFTER BODY STARTS AT X/REFL = 8.000000 AND ENDS AT X/REFL = 8.800000
 THE BODY SLOPE AT THE NOSE IS = .250130

i	x/refl	x/refl	x/refl	x/refl	x/refl
1	0.00000	0.00000	0.00000	3.50000	3.50000
2	*1.00000	*0.25015	*0.50026	*3.60000	*3.60000
3	*2.00000	*0.50026	*0.75038	*3.70000	*3.70000
4	*3.00000	*0.75038	*1.00051	*3.80000	*3.80000
5	*4.00000	*1.00051	*1.25064	*3.90000	*3.90000
6	*5.00000	*1.25064	*1.50077	*4.00000	*4.00000
7	*6.00000	*1.50077	*1.75090	*4.10000	*4.10000
8	*7.00000	*1.75090	*2.00102	*4.20000	*4.20000
9	*8.00000	*2.00102	*2.25115	*4.30000	*4.30000
10	*9.00000	*2.25115	*2.50128	*4.40000	*4.40000
11	*1.00000	*2.50128	*2.75141	*4.50000	*4.50000
12	*1.10000	*2.75141	*3.00154	*4.60000	*4.60000
13	*1.20000	*3.00154	*3.25166	*4.70000	*4.70000
14	*1.30000	*3.25166	*3.50179	*4.80000	*4.80000
15	*1.40000	*3.50179	*3.75192	*4.90000	*4.90000
16	*1.50000	*3.75192	*4.00205	*5.00000	*5.00000
17	*1.60000	*4.00205	*4.25218	*5.10000	*5.10000
18	*1.70000	*4.25218	*4.50230	*5.20000	*5.20000
19	*1.80000	*4.50230	*4.75343	*5.30000	*5.30000
20	*1.90000	*4.75343	*5.00000	*5.40000	*5.40000
21	*2.00000	*5.00000	*5.49976	*5.50000	*5.50000
22	*2.10000	*5.49976	*5.98366	*5.60000	*5.60000
23	*2.20000	*5.98366	*5.00000	*5.70000	*5.70000
24	*2.30000	*5.00000	*5.00000	*5.80000	*5.80000
25	*2.40000	*5.00000	*5.00000	*5.90000	*5.90000
26	*2.50000	*5.00000	*5.00000	*6.00000	*6.00000
27	*2.60000	*5.00000	*5.00000	*6.10000	*6.10000
28	*2.70000	*5.00000	*5.00000	*6.20000	*6.20000
29	*2.80000	*5.00000	*5.00000	*6.30000	*6.30000
30	*2.90000	*5.00000	*5.00000	*6.40000	*6.40000
31	*3.00000	*5.00000	*5.00000	*6.50000	*6.50000
32	*3.10000	*5.00000	*5.00000	*6.60000	*6.60000
33	*3.20000	*5.00000	*5.00000	*6.70000	*6.70000
34	*3.30000	*5.00000	*5.00000	*6.80000	*6.80000
35	*3.40000	*5.00000	*5.00000	*6.90000	*6.90000

APPENDIX

	X/REFL	X/REFL
1		
71	7.000000	* 500000
72	7.100000	* 500000
73	7.200000	* 500000
74	7.300000	* 500000
75	7.400000	* 500000
76	7.500000	* 500000
77	7.600000	* 500000
78	7.700000	* 500000
79	7.800000	* 500000
80	7.900000	* 500000
81	8.000000	* 500000
82	8.100000	* 496496
83	8.200000	* 485932
84	8.300000	* 468146
85	8.400000	* 442860
86	8.500000	* 409640
87	8.600000	* 367697
88	8.700000	* 316754
89	8.800000	* 255000
90	9.050000	* 250000
91	9.300000	* 250000
92	9.550000	* 250000
93	9.800000	* 250000
94	10.050000	* 250000
95	10.300000	* 250000
96	10.550000	* 250000
97	10.800000	* 250000
98	11.050000	* 250000
99	11.300000	* 250000

$L/D = 0.8$, $Dh/D = 0.51$ CIRCULAR ARC BLUFFTAIL - $M = 0.8$, $NPK = 5,0$
 $MO = .800$ JET PRESSURE RATIO = 5.000 $L = .1524$ METERS

BOUNDARY LAYER SEPARATION AT $X/L = 8.5380$

I	x/L	R/L	CP	ML	CF	MD/L	REF/L	RV/L	DEL/L	THETA/L	H
51	7.8975	.5000	-1851	.9839	.0025	.5000	.5123	.5973	.0123	.0079	1.5565
52	8.0098	.4997	-3003	.9368	.0026	.4997	.5106	.5965	.0110	.0070	1.5570
53	8.1121	.4952	-4010	.9840	.0028	.4952	.5055	.5928	.0102	.0065	1.5586
54	8.2046	.4851	-4009	.9844	.0027	.4851	.4959	.5852	.0108	.0068	1.5752
55	8.2882	.4702	-3085	.9407	.0025	.4702	.4829	.5747	.0127	.0079	1.5757
56	8.3637	.4520	-1836	.8852	.0025	.4520	.4678	.5629	.0156	.0096	1.5857
57	8.4322	.4322	-0646	.8292	.0020	.4322	.4522	.5514	.0200	.0119	1.6139
58	8.4952	.4112	.0412	.7814	.0017	.4112	.4370	.5410	.0260	.0146	1.6645
59	8.5544	.3870	.1072	.7516	0.0000	.5895	.4233	.5315	.0323	.0174	1.7146
60	8.6118	.3619	.1225	.7447	0.0000	.5746	.4115	.5283	.0364	.0191	1.7258
61	8.6699	.3321	.1130	.7490	0.0000	.5397	.4001	.5274	.0398	.0205	1.7117
62	8.7316	.2973	.1023	.7558	0.0000	.3444	.3886	.5316	.0445	.0226	1.6987
63	8.8000	.2550	.1663	.7246	0.0000	.5235	.3745	.5500	.0539	.0295	1.7686
64	8.8780	.2534	.2570	.6634	0.0000	.2714	.3576	.5358	.0806		
65	8.9704	.2516	.2503	.6865	0.0000	.2895	.3451	.5112	.0529		
66	9.0788	.2500	.1904	.7159	0.0000	.3036	.3346	.5043	.0281		
67	9.2089	.2500	.1378	.7377	0.0000	.3119	.3253	.4996	.0125		
68	9.3679	.2500	.1112	.7498	0.0000	.3079	.3147	.4936	.0070		
69	9.5666	.2500	.1033	.7534	0.0000	.2967	.3027	.4843	.0033		
70	9.8222	.2500	.0839	.7621	0.0000	.2902	.2920	.4777	.0014		
71	10.1629	.2500	.0568	.7744	0.0000	.2866	.2833	.4724	.0071		
72	10.0399	.2500	.0326	.7853	0.0000	.2873	.2769	.4700	.0126		
73	11.3554	.2500	.0170	.7923	0.0000	.2878	.2712	.4678	.0183		
74	12.5479	.2500	.0080	.7964	0.0000	.2881	.2663	.4773	.0250		
75	14.9129	.2500	.0024	.7989	0.0000	.2882	.2635	.4826	.0268		
76	22.0860	.2500	.0003	.7999	0.0000	.2883	.2635	.4826	.0268		

APPENDIX

APPENDIX

DRAG COEFFICIENTS (REFERENCE AREA = .010241 SQ METERS)		CDP, AFT					CDT, AFT					CDP, 800					CDT, AFT				
ITERATION	CDP, AFT	CDP, AFT	CUT, AFT	CDP, 800	CDT, AFT																
1	.0123	.0066		.0190		.0352		.0645		.1197											
2	.0126	.0068		.0194		.0256		.0850		.1106											
3	.0090	.0068		.0158		.0174		.0851		.1025											
4	.0033	.0067		.0100		.0091		.0850		.0941											
5	.0020	.0066		.0045		.0021		.0849		.0870											
6	.0011	.0065		.0054		.0019		.0848		.0867											
7	.0065	.0065		.0126		.0085		.0847		.0932											
8	.0164	.0065		.0229		.0181		.0847		.1026											
9	.0259	.0065		.0325		.0271		.0847		.1119											
10	.0283	.0066		.0349		.0292		.0848		.1140											
11	.0255	.0066		.0321		.0261		.0849		.109											
12	.0228	.0066		.0293		.0251		.0849		.1079											
13	.0221	.0066		.0287		.0222		.0849		.1070											
14	.0219	.0066		.0283		.0216		.0849		.1066											
15	.0218	.0066		.0284		.0216		.0849		.1064											
16	.0221	.0066		.0286		.0217		.0849		.1065											
17	.0223	.0066		.0288		.0218		.0849		.1066											
18	.0226	.0066		.0291		.0220		.0849		.1068											
19	.0227	.0066		.0292		.0221		.0849		.1069											
20	.0229	.0056		.0285		.0223		.0839		.1061											

APPENDIX

RAXBOD CONVERGENCE HISTORY FOR INVISCID RELAXATION SOLUTION
FOR CONVERGENCE, RPAVG MUST BE LESS THAN .17E-03 IN 40 RELAXATION CYCLES

ITERATION	RPMAX	RPAVG	CONVERGED?
1	.52E+00	.12E-01	NO
2	.22E+00	.56E-02	NO
3	.13E+00	.33E-02	NO
4	.85E-01	.21E-02	NO
5	.61E-01	.14E-02	NO
6	.46E-01	.11E-02	NO
7	.35E-01	.85E-03	NO
8	.28E-01	.77E-03	NO
9	.23E-01	.74E-03	NO
10	.19E-01	.56E-03	NO
11	.16E-01	.42E-03	NO
12	.14E-01	.33E-03	NO
13	.12E-01	.26E-03	NO
14	.10E-01	.25E-03	NO
15	.87E-02	.22E-03	NO
16	.77E-02	.20E-03	NO
17	.68E-02	.19E-03	NO
18	.61E-02	.17E-03	NO
19	.57E-02	.17E-03	YES
20	.59E-02	.17E-03	YES

APPENDIX

FLUID FIELD RESULTS FROM X/L = 0.0000 TO X/L = 9.4000 AND TO R/L = .7500

NOTE: POINTS DENOTED BY (BL) ARE BOUNDARY-LAYER PROPERTIES CALCULATED FROM POWER-LAW PROFILE,
 POINTS DENOTED BY (I) ARE INVISCID JET PROPERTIES CALCULATED FROM 1-D ISENTROPIC THEORY,
 POINTS DENOTED BY (EL) ARE MIXING LAYER PROPERTIES FROM LAST X/L=STATION & SHOULD NOT BE USED.

I	X/L	R/L	P/PINF	T/TINF	U/UINF	V/UINF	M	GAMMA	PT/PTINF
BL	1	7.8975	.5000	.9171	1.1280	0.0000	0.0000	1.4000	.6016
BL	2	7.8975	.5144	.9171	1.0387	.8354	.0060	.6558	.6030
BL	3	7.8975	.5208	.9179	1.0231	.9051	.0078	.7159	.6473
BL	4	7.8975	.5312	.9190	1.0128	.9486	.0087	.7541	.6790
BL	5	7.8975	.5417	.9201	1.0049	.9807	.0095	.7827	.7045
BL	6	7.8975	.5521	.9212	.9984	1.0063	.0103	.8057	.7264
BL	7	7.8975	.5625	.9222	.9928	1.0277	.0110	.8252	.7459
BL	8	7.8975	.5729	.9233	.9879	1.0462	.0118	.8422	.7636
BL	9	7.8975	.5833	.9244	.9835	1.0625	.0125	.8572	.7799
BL	10	7.8975	.5937	.9254	.9795	1.0771	.0131	.8707	.7950
BL	11	7.8975	.6042	.9264	.9784	1.0810	.0135	.8744	.8000
BL	12	7.8975	.6146	.9274	.9787	1.0799	.0139	.8734	.8000
BL	13	7.8975	.6250	.9284	.9790	1.0788	.0143	.8724	.8000
BL	14	7.8975	.6354	.9294	.9793	1.0778	.0146	.8714	.8000
BL	15	7.8975	.6458	.9304	.9796	1.0767	.0150	.8703	.8000
BL	16	7.8975	.6562	.9314	.9799	1.0756	.0154	.8693	.8000
BL	17	7.8975	.6667	.9323	.9802	1.0745	.0157	.8684	.8000
BL	18	7.8975	.6771	.9332	.9805	1.0735	.0159	.8674	.8000
BL	19	7.8975	.6875	.9342	.9807	1.0725	.0161	.8665	.8000
BL	20	7.8975	.6979	.9351	.9810	1.0715	.0163	.8656	.8000
BL	21	7.8975	.7083	.9360	.9813	1.0705	.0165	.8646	.8000
BL	22	7.8975	.7187	.9369	.9815	1.0693	.0168	.8637	.8000
BL	23	7.8975	.7292	.9378	.9818	1.0685	.0170	.8628	.8000
BL	24	7.8975	.7396	.9387	.9821	1.0675	.0172	.8619	.8000
BL	25	7.8975	.7500	.9396	.9824	1.0665	.0174	.8610	.8000
BL	1	8.0098	.4997	.8655	1.1280	0.0000	0.0000	1.4000	.5676
BL	2	8.0098	.5101	.8655	1.0248	.8975	.0255	.7096	.4000
BL	3	8.0098	.5205	.8685	1.0096	.9614	.0276	.7657	.3999
BL	4	8.0098	.5309	.8717	.9997	1.0008	.0288	.8011	.7226
BL	5	8.0098	.5414	.8749	.9922	1.0297	.0297	.8274	.8993
BL	6	8.0098	.5518	.8780	.9860	1.0528	.0304	.8465	.9224
BL	7	8.0098	.5622	.8812	.9808	1.0720	.0310	.8663	.9431
BL	8	8.0098	.5727	.8844	.9762	1.0885	.0315	.8817	.9621
BL	9	8.0098	.5831	.8876	.9722	1.1050	.0320	.8953	.9798
EL	10	8.0098	.5935	.8901	.9685	1.1159	.0324	.9075	.9957
EL	11	8.0098	.6040	.8925	.9680	1.1174	.0325	.9090	.0000

APPENDIX

	x/L	R/L	P/PINF	T/TINF	U/UINF	V/VINF	H	GAMMA	PT/PINF
1	12	8.0098	.6144	.8950	.9688	1.1146	.0325	1.4000	1.0000
	13	8.0098	.6248	.8974	.9695	1.1121	.0324	.9040	1.0000
	14	8.0098	.6353	.8999	.9703	1.1095	.0324	.9015	1.0000
	15	8.0098	.6457	.9023	.9711	1.1068	.0324	.8989	1.0000
	16	8.0098	.5561	.9048	.9718	1.1042	.0323	.8964	1.0000
	17	8.0098	.6666	.9070	.9725	1.1018	.0323	.8942	1.0000
	18	8.0098	.6770	.9089	.9731	1.0997	.0322	.8922	1.0000
	19	8.0098	.6874	.9108	.9737	1.0976	.0321	.8903	1.0000
	20	8.0098	.6978	.9127	.9742	1.0955	.0320	.8883	1.0000
	21	8.0098	.7165	.9146	.9748	1.0935	.0320	.8864	1.0000
	22	8.0098	.7187	.9165	.9754	1.0914	.0319	.8844	1.0000
	23	8.0098	.7291	.9185	.9760	1.0893	.0318	.8825	1.0000
	24	8.0098	.7390	.9204	.9766	1.0872	.0317	.8805	1.0000
	25	8.0098	.7500	.9221	.9771	1.0853	.0316	.8787	1.0000
	BL	1	8.1121	.4952	.6204	1.1260	0.0000	0.0000	1.4000
	BL	2	8.1121	.5056	.6206	1.0135	.9431	.0718	.7516
	BL	3	8.1121	.5165	.6259	.9986	1.0026	.0746	.8051
	BL	4	8.1121	.5271	.8312	.9889	1.0395	.0759	.8485
	BL	5	8.1121	.5377	.8365	.9817	1.0664	.0762	.8632
	BL	6	8.1121	.5483	.8416	.9758	1.0877	.0760	.8831
	BL	7	8.1121	.5599	.8471	.9708	1.1053	.0755	.8997
	BL	8	8.1121	.5695	.8524	.9665	1.1208	.0747	.9141
	BL	9	8.1121	.5801	.8575	.9626	1.1342	.0738	.9268
	BL	10	8.1121	.5908	.8614	.9592	1.1462	.0733	.9382
	BL	11	8.1121	.6014	.8654	.9595	1.1450	.0720	.9370
	BL	12	8.1121	.6120	.8693	.9608	1.1408	.0705	.9329
	BL	13	8.1121	.6226	.8733	.9620	1.1366	.0690	.9288
	BL	14	8.1121	.6332	.8772	.9632	1.1324	.0675	.9247
	BL	15	8.1121	.6438	.8812	.9645	1.1282	.0660	.9206
	BL	16	8.1121	.6545	.8851	.9657	1.1241	.0644	.9166
	BL	17	8.1121	.6651	.8883	.9667	1.1207	.0633	.9133
	BL	18	8.1121	.6757	.8912	.9676	1.1176	.0622	.9104
	BL	19	8.1121	.6863	.8941	.9685	1.1145	.0611	.9074
	BL	20	8.1121	.6969	.8970	.9694	1.1114	.0600	.9044
	BL	21	8.1121	.7075	.8999	.9703	1.1083	.0589	.9014
	BL	22	8.1121	.7182	.9029	.9712	1.1052	.0578	.8984
	BL	23	8.1121	.7288	.9058	.9721	1.1021	.0567	.8954
	BL	24	8.1121	.7394	.9187	.9730	1.0990	.0556	.8924
	BL	25	8.1121	.7500	.9109	.9737	1.0966	.0546	.8901
	BL	1	8.2046	.4851	.8204	1.1280	0.0000	0.0000	1.4000
	BL	2	8.2046	.4961	.8205	1.0147	.9331	.1216	.7473

APPENDIX

<i>R/L</i>	<i>X/L</i>	<i>T/TINF</i>	<i>U/UINF</i>	<i>V/VINF</i>	<i>H</i>	<i>GAMMA</i>	<i>P1/P1TINF</i>
BL	3	0.2046	0.5072	0.9262	0.9996	0.1262	0.8275
BL	4	0.2046	0.5182	0.9319	0.9896	0.1276	1.4000
BL	5	0.2046	0.5293	0.9376	0.9824	0.1274	1.4000
BL	6	0.2046	0.5403	0.9433	0.9764	0.1265	0.8606
BL	7	0.2046	0.5513	0.9490	0.9713	0.1092	0.9167
BL	8	0.2046	0.5624	0.9547	0.9669	0.1151	0.9390
BL	9	0.2046	0.5734	0.9597	0.9630	0.1290	0.9614
BL	10	0.2046	0.5844	0.9640	0.9594	0.1413	0.9811
BL	11	0.2046	0.5955	0.9682	0.9604	0.1382	0.9981
BL	12	0.2046	0.6065	0.9724	0.9617	0.1340	1.0000
BL	13	0.2046	0.6176	0.9767	0.9631	0.1297	1.0000
BL	14	0.2046	0.6286	0.9809	0.9644	0.1253	1.0000
BL	15	0.2046	0.6396	0.9851	0.9657	0.1212	1.0000
BL	16	0.2046	0.6507	0.9890	0.9669	0.1173	1.0000
BL	17	0.2046	0.6617	0.9921	0.9679	0.1141	1.0000
BL	18	0.2046	0.6727	0.9952	0.9688	0.1109	1.0000
BL	19	0.2046	0.6838	0.9983	0.9698	0.1077	1.0000
BL	20	0.2046	0.6948	0.9014	0.9708	0.1046	1.0000
BL	21	0.2046	0.7059	0.9045	0.9717	0.1014	1.0000
BL	22	0.2046	0.7169	0.9076	0.9727	0.0982	1.0000
BL	23	0.2046	0.7279	0.9107	0.9736	0.0950	1.0000
BL	24	0.2046	0.7390	0.9132	0.9744	0.0924	1.0000
BL	25	0.2046	0.7500	0.9155	0.9751	0.0901	1.0000
BL	1	0.2662	0.4702	0.9010	1.1260	0.0000	0.0000
BL	2	0.2662	0.4819	0.8610	1.0271	0.8734	0.5653
BL	3	0.2662	0.4936	0.8657	1.0114	0.9400	0.4000
BL	4	0.2662	0.5052	0.8701	1.0011	0.9815	0.3221
BL	5	0.2662	0.5169	0.8745	0.9933	1.0123	0.2356
BL	6	0.2662	0.5285	0.8788	0.9869	1.0371	0.1666
BL	7	0.2662	0.5402	0.8832	0.9814	1.0579	0.1649
BL	8	0.2662	0.5518	0.8875	0.9760	1.0759	0.1590
BL	9	0.2662	0.5635	0.8912	0.9723	1.0917	0.1564
BL	10	0.2662	0.5751	0.8944	0.9686	1.1052	0.1538
BL	11	0.2662	0.5868	0.8976	0.9696	1.1023	0.1489
BL	12	0.2662	0.5982	0.9008	0.9700	1.0994	0.1441
BL	13	0.2662	0.6101	0.9041	0.9716	1.0965	0.1392
BL	14	0.2662	0.6218	0.9073	0.9726	1.0936	0.1343
BL	15	0.2662	0.6334	0.9105	0.9736	1.0908	0.1294
BL	16	0.2662	0.6451	0.9130	0.9743	1.0865	0.1256
BL	17	0.2662	0.6567	0.9154	0.9750	1.0862	0.1223
BL	18	0.2662	0.6684	0.9176	0.9758	1.0844	0.1187
BL	19	0.2662	0.6801	0.9202	0.9763	0.1152	0.1000

APPENDIX

I	x/L	w/L	p/p _{INF}	r/r _{INF}	u/u _{INF}	v/v _{INF}	w/w _{INF}	gamma	pT/pT _{INF}
20	0.2982	0.917	0.9226	0.9772	1.0794	-1.117	0.8783	1.4000	1.0000
21	0.2982	0.7034	0.9250	0.9780	1.0772	-1.081	0.8756	1.4000	1.0000
22	0.2982	0.7150	0.9274	0.9787	1.0749	-1.046	0.8734	1.4000	1.0000
23	0.2982	0.7267	0.9294	0.9793	1.0730	-1.018	0.8714	1.4000	1.0000
24	0.2982	0.7383	0.9312	0.9798	1.0713	-0.992	0.8695	1.4000	1.0000
25	0.2982	0.7500	0.9330	0.9804	1.0695	-0.967	0.8677	1.4000	1.0000
BL	1	0.3637	0.4520	0.9177	1.1280	0.0000	0.0000	1.4000	1.0021
BL	2	0.3637	0.4644	0.9177	1.0435	0.7922	-1.1800	0.6362	1.0000
BL	3	0.3637	0.4769	0.9194	1.0272	0.8680	-1.035	0.7003	1.0000
BL	4	0.3637	0.4893	0.9216	1.0163	0.9153	-1.066	0.7413	1.0000
BL	5	0.3637	0.5017	0.9238	1.0078	0.9508	-1.066	0.7721	1.0000
BL	6	0.3637	0.5111	0.9260	1.0008	0.9793	-1.048	0.7971	1.0000
BL	7	0.3637	0.5265	0.9282	0.9948	1.0038	-1.016	0.8163	1.0000
BL	8	0.3637	0.5369	0.9304	0.9895	1.0250	-1.077	0.8367	1.0000
BL	9	0.3637	0.5514	0.9322	0.9847	1.0436	-1.151	0.8531	1.0000
BL	10	0.3637	0.5638	0.9338	0.9806	1.0590	-1.20	0.8668	1.0000
BL	11	0.3637	0.5762	0.9355	0.9811	1.0581	-1.26	0.8651	1.0000
BL	12	0.3637	0.5886	0.9372	0.9816	1.0571	-1.30	0.8634	1.0000
BL	13	0.3637	0.6010	0.9388	0.9821	1.0562	-1.34	0.8618	1.0000
BL	14	0.3637	0.6134	0.9405	0.9826	1.0555	-1.38	0.8601	1.0000
BL	15	0.3637	0.6258	0.9420	0.9831	1.0545	-1.43	0.8596	1.0000
BL	16	0.3637	0.6383	0.9433	0.9835	1.0534	-1.49	0.8572	1.0000
BL	17	0.3637	0.6507	0.9446	0.9839	1.0525	-1.54	0.8559	1.0000
BL	18	0.3637	0.6631	0.9460	0.9843	1.0515	-1.58	0.8545	1.0000
BL	19	0.3637	0.6755	0.9473	0.9846	1.0506	-1.64	0.8532	1.0000
BL	20	0.3637	0.6879	0.9486	0.9850	1.0497	-1.72	0.8518	1.0000
BL	21	0.3637	0.7003	0.9500	0.9854	1.0487	-1.79	0.8505	1.0000
BL	22	0.3637	0.7128	0.9511	0.9858	1.0478	-1.85	0.8494	1.0000
BL	23	0.3637	0.7252	0.9522	0.9861	1.0470	-1.91	0.8483	1.0000
BL	24	0.3637	0.7376	0.9532	0.9864	1.0461	-1.98	0.8472	1.0000
BL	25	0.3637	0.7500	0.9543	0.9867	1.0452	-2.05	0.8461	1.0000
BL	1	0.4322	0.4322	0.9711	1.1280	0.0000	0.0000	1.4000	0.8370
BL	2	0.4322	0.4454	0.9711	1.0595	0.7075	-1.154	0.5604	1.0000
BL	3	0.4322	0.4586	0.9710	1.0429	0.7941	-1.148	0.6367	1.0000
BL	4	0.4322	0.4719	0.9710	1.0314	0.8479	-1.196	0.6844	1.0000
BL	5	0.4322	0.4851	0.9709	1.0222	0.8888	-1.196	0.7192	1.0000
BL	6	0.4322	0.4984	0.9708	1.0146	0.9221	-1.194	0.7476	1.0000
BL	7	0.4322	0.5110	0.9707	1.0079	0.9505	-1.166	0.7719	1.0000
BL	8	0.4322	0.5249	0.9707	1.0020	0.9754	-1.127	0.7931	1.0000
BL	9	0.4322	0.5381	0.9707	0.9966	0.9972	-1.03	0.8121	1.0000
BL	10	0.4322	0.5513	0.9708	0.9916	1.0169	-1.74	0.8293	1.0000

APPENDIX

I	X/L	R/L	P/PINF	T/TINF	U/UINF	V/VINF	W/WINF	GAMMA	PT/PINF
11	0.4322	5646	.9709	.9916	1.0179	-1.1711	.8293	1.4000	1.0000
12	0.4322	5776	.9710	.9916	1.0186	-1.1646	.8293	1.4000	1.0000
13	0.4322	5911	.9710	.9916	1.0196	-1.1585	.8292	1.4000	1.0000
14	0.4322	6043	.9711	.9917	1.0206	-1.1523	.8291	1.4000	1.0000
15	0.4322	6176	.9713	.9917	1.0212	-1.1476	.8289	1.4000	1.0000
16	0.4322	6308	.9715	.9918	1.0215	-1.1430	.8287	1.4000	1.0000
17	0.4322	6441	.9717	.9918	1.0219	-1.1384	.8285	1.4000	1.0000
18	0.4322	6573	.9720	.9919	1.0223	-1.1338	.8283	1.4000	1.0000
19	0.4322	6705	.9722	.9920	1.0227	-1.1292	.8281	1.4000	1.0000
20	0.4322	6838	.9724	.9920	1.0231	-1.1246	.8278	1.4000	1.0000
21	0.4322	6970	.9727	.9921	1.0232	-1.1208	.8276	1.4000	1.0000
22	0.4322	7103	.9730	.9922	1.0233	-1.1174	.8273	1.4000	1.0000
23	0.4322	7235	.9733	.9923	1.0233	-1.1140	.8270	1.4000	1.0000
24	0.4322	7368	.9736	.9924	1.0233	-1.106	.8266	1.4000	1.0000
25	0.4322	7500	.9739	.9925	1.0234	-1.072	.8263	1.4000	1.0000
BL	1	8.4952	.4112	1.0185	1.1280	0.000	0.000	1.4000	1.4000
BL	2	8.4952	.4254	1.0185	1.0742	.0211	.5005	1.4000	1.4000
BL	3	8.4952	.4395	1.0180	1.0575	.7215	.5771	1.4000	1.4000
BL	4	8.4952	.4536	1.0154	1.0455	.7824	.6280	1.4000	1.4000
BL	5	8.4952	.4677	1.0126	1.0358	.8291	.6673	1.4000	1.4000
BL	6	8.4952	.4818	1.0102	1.0274	.8676	.6997	1.4000	1.4000
BL	7	8.4952	.4959	1.0076	1.0200	.9006	.7275	1.4000	1.4000
BL	8	8.4952	.5100	1.0050	1.0134	.9297	.7521	1.4000	1.4000
BL	9	8.4952	.5242	1.0036	1.0072	.9553	.7742	1.4000	1.4000
BL	10	8.4952	.5383	1.0021	1.0016	.9786	.7944	1.4000	1.4000
BL	11	8.4952	.5524	1.0006	1.0002	.9850	.8176	1.4000	1.4000
BL	12	8.4952	.5665	.9991	.9996	.9877	.8314	1.4000	1.4000
BL	13	8.4952	.5806	.9977	.9993	.9905	.8552	1.4000	1.4000
BL	14	8.4952	.5947	.9965	.9990	.9927	.8798	1.4000	1.4000
BL	15	8.4952	.6088	.9957	.9986	.9942	.8944	1.4000	1.4000
BL	16	8.4952	.6230	.9949	.9985	.9958	.9105	1.4000	1.4000
BL	17	8.4952	.6371	.9941	.9983	.9975	.9159	1.4000	1.4000
BL	18	8.4952	.6512	.9933	.9981	.9989	.9112	1.4000	1.4000
BL	19	8.4952	.6653	.9924	.9978	1.0004	.9166	1.4000	1.4000
BL	20	8.4952	.6794	.9918	.9977	1.0016	.9225	1.4000	1.4000
BL	21	8.4952	.6935	.9914	.9975	1.0025	.9190	1.4000	1.4000
BL	22	8.4952	.7077	.9910	.9974	1.0055	.9155	1.4000	1.4000
BL	23	8.4952	.7218	.9906	.9973	1.0041	.9120	1.4000	1.4000
BL	24	8.4952	.7359	.9902	.9972	1.0050	.9085	1.4000	1.4000
BL	25	8.4952	.7500	.9898	.9971	1.0058	.9050	1.4000	1.4000
1	8.5544	3870	1	*** SEPARATED FLOW ***					

APPENDIX

	X/L	R/L	P/PINF	T/TINF	U/UINF	V/VINF	W	GAMMA	P1/P1INF
2	0.5544	• 4021	*** SEPARATED FLOW ***						1.0000
3	0.5544	• 4172	*** SEPARATED FLOW ***						1.0000
4	0.5544	• 4323	*** SEPARATED FLOW ***						1.0000
5	0.5544	• 4475	*** SEPARATED FLOW ***						1.0000
6	0.5544	• 4626	*** SEPARATED FLOW ***						1.0000
7	0.5544	• 4777	*** SEPARATED FLOW ***						1.0000
8	0.5544	• 4928	*** SEPARATED FLOW ***						1.0000
9	0.5544	• 5080	*** SEPARATED FLOW ***						1.0000
10	0.5544	• 5231	*** SEPARATED FLOW ***						1.0000
11	0.5544	• 5382	1.0222	1.0063	0.9621	• 1582	• 7776	1.4000	1.0000
12	0.5544	• 5533	1.0198	1.0056	0.9657	• 1529	• 7801	1.4000	1.0000
13	0.5544	• 5685	1.0173	1.0049	0.9694	• 1476	• 7826	1.4000	1.0000
14	0.5544	• 5836	1.0154	1.0044	0.9722	• 1429	• 7845	1.4000	1.0000
15	0.5544	• 5987	1.0139	1.0040	0.9746	• 1385	• 7860	1.4000	1.0000
16	0.5544	• 6139	1.0124	1.0035	0.9769	• 1342	• 7875	1.4000	1.0000
17	0.5544	• 6290	1.0109	1.0031	0.9792	• 1299	• 7891	1.4000	1.0000
18	0.5544	• 6441	1.0093	1.0027	0.9815	• 1256	• 7906	1.4000	1.0000
19	0.5544	• 6592	1.0078	1.0022	0.9838	• 1213	• 7921	1.4000	1.0000
20	0.5544	• 6744	1.0069	1.0020	0.9852	• 1179	• 7931	1.4000	1.0000
21	0.5544	• 6895	1.0059	1.0017	0.9857	• 1144	• 7940	1.4000	1.0000
22	0.5544	• 7046	1.0050	1.0014	0.9881	• 1110	• 7950	1.4000	1.0000
23	0.5544	• 7197	1.0040	1.0012	0.9896	• 1076	• 7959	1.4000	1.0000
24	0.5544	• 7349	1.0031	1.0009	0.9910	• 1042	• 7969	1.4000	1.0000
25	0.5544	• 7500	1.0022	1.0006	0.9925	• 1008	• 7976	1.4000	1.0000
1	0.6116	• 5619	*** SEPARATED FLOW ***						
2	0.6116	• 3790	*** SEPARATED FLOW ***						
3	0.6116	• 3942	*** SEPARATED FLOW ***						
4	0.6116	• 4104	*** SEPARATED FLOW ***						
5	0.6116	• 4266	*** SEPARATED FLOW ***						
6	0.6116	• 4427	*** SEPARATED FLOW ***						
7	0.6116	• 4589	*** SEPARATED FLOW ***						
8	0.6116	• 4751	*** SEPARATED FLOW ***						
9	0.6116	• 4912	*** SEPARATED FLOW ***						
10	0.6116	• 5074	*** SEPARATED FLOW ***						
11	0.6116	• 5236	*** SEPARATED FLOW ***						
12	0.6116	• 5398	1.0326	1.0092	0.9525	• 1436	• 7672	1.4000	1.0000
13	0.6116	• 5559	1.0302	1.0085	0.9560	• 1391	• 7696	1.4000	1.0000
14	0.6116	• 5721	1.0281	1.0079	0.9590	• 1348	• 7717	1.4000	1.0000
15	0.6116	• 5883	1.0263	1.0074	0.9615	• 1309	• 7735	1.4000	1.0000
16	0.6116	• 6045	1.0245	1.0069	0.9641	• 1269	• 7753	1.4000	1.0000
17	0.6116	• 6206	1.0227	1.0064	0.9666	• 1229	• 7771	1.4000	1.0000
18	0.6116	• 6368	1.0210	1.0059	0.9692	• 1189	• 7789	1.4000	1.0000

APPENDIX

	x/l	K/L	P/PINF	T/TINF	U/UINF	V/VINF	W	GAMMA	PT/PTINF
I	0.6118	.6510	1.0194	1.0055	.9715	.1152	.7805	1.4000	1.0000
20	0.6118	.6891	1.0181	1.0051	.9733	.1119	.7818	1.4000	1.0000
21	0.6118	.6853	1.0168	1.0048	.9751	.1086	.7831	1.4000	1.0000
22	0.6118	.7015	1.0155	1.0044	.9769	.1053	.7843	1.4000	1.0000
23	0.6118	.7177	1.0143	1.0041	.9787	.1020	.7856	1.4000	1.0000
24	0.6118	.7338	1.0130	1.0037	.9805	.0986	.7869	1.4000	1.0000
25	0.6118	.7500	1.0120	1.0034	.9818	.0960	.7879	1.4000	1.0000
	0.6699	.3521	** SEPARATED FLOW ***						
	0.6699	.3490	** SEPARATED FLOW ***						
	0.6699	.3670	** SEPARATED FLOW ***						
	0.6699	.3844	** SEPARATED FLOW ***						
	0.6699	.4014	** SEPARATED FLOW ***						
	0.6699	.4192	** SEPARATED FLOW ***						
	0.6699	.4366	** SEPARATED FLOW ***						
	0.6699	.4540	** SEPARATED FLOW ***						
	0.6699	.4714	** SEPARATED FLOW ***						
	0.6699	.4889	** SEPARATED FLOW ***						
	0.6699	.5062	** SEPARATED FLOW ***						
	0.6699	.5237	** SEPARATED FLOW ***						
	0.6699	.5411	1.0361	1.0107	.9478	.1329	.7616	1.4000	1.0000
	0.6699	.5585	1.0363	1.0102	.9505	.1215	.7634	1.4030	1.0000
	0.6699	.5759	1.0346	1.0098	.9529	.1216	.7651	1.4000	1.0000
	0.6699	.5933	1.0329	1.0093	.9554	.1207	.7668	1.4000	1.0000
	0.6699	.6107	1.0312	1.0088	.9578	.1168	.7686	1.4000	1.0000
	0.6699	.6281	1.0295	1.0063	.9603	.1128	.7703	1.4000	1.0000
	0.6699	.6455	1.0279	1.0079	.9624	.1093	.7719	1.4000	1.0000
	0.6699	.6629	1.0265	1.0075	.9644	.1061	.7733	1.4000	1.0000
	0.6699	.6804	1.0251	1.0071	.9664	.1029	.7747	1.4000	1.0000
	0.6699	.6978	1.0236	1.0067	.9683	.0996	.7762	1.4000	1.0000
	0.6699	.7152	1.0222	1.0063	.9703	.0954	.7776	1.4000	1.0000
	0.6699	.7326	1.0209	1.0059	.9721	.0914	.7790	1.4000	1.0000
	0.6699	.7500	1.0198	1.0056	.9736	.0908	.7801	1.4000	1.0000
	0.7316	.2973	** SEPARATED FLOW ***						
	0.7316	.3161	** SEPARATED FLOW ***						
	0.7316	.3350	** SEPARATED FLOW ***						
	0.7316	.3539	** SEPARATED FLOW ***						
	0.7316	.3727	** SEPARATED FLOW ***						
	0.7316	.3916	** SEPARATED FLOW ***						
	0.7316	.4104	** SEPARATED FLOW ***						
	0.7316	.4293	** SEPARATED FLOW ***						
	0.7316	.4482	** SEPARATED FLOW ***						

APPENDIX

	X/L	R/L	P/PIPE	T/TINF	U/UINF	V/VINF	W	GAMMA	PT/PTINF
1	0.7316	0.4670	*** SEPARATED FLOW ***						
1-1	0.7316	0.4859	*** SEPARATED FLOW ***						
1-2	0.7316	0.5048	*** SEPARATED FLOW ***						
1-3	0.7316	0.5239	*** SEPARATED FLOW ***						
1-4	0.7316	0.5425	1.0433	1.0122	0.9431				
1-5	0.7316	0.5614	1.0417	1.0117	0.9454				
1-6	0.7316	0.5802	1.0400	1.0113	0.9478				
1-7	0.7316	0.5991	1.0384	1.0108	0.9502				
1-8	0.7316	0.6180	1.0368	1.0104	0.9526				
1-9	0.7316	0.6366	1.0352	1.0099	0.9548				
2-0	0.7316	0.6557	1.0336	1.0095	0.9569				
2-1	0.7316	0.6745	1.0320	1.0091	0.9590				
2-2	0.7316	0.6934	1.0305	1.0082	0.9612				
2-3	0.7316	0.7125	1.0289	1.0082	0.9635				
2-4	0.7316	0.7311	1.0276	1.0078	0.9651				
2-5	0.7316	0.7500	1.0262	1.0074	0.9668				
2-6	0.7316	0.7690	0.4859	0.4860	0.9145	0.0000	1.0500	1.3986	3.2735
2-7	0.7316	0.7880	0.4859	0.4860	0.9145	0.0000	1.0500	1.3986	3.2735
2-8	0.7316	0.8070	0.4859	0.4860	0.9145	0.0000	1.0500	1.3986	3.2735
2-9	0.7316	0.8259	0.4859	0.4860	0.9145	0.0000	1.0500	1.3986	3.2735
2-10	0.7316	0.8447	0.4859	0.4860	0.9145	0.0000	1.0500	1.3986	3.2735
2-11	0.7316	0.8636	0.4859	0.4860	0.9145	0.0000	1.0500	1.3986	3.2735
2-12	0.7316	0.8825	0.4859	0.4860	0.9145	0.0000	1.0500	1.3986	3.2735
2-13	0.7316	0.9013	0.4859	0.4860	0.9145	0.0000	1.0500	1.3986	3.2735
2-14	0.7316	0.9199	0.4859	0.4860	0.9145	0.0000	1.0500	1.3986	3.2735
2-15	0.7316	0.9386	0.4859	0.4860	0.9145	0.0000	1.0500	1.3986	3.2735
2-16	0.7316	0.9573	0.4859	0.4860	0.9145	0.0000	1.0500	1.3986	3.2735
2-17	0.7316	0.9760	0.4859	0.4860	0.9145	0.0000	1.0500	1.3986	3.2735
2-18	0.7316	0.9947	0.4859	0.4860	0.9145	0.0000	1.0500	1.3986	3.2735
2-19	0.7316	0.1034	0.4859	0.4860	0.9145	0.0000	1.0500	1.3986	3.2735
2-20	0.7316	0.1221	0.4859	0.4860	0.9145	0.0000	1.0500	1.3986	3.2735
2-21	0.7316	0.1408	0.4859	0.4860	0.9145	0.0000	1.0500	1.3986	3.2735
2-22	0.7316	0.1595	0.4859	0.4860	0.9145	0.0000	1.0500	1.3986	3.2735
2-23	0.7316	0.1782	0.4859	0.4860	0.9145	0.0000	1.0500	1.3986	3.2735
2-24	0.7316	0.1969	0.4859	0.4860	0.9145	0.0000	1.0500	1.3986	3.2735
2-25	0.7316	0.2156	0.4859	0.4860	0.9145	0.0000	1.0500	1.3986	3.2735
2-26	0.7316	0.2343	0.4859	0.4860	0.9145	0.0000	1.0500	1.3986	3.2735

APPENDIX

<i>x/L</i>	<i>H/L</i>	<i>P/PINF</i>	<i>T/TINF</i>	<i>U/UINF</i>	<i>V/VINF</i>	<i>H</i>	<i>GAMMA</i>	<i>PT/PTINF</i>
27	0.8000	2917	*** SEPARATED FLOW ***					
28	0.8000	3125	*** SEPARATED FLOW ***					
29	0.8000	3333	*** SEPARATED FLOW ***					
30	0.8000	3542	*** SEPARATED FLOW ***					
31	0.8000	3750	*** SEPARATED FLOW ***					
32	0.8000	3956	*** SEPARATED FLOW ***					
33	0.8000	4167	*** SEPARATED FLOW ***					
34	0.8000	4375	*** SEPARATED FLOW ***					
35	0.8000	4583	*** SEPARATED FLOW ***					
36	0.8000	4792	*** SEPARATED FLOW ***					
37	0.8000	5000	*** SEPARATED FLOW ***					
38	0.8000	5208	*** SEPARATED FLOW ***					
39	0.8000	5417	*** SEPARATED FLOW ***					
40	0.8000	5625	1.0142	0.9361	-0.1122	0.7490	1.44000	1.44000
41	0.8000	5833	1.0402	1.0135	0.9195	0.7514	1.44000	1.44000
42	0.8000	6042	1.0458	1.0129	0.9426	0.7539	1.44000	1.44000
43	0.8000	6250	1.0437	1.0123	0.9457	0.7560	1.44000	1.44000
44	0.8000	6458	1.0416	1.0117	0.9484	0.7581	1.44000	1.44000
45	0.8000	6667	1.0396	1.0111	0.9511	0.7601	1.44000	1.44000
46	0.8000	6875	1.0375	1.0106	0.9538	0.7622	1.44000	1.44000
47	0.8000	7083	1.0356	1.0100	0.9562	0.7641	1.44000	1.44000
48	0.8000	7292	1.0339	1.0096	0.9584	0.7658	1.44000	1.44000
49	0.8000	7500	1.0323	1.0091	0.9605	0.7675	1.44000	1.44000
50	0.8000	7708	1.0307	1.0085	0.9625	0.7694	1.44000	1.44000
51	0.8000	7916	1.0293	1.0078	0.9643	0.7713	1.44000	1.44000
52	0.8000	8125	1.0280	1.0072	0.9662	0.7732	1.44000	1.44000
53	0.8000	8333	0.8226	2.3874	0.9380	0.7750	1.44000	1.44000
54	0.8002	8542	0.0339	2.3510	0.4781	0.0102	1.0959	1.2716
55	0.8002	8750	0.0452	2.3248	0.4769	0.9530	1.047	1.2699
56	0.8002	8958	0.0565	2.2816	0.4741	0.9635	1.0200	1.2699
57	0.8002	9166	0.0678	2.2376	0.4716	0.9737	1.0352	1.2699
58	0.8002	9375	0.0792	2.1781	0.4680	0.9880	0.0286	1.2619
59	0.8002	9583	0.0905	2.1112	0.4656	1.0044	0.0361	1.2564
60	0.8002	9792	0.1016	2.0343	0.4590	1.0225	0.0496	1.2474
61	0.8002	9900	0.1131	1.9476	0.4535	1.0430	0.0640	1.2423
62	0.8002	10008	0.1244	1.8545	0.4470	1.0651	0.0816	1.2376
63	0.8002	10116	0.1357	1.7544	0.4400	1.0888	0.1021	1.2178
64	0.8002	10224	0.1470	1.6489	0.4325	1.1137	0.1262	1.1942
65	0.8002	10332	0.1583	1.5400	0.4240	1.1391	0.1540	1.1641
66	0.8002	10439	0.1696	1.4507	0.4156	1.1630	0.1856	1.1251
67	0.8002	10547	0.1809	1.3183	0.4084	1.1814	0.2189	1.0986
68	0.8002	10655	0.1922	1.2096	0.4004	1.2001	0.2500	1.0669
69	0.8002	10763	0.2035	1.1038	0.3914	1.2193	0.2967	1.0370

APPENDIX

I	X/L	R/L	P/PINF	T/TINF	V/UINF	U/UINF	M	GAMMA	P1/P1INF
20	6.8802	.2149	1.0024	.1817	1.2405	.3352	1.3986	2.6774	
21	6.8802	.2262	0.9355	.3742	1.2557	.3626	1.7102	2.6175	
22	6.8786	.2375	0.9645	.4114	1.1340	0.0000	1.4115	1.4006	1.9553
23	6.8786	.2486	0.9906	.5316	.5072	0.0003	.5629	1.4002	.8050
24	6.8786	.2601	1.0154	.6581	1.1156	.0028	1.130	1.3998	.6721
25	6.8786	.2714	1.0554	.6437	1.462	.0069	1.257	1.3992	.7001
26	6.8786	.2913	1.1151	1.1197	2.036	.0154	1.538	1.3983	.7437
27	6.8786	.3113	1.1151	1.1150	2.819	.0309	2.133	1.3983	.7551
28	6.8786	.3512	1.1151	1.1082	3.644	.0529	2.765	1.3983	.7714
29	6.8786	.3512	1.1151	1.0994	4.486	.0810	3.418	1.3984	.7931
30	6.8786	.3711	1.1151	1.0890	5.330	.1150	4.079	1.3985	.8203
31	6.8786	.3910	1.1151	1.0772	6.144	.1281	4.725	1.3985	.8523
32	6.8786	.4110	1.1151	1.0646	6.900	.1332	5.341	1.3986	.8852
33	6.8786	.4309	1.1151	1.0521	7.582	.1345	5.903	1.3986	.9246
34	6.8786	.4509	1.097	1.0406	8.157	.1329	6.586	1.3986	.9576
35	6.8786	.4708	1.050	1.0309	8.606	.1328	6.770	1.3987	.9856
36	6.8786	.4908	1.012	1.0243	8.907	.1296	7.026	1.3987	1.0043
37	6.8786	.5107	1.0960	1.0214	9.033	.1236	7.138	1.3987	1.0100
38	6.8786	.5306	1.0657	1.0184	9.196	.1039	7.337	1.4000	1.0000
39	6.8786	.5505	1.0624	1.0174	9.239	.0999	7.371	1.4000	1.0000
40	6.8786	.5705	1.0591	1.0165	9.282	.0960	7.404	1.4000	1.0000
41	6.8786	.5905	1.0558	1.0156	9.324	.0920	7.438	1.4000	1.0000
42	6.8786	.6104	1.0532	1.0149	9.357	.0889	7.464	1.4000	1.0000
43	6.8786	.6303	1.0508	1.0142	9.387	.0860	7.489	1.4000	1.0000
44	6.8786	.6503	1.0483	1.0136	9.416	.0830	7.513	1.4000	1.0000
45	6.8786	.6702	1.0459	1.0129	9.449	.0801	7.536	1.4000	1.0000
46	6.8786	.6902	1.0436	1.0123	9.477	.0774	7.561	1.4000	1.0000
47	6.8786	.7101	1.0417	1.0117	9.500	.0751	7.580	1.4000	1.0000
48	6.8786	.7301	1.0399	1.0112	9.523	.0728	7.598	1.4000	1.0000
49	6.8786	.7500	1.0380	1.0107	9.546	.0706	7.617	1.4000	1.0000
1	6.9716	0.0000	1.3728	4.099	1.1952	0.0000	1.4945	1.3986	3.0526
2	6.9716	.0121	1.3728	.4100	1.1951	.0189	1.4942	1.3986	.3024
3	6.9716	.0241	1.3648	.4094	1.1968	.0373	1.4979	1.3986	.30473
4	6.9716	.0362	1.3459	.4078	1.2015	.0544	1.5076	1.3986	.30373
5	6.9716	.0482	1.3270	.4062	1.2056	.0749	1.5170	1.3986	.30271
6	6.9716	.0603	1.3010	.4058	1.2117	.0948	1.5309	1.3986	.30122
7	6.9716	.0724	1.2681	.4009	1.2194	.1154	1.5484	1.3986	.29925
8	6.9716	.0844	1.2311	.3975	1.2279	.1372	1.5687	1.3986	.29996
9	6.9716	.0965	1.190	.3936	1.2370	.1601	1.5923	1.3986	.29419
10	6.9716	.1085	1.1429	.3891	1.2482	.1842	1.6190	1.3986	.29090
11	6.9716	.1206	1.0936	.3843	1.2592	.2103	1.6485	1.3986	.28715
12	6.9716	.1327	1.0431	.3791	1.2703	.2381	1.6801	1.3986	.28302

APPENDIX

<i>I</i>	<i>x/l</i>	<i>w/l</i>	<i>P/PINF</i>	<i>T/TINF</i>	<i>U/UINF</i>	<i>V/VINF</i>	<i>W/WINF</i>	<i>PT/PTINF</i>	<i>GAMMA</i>
13	6.9716	0.1447	.9885	.3733	1.2823	2669	1.7157	1.3986	2.7615
14	6.9716	0.1568	.9326	.3672	1.2941	2976	1.7543	1.3986	2.7264
15	6.9716	0.1689	.8754	.3606	1.3064	3269	1.7956	1.3986	2.6686
16	6.9716	0.1809	.8204	.3538	1.3188	3600	1.8395	1.3986	2.6102
17	6.9716	0.1930	.7779	.3493	1.3248	3634	1.8678	1.3986	2.5432
18	6.9716	0.2050	.7743	.3506	1.3215	3625	1.8596	1.3986	2.5116
19	6.9716	0.2171	.8304	.3596	1.3060	3435	1.8025	1.3986	2.5483
20	6.9716	0.2292	.8936	.3685	1.2888	3043	1.7460	1.3986	2.5926
21	6.9716	0.2412	.9426	.3771	1.2752	2765	1.7054	1.3986	2.6247
22	6.9746	0.2533	1.0068	.3763	1.2509	1866	1.6453	1.4007	2.6370
23	6.9746	0.2653	1.0416	.5011	1.0490	2020	1.9873	1.4003	1.2746
24	6.9746	0.2774	1.0630	.7764	1.4228	1065	1.4061	1.3994	1.7959
25	6.9746	0.2895	1.0855	.9735	1.3114	1065	1.2529	1.3988	1.7620
26	6.9746	0.3066	1.1111	1.0763	1.2752	1039	1.2673	1.3985	1.7660
27	6.9746	0.3278	1.1111	1.0959	1.2509	1186	1.3155	1.3984	1.7809
28	6.9746	0.3470	1.0416	.5011	1.0490	1849	1.2020	1.4003	1.8016
29	6.9746	0.3662	1.0630	.7764	1.4228	1065	1.4305	1.3985	1.8278
30	6.9746	0.3854	1.0855	.9735	1.3114	1065	1.2529	1.3988	1.8582
31	6.9746	0.4046	1.1111	1.0763	1.2752	1039	1.2673	1.3985	1.8916
32	6.9746	0.4256	1.1095	1.1095	1.0407	1015	1.0648	1.3986	1.9250
33	6.9746	0.4430	1.1062	1.1062	1.0407	1015	1.0648	1.3986	1.9559
34	6.9746	0.4622	1.1027	1.1027	1.0316	1.0593	1.0640	1.3986	1.9827
35	6.9746	0.4814	1.0990	1.0990	1.0248	1.0248	1.0588	1.3985	1.9882
36	6.9746	0.5005	1.0951	1.0951	1.0218	1.0218	1.0614	1.3986	1.9916
37	6.9746	0.5197	1.0693	1.0693	1.0193	1.0193	1.0813	1.3987	1.9946
38	6.9704	0.5349	1.0662	1.0662	1.0185	1.0185	1.0793	1.3987	1.9987
39	6.9704	0.5541	1.0630	1.0630	1.0176	1.0176	1.0774	1.3987	1.9987
40	6.9704	0.5773	1.0599	1.0599	1.0168	1.0168	1.0754	1.3986	1.9986
41	6.9704	0.5965	1.0574	1.0574	1.0161	1.0161	1.0735	1.3987	1.9987
42	6.9704	0.6157	1.0550	1.0550	1.0154	1.0154	1.0717	1.3987	1.9987
43	6.9704	0.6349	1.0526	1.0526	1.0148	1.0148	1.0699	1.3987	1.9987
44	6.9704	0.6541	1.0502	1.0502	1.0141	1.0141	1.0681	1.3986	1.9986
45	6.9704	0.6732	1.0479	1.0479	1.0135	1.0135	1.0663	1.3986	1.9986
46	6.9704	0.6924	1.0461	1.0461	1.0130	1.0130	1.0647	1.3986	1.9986
47	6.9704	0.7116	1.0443	1.0443	1.0125	1.0125	1.0631	1.3986	1.9986
48	6.9704	0.7308	1.0425	1.0425	1.0120	1.0120	1.0616	1.3986	1.9986
49	6.9704	0.7500	1.0408	1.0408	1.0114	1.0114	1.0600	1.3986	1.9986
50	6.9704	0.7680	1.0388	1.0388	1.0108	1.0108	1.0581	1.3986	1.9986
51	6.9704	0.7862	1.0370	1.0370	1.0102	1.0102	1.0563	1.3986	1.9986
52	6.9704	0.8044	1.0354	1.0354	1.0096	1.0096	1.0545	1.3986	1.9986
53	6.9704	0.8226	1.0338	1.0338	1.0090	1.0090	1.0527	1.3986	1.9986
54	6.9704	0.8408	1.0322	1.0322	1.0084	1.0084	1.0510	1.3986	1.9986
55	6.9704	0.8580	1.0306	1.0306	1.0078	1.0078	1.0492	1.3986	1.9986
56	6.9704	0.8752	1.0290	1.0290	1.0072	1.0072	1.0475	1.3986	1.9986
57	6.9704	0.8924	1.0274	1.0274	1.0066	1.0066	1.0458	1.3986	1.9986
58	6.9704	0.9096	1.0258	1.0258	1.0060	1.0060	1.0441	1.3986	1.9986
59	6.9704	0.9268	1.0242	1.0242	1.0054	1.0054	1.0424	1.3986	1.9986
60	6.9704	0.9440	1.0226	1.0226	1.0048	1.0048	1.0407	1.3986	1.9986
61	6.9704	0.9612	1.0210	1.0210	1.0042	1.0042	1.0390	1.3986	1.9986
62	6.9704	0.9784	1.0194	1.0194	1.0036	1.0036	1.0373	1.3986	1.9986
63	6.9704	0.9956	1.0178	1.0178	1.0030	1.0030	1.0356	1.3986	1.9986
64	6.9704	0.1028	1.0162	1.0162	1.0024	1.0024	1.0339	1.3986	1.9986
65	6.9704	0.1100	1.0146	1.0146	1.0018	1.0018	1.0322	1.3986	1.9986
66	6.9704	0.1172	1.0130	1.0130	1.0012	1.0012	1.0315	1.3986	1.9986
67	6.9704	0.1244	1.0114	1.0114	1.0006	1.0006	1.0301	1.3986	1.9986
68	6.9704	0.1316	1.0098	1.0098	1.0000	1.0000	1.0284	1.3986	1.9986
69	6.9704	0.1388	1.0082	1.0082	1.0000	1.0000	1.0267	1.3986	1.9986
70	6.9704	0.1460	1.0066	1.0066	1.0000	1.0000	1.0250	1.3986	1.9986
71	6.9704	0.1532	1.0050	1.0050	1.0000	1.0000	1.0233	1.3986	1.9986
72	6.9704	0.1604	1.0034	1.0034	1.0000	1.0000	1.0216	1.3986	1.9986
73	6.9704	0.1676	1.0018	1.0018	1.0000	1.0000	1.0200	1.3986	1.9986
74	6.9704	0.1748	1.0002	1.0002	1.0000	1.0000	1.0183	1.3986	1.9986
75	6.9704	0.1820	0.9986	0.9986	1.0000	1.0000	1.0166	1.3986	1.9986
76	6.9704	0.1892	0.9970	0.9970	1.0000	1.0000	1.0150	1.3986	1.9986
77	6.9704	0.1964	0.9954	0.9954	1.0000	1.0000	1.0133	1.3986	1.9986
78	6.9704	0.2036	0.9938	0.9938	1.0000	1.0000	1.0116	1.3986	1.9986
79	6.9704	0.2108	0.9922	0.9922	1.0000	1.0000	1.0099	1.3986	1.9986
80	6.9704	0.2180	0.9906	0.9906	1.0000	1.0000	1.0082	1.3986	1.9986
81	6.9704	0.2252	0.9890	0.9890	1.0000	1.0000	1.0065	1.3986	1.9986
82	6.9704	0.2324	0.9874	0.9874	1.0000	1.0000	1.0048	1.3986	1.9986
83	6.9704	0.2396	0.9858	0.9858	1.0000	1.0000	1.0031	1.3986	1.9986
84	6.9704	0.2468	0.9842	0.9842	1.0000	1.0000	1.0014	1.3986	1.9986
85	6.9704	0.2540	0.9826	0.9826	1.0000	1.0000	1.0000	1.3986	1.9986
86	6.9704	0.2612	0.9810	0.9810	1.0000	1.0000	1.0000	1.3986	1.9986
87	6.9704	0.2684	0.9794	0.9794	1.0000	1.0000	1.0000	1.3986	1.9986
88	6.9704	0.2756	0.9778	0.9778	1.0000	1.0000	1.0000	1.3986	1.9986
89	6.9704	0.2828	0.9762	0.9762	1.0000	1.0000	1.0000	1.3986	1.9986
90	6.9704	0.2890	0.9746	0.9746	1.0000	1.0000	1.0000	1.3986	1.9986
91	6.9704	0.2962	0.9730	0.9730	1.0000	1.0000	1.0000	1.3986	1.9986
92	6.9704	0.3034	0.9714	0.9714	1.0000	1.0000	1.0000	1.3986	1.9986
93	6.9704	0.3106	0.9698	0.9698	1.0000	1.0000	1.0000	1.3986	1.9986
94	6.9704	0.3178	0.9682	0.9682	1.0000	1.0000	1.0000	1.3986	1.9986
95	6.9704	0.3250	0.9666	0.9666	1.0000	1.0000	1.0000	1.3986	1.9986
96	6.9704	0.3322	0.9650	0.9650	1.0000	1.0000	1.0000	1.3986	1.9986
97	6.9704	0.3394	0.9634	0.9634	1.0000	1.0000	1.0000	1.3986	1.9986
98	6.9704	0.3466	0.9618	0.9618	1.0000	1.0000	1.0000	1.3986	1.9986
99	6.9704	0.3538	0.9602	0.9602	1.0000	1.0000	1.0000	1.3986	1.9986
100	6.9704	0.3610	0.9586	0.9586	1.0000	1.0000	1.0000	1.3986	1.9986
101	6.9704	0.3682	0.9570	0.9570	1.0000	1.0000	1.0000	1.3986	1.9986
102	6.9704	0.3754	0.9554	0.9554	1.0000	1.0000	1.0000	1.3986	1.9986
103	6.9704	0.3826	0.9538	0.9538	1.0000	1.0000	1.0000	1.3986	1.9986
104	6.9704	0.3898	0.9522	0.9522	1.0000	1.0000	1.0000	1.3986	1.9986
105	6.9704	0.3970	0.9506	0.9506	1.0000	1.0000	1.0000	1.3986	1.9986
106	6.9704	0.4042	0.9490	0.9490	1.0000	1.0000	1.0000	1.3986	1.9986
107	6.9704	0.4114	0.9474	0.9474	1.0000	1.0000	1.0000	1.3986	1.9986
108	6.9704	0.4186	0.9458	0.9458	1.0000	1.0000	1.0000	1.3986	1.9986
109	6.9704	0.4258	0.9442	0.9442	1.0000	1.0000	1.0000	1.3986	1.9986
110	6.9704	0.4330	0.9426	0.9426	1.0000	1.0000	1.0000	1.3986	1.9986
111	6.9704	0.4402	0.9410	0.9410	1.0000	1.0000	1.0000	1.3986	1.9986
1									

APPENDIX

I	X/L	H/L	P/PINF	T/TINF	U/UINF	V/UINF	W	GAMMA	PT/PTINF
1	9.0840	• 0633	• 6578	• 3323	1.4200	• 1376	1.9811	1.3986	2.3908
2	9.0840	• 0759	• 6449	• 3304	1.4221	• 1660	1.9936	1.3986	2.3714
3	9.0840	• 0880	• 6300	• 3262	1.4245	.1947	2.0099	1.3986	2.3485
4	9.0840	• 1012	• 6136	• 3257	1.4270	• 2240	2.0259	1.3986	2.3227
5	9.0840	• 1139	• 5955	• 3230	1.4296	• 2539	2.0452	1.3986	2.2933
6	9.0840	• 1265	• 5757	• 3198	1.4325	• 2838	2.0669	1.3986	2.2603
7	9.0840	• 1392	• 5557	• 3166	1.4350	• 3136	2.0896	1.3986	2.2257
8	9.0840	• 1518	• 5375	• 3136	1.4366	• 3419	2.1110	1.3986	2.1932
9	9.0840	• 1645	• 5286	• 3121	1.4361	• 3610	2.1217	1.3986	2.1770
10	9.0840	• 1771	• 5540	• 3164	1.4277	• 3489	2.0917	1.3986	2.2231
11	9.0840	• 1898	• 6517	• 3315	1.4005	• 2805	1.9856	1.3986	2.3701
12	9.0840	• 2024	• 7689	• 3474	1.3683	• 2145	1.8812	1.3986	2.5461
13	9.0840	• 2151	• 8452	• 3577	1.3439	• 1609	1.8149	1.3986	2.6253
14	9.0840	• 2277	• 8902	• 3650	1.3239	• 1679	1.7682	1.3986	2.6409
15	9.0840	• 2404	• 9283	• 3715	1.3056	• 1590	1.7276	1.3986	2.6440
16	9.0840	• 2530	• 9670	• 3773	1.2892	• 1495	1.6910	1.3986	2.6532
17	9.0840	• 2657	• 9999	• 3699	1.2712	• 0839	1.6716	1.4007	2.6917
18	9.0840	• 2784	• 10242	• 4895	• 9661	• 1528	1.1162	1.4003	1.4615
19	9.0840	• 2910	• 10360	• 7047	• 6620	• 0978	1.4997	1.3986	0.8962
20	9.0840	• 3036	• 10844	• 9348	• 5032	• 0374	4.174	1.3986	0.8019
21	9.0840	• 3222	• 10844	• 4982	• 0526	• 0037	3879	1.3986	1.7891
22	9.0838	• 3408	• 3410	• 10844	• 0757	• 5468	• 0219	1.3985	0.8037
23	9.0838	• 3594	• 3594	• 10844	• 0754	• 6078	• 0337	1.3985	0.8268
24	9.0838	• 3780	• 3780	• 10844	• 0674	• 6711	• 0423	1.3986	0.8595
25	9.0838	• 3966	• 3966	• 10844	• 0569	• 7322	• 0486	1.3986	0.8666
26	9.0838	• 4152	• 4152	• 10835	• 0462	• 7880	• 0532	1.3986	0.9185
27	9.0838	• 4338	• 4338	• 10817	• 0362	• 8364	• 0563	1.3987	0.9485
28	9.0838	• 4524	• 4524	• 10797	• 0275	• 8762	• 0584	1.3987	0.9751
29	9.0838	• 4710	• 4710	• 10775	• 0208	• 9059	• 0594	1.3987	0.9959
30	9.0838	• 4896	• 4896	• 10753	• 0170	• 9222	• 0596	1.3987	1.0069
31	9.0838	• 5082	• 5082	• 10631	• 0176	• 9264	• 0629	1.3987	1.0000
32	9.0838	• 5268	• 5268	• 10610	• 0171	• 9284	• 0618	1.3987	1.0000
33	9.0838	• 5454	• 5454	• 10589	• 0165	• 9314	• 0607	1.4000	1.0000
34	9.0838	• 5640	• 5640	• 10567	• 0159	• 9340	• 0596	1.4000	1.0000
35	9.0838	• 5826	• 5826	• 10548	• 0154	• 9362	• 0585	1.4000	1.0000
36	9.0788	• 6012	• 6012	• 10531	• 0149	• 9383	• 0574	1.4000	1.0000
37	9.0788	• 6198	• 6198	• 10513	• 0144	• 9404	• 0563	1.4000	1.0000
38	9.0788	• 6384	• 6384	• 10495	• 0139	• 9425	• 0553	1.4000	1.0000
39	9.0788	• 6570	• 6570	• 10477	• 0134	• 9447	• 0542	1.4000	1.0000
40	9.0788	• 6756	• 6756	• 10458	• 0130	• 9465	• 0532	1.4000	1.0000
41	9.0788	• 6942	• 6942	• 10437	• 0126	• 9482	• 0522	1.4000	1.0000
42	9.0788	• 7128	• 7128	• 10422	• 0122	• 9499	• 0512	1.4000	1.0000
43	9.0788	• 7314	• 7314	• 10417	• 0117	• 9517	• 0502	1.4000	1.0000

APPENDIX

I	X/L	K/L	P/PINF	T/TINF	U/UINT	V/VINF	W/WINF	GAMMA	PI/PIINF
49	9.0768	.7500	1.0402	1.0113	.9534	*.0492	*.7595	1.4000	1.0000
1	9.2144	0.0000	.3440	.2760	1.5729	0.0000	2.3967	1.3986	1.7760
2	9.2144	.0130	.3440	.2762	1.5727	.0299	2.3958	1.3986	1.7748
3	9.2144	.0260	.3425	.2757	1.5727	.0593	2.3992	1.3986	1.7717
4	9.2144	.0390	.3402	.2752	1.5727	.0886	2.4035	1.3986	1.7658
5	9.2144	.0520	.3371	.2745	1.5724	.1184	2.4093	1.3986	1.7579
6	9.2144	.0650	.3332	.2735	1.5722	.1481	2.4168	1.3986	1.7477
7	9.2144	.0780	.3285	.2724	1.5719	.1779	2.4257	1.3986	1.7352
8	9.2144	.0910	.3233	.2712	1.5714	.2075	2.4362	1.3986	1.7213
9	9.2144	.1040	.3179	.2699	1.5704	.2364	2.4469	1.3986	1.7067
10	9.2144	.1170	.3134	.2688	1.5699	.2633	2.4562	1.3986	1.6944
11	9.2144	.1300	.3165	.2696	1.5644	.2787	2.4497	1.3986	1.7029
12	9.2144	.1430	.3806	.2846	1.5355	.2184	2.3299	1.3986	1.8642
13	9.2144	.1560	.5792	.3214	1.4552	.0516	2.0562	1.3986	2.2526
14	9.2144	.1690	.6400	.3299	1.4331	.0352	1.9979	1.3986	2.3622
15	9.2144	.1820	.6742	.3347	1.4198	.0368	1.9652	1.3986	2.4150
16	9.2144	.1950	.7227	.3415	1.4013	.0327	1.9200	1.3986	2.4022
17	9.2144	.2079	.7644	.3467	1.3866	.0314	1.8854	1.3986	2.5414
18	9.2144	.2209	.8053	.3523	1.3709	.0302	1.8492	1.3986	2.5063
19	9.2144	.2339	.8457	.3591	1.3512	.0290	1.8052	1.3986	2.6023
20	9.2144	.2469	.8850	.3660	1.3311	.0279	1.7615	1.3986	2.6077
21	9.2144	.2599	.9230	.3722	1.3130	.0268	1.7230	1.3986	2.6166
22	9.2120	.2729	.9593	.3916	1.2255	.0083	1.5645	1.4006	2.3058
23	9.2120	.2859	.9855	.5032	1.0232	.0854	1.1558	1.4003	1.4756
24	9.2120	.2989	.1.0020	.6644	.8282	.0713	.6151	1.3996	1.0171
25	9.2120	.3119	1.0615	.8532	.6778	.0350	.5877	1.3992	.8797
26	9.2120	.3350	1.0615	.0036	.6235	.0012	.4971	1.3987	.8243
27	9.2120	.3484	1.0615	.0468	.6471	.0172	.5052	1.3986	.8268
28	9.2120	.3667	1.0615	.0561	.6911	.0257	.5375	1.3986	.8475
29	9.2120	.3849	1.0615	.0530	.7412	.0303	.5773	1.3986	.8727
30	9.2120	.4032	1.0615	.0450	.7914	.0329	.6188	1.3986	.9012
31	9.2120	.4214	1.0604	.0358	.8378	.0345	.6580	1.3987	.9301
32	9.2120	.4397	1.0595	.0271	.8764	.0353	.6926	1.3987	.9575
33	9.2120	.4579	1.0584	.0197	.9107	.0355	.7207	1.3987	.9810
34	9.2120	.4762	1.0573	.0145	.9311	.0354	.7403	1.3987	.9979
35	9.2120	.4945	1.0561	.0128	.9399	.0351	.7463	1.3987	1.0024
36	9.2089	.5127	1.0512	.0144	.9410	.0492	.7484	1.4000	1.0000
37	9.2089	.5310	1.0500	.0140	.9425	.0483	.7498	1.4000	1.0000
38	9.2089	.5492	1.0489	.0137	.9437	.0474	.7508	1.4000	1.0000
39	9.2089	.5675	1.0477	.0134	.9450	.0466	.7519	1.4000	1.0000
40	9.2089	.5857	1.0466	.0131	.9464	.0458	.7531	1.4000	1.0000
41	9.2089	.6040	1.0455	.0128	.9477	.0450	.7542	1.4000	1.0000

APPENDIX

T	X/L	H/L	P/PINF	T/TINF	U/UINF	V/VINF	W/WINF	GAMMA	PT/PTINF
42	9.2089	0.6222	1.0444	1.0125	0.949	-0.0443	0.7554	1.4000	1.0000
43	9.2089	0.6405	1.0432	1.0122	0.9503	-0.0435	0.7564	1.4000	1.0000
44	9.2089	0.6587	1.0422	1.0119	0.9516	-0.0426	0.7575	1.4000	1.0000
45	9.2089	0.6770	1.0411	1.0116	0.9527	-0.0421	0.7586	1.4000	1.0000
46	9.2089	0.6952	1.0401	1.0115	0.9539	-0.0415	0.7596	1.4000	1.0000
47	9.2089	7.115	1.0591	1.0110	0.9551	-0.0406	0.7606	1.4000	1.0000
48	9.2089	7.317	1.0581	1.0107	0.9563	-0.0401	0.7617	1.4000	1.0000
49	9.2089	7.500	1.0370	1.0104	0.9575	-0.0394	0.7627	1.4000	1.0000
1	9.3692	0.0000	0.1727	0.2266	1.6909	0.0000	2.8429	1.3986	1.2321
2	9.3692	0.126	0.1725	0.2266	1.6910	-0.0275	2.8438	1.3986	1.2313
3	9.3692	0.257	0.1722	0.2265	1.6905	-0.0549	2.8445	1.3986	1.2298
4	9.3692	0.385	0.1715	0.2262	1.6900	-0.0822	2.8476	1.3986	1.2273
5	9.3692	0.513	0.1708	0.2259	1.6891	-0.1090	2.8504	1.3986	1.2244
6	9.3692	0.641	0.1701	0.2261	1.6872	-0.1337	2.8488	1.3986	1.2242
7	9.3692	0.770	0.1957	0.2349	1.6685	-0.1072	2.7616	1.3986	1.3075
8	9.3692	0.898	0.4689	0.3082	1.4743	-0.2091	2.1520	1.3986	1.9821
9	9.3692	1.020	0.5022	0.3109	1.4715	-0.1952	2.1508	1.3986	2.0847
10	9.3692	1.154	0.5377	0.3155	1.4606	-0.1837	2.0977	1.3986	2.1690
11	9.3692	1.283	0.5820	0.3219	1.4441	-0.1789	2.0530	1.3986	2.2569
12	9.3692	1.411	0.6195	0.3271	1.4307	-0.1703	2.0164	1.3986	2.3248
13	9.3692	1.539	0.6595	0.3328	1.4161	-0.1643	1.9779	1.3986	2.3900
14	9.3692	1.666	0.6983	0.3381	1.4019	-0.1582	1.9420	1.3986	2.4483
15	9.3692	1.790	0.7361	0.3452	1.3865	-0.1521	1.9087	1.3986	2.5018
16	9.3692	1.924	0.7730	0.361	1.3753	-0.1460	1.8765	1.3986	2.5463
17	9.3692	2.152	0.8094	0.3524	1.3636	-0.1403	1.8485	1.3986	2.5977
18	9.3692	2.141	0.8450	0.3575	1.3494	-0.1347	1.8155	1.3986	2.6263
19	9.3692	2.309	0.8790	0.3637	1.3325	-0.1279	1.7764	1.3986	2.6286
20	9.3692	2.457	0.9111	0.3695	1.3155	-0.1214	1.7496	1.3986	2.6265
21	9.3692	2.565	0.9418	0.3746	1.3010	-0.1152	1.7083	1.3986	2.6302
22	9.3722	2.094	0.9694	0.4166	1.1794	-0.0365	1.4555	1.4005	2.0661
23	9.3722	2.222	0.9984	0.5206	1.0109	-0.0262	1.1129	1.4002	1.4048
24	9.3722	2.295	1.0012	0.6093	0.8526	-0.0199	0.8322	1.3998	1.0342
25	9.3722	3.079	1.0498	0.6283	0.7323	-0.0201	0.6428	1.3993	0.9092
26	9.3722	3.263	1.0498	0.6216	0.6703	-0.0253	0.5407	1.3986	0.8401
27	9.3722	3.447	1.0498	1.0533	0.6862	-0.0300	0.5396	1.3987	0.8394
28	9.3722	3.631	1.0498	1.0468	0.7240	-0.0334	0.5657	1.3986	0.8555
29	9.3722	3.815	1.0498	1.0462	0.7684	-0.0357	0.6010	1.3986	0.8789
30	9.3722	4.000	1.0495	1.0398	0.8146	-0.0371	0.6387	1.3986	0.9058
31	9.3722	4.144	1.0489	1.0315	0.8576	-0.0379	0.6750	1.3987	0.9335
32	9.3722	4.308	1.0482	1.0232	0.8954	-0.0382	0.7074	1.3987	0.9600
33	9.3722	4.552	1.0475	1.0162	0.9255	-0.0381	0.7338	1.3987	0.9827
34	9.3722	4.737	1.0467	1.0115	0.9454	-0.0377	0.7513	1.3987	0.9882

APPENDIX

I	X/L	R/L	P/PINF	T/TINF	U/UINF	V/VINF	H	GAMMA	PT/PTINF
35	9.3722	4.921	1.0460	1.0110	.9470	.0368	1.3987	1.9993	
36	9.3679	5.105	1.0425	1.0120	.9512	.0414	1.4000	1.0000	
37	9.3679	5.289	1.0417	1.0110	.9521	.0403	1.4000	1.0000	
38	9.3679	5.474	1.0410	1.0115	.9531	.0392	1.4000	1.0000	
39	9.3679	5.658	1.0402	1.0113	.9539	.0383	1.4000	1.0000	
40	9.3679	5.842	1.0395	1.0111	.9540	.0375	1.4000	1.0000	
41	9.3679	6.020	1.0387	1.0109	.9557	.0367	1.4000	1.0000	
42	9.3679	6.214	1.0380	1.0107	.9560	.0359	1.4000	1.0000	
43	9.3679	6.395	1.0375	1.0105	.9575	.0351	1.4000	1.0000	
44	9.3679	6.579	1.0365	1.0103	.9585	.0345	1.4000	1.0000	
45	9.3679	6.763	1.0358	1.0101	.9592	.0339	1.4000	1.0000	
46	9.3679	6.947	1.0350	1.0099	.9600	.0333	1.4000	1.0000	
47	9.3679	7.132	1.0343	1.0097	.9609	.0327	1.4000	1.0000	
48	9.3679	7.510	1.0336	1.0095	.9617	.0321	1.4000	1.0000	
49	9.3679	7.500	1.0329	1.0093	.9625	.0315	1.4000	1.0000	
*	1	9.5660	0.0000	1.2988	1.0994	0.0000	1.3292	1.3986	2.3916
*	2	9.5660	0.124	1.2968	1.0993	0.0000	1.3292	1.3986	2.1917
*	3	9.5660	0.247	1.2968	1.0983	1.0993	1.3291	1.3986	2.3915
*	4	9.5660	0.571	1.0176	1.4124	1.1756	1.1585	1.4805	2.2285
*	5	9.5660	0.494	0.6510	1.3472	1.3490	1.3126	1.8822	2.1575
*	6	9.5660	0.616	0.6259	1.3355	1.3955	1.2524	1.9593	2.2298
*	7	9.5660	0.742	0.6711	1.3400	1.3832	1.2492	1.9295	2.3257
*	8	9.5660	0.865	0.6914	1.3401	1.4860	1.2328	1.9290	2.3948
*	9	9.5660	0.999	0.7185	1.3427	1.3802	1.2232	1.9110	2.4489
*	10	9.5660	1.113	0.7442	1.3453	1.3742	1.2142	1.8945	2.4956
*	11	9.5660	1.236	0.7691	1.3480	1.3677	1.2057	1.8766	2.5155
*	12	9.5660	1.560	0.7938	1.3509	1.3606	1.1980	1.8580	2.5709
*	13	9.5660	1.413	0.6182	1.3538	1.3534	1.1907	1.8394	2.6029
*	14	9.5660	1.607	0.8418	1.3566	1.3463	1.1834	1.8212	2.6311
*	15	9.5660	1.731	0.8644	1.3593	1.3395	1.1763	1.8042	2.6572
*	16	9.5660	1.854	0.8865	1.3610	1.3330	1.1693	1.7802	2.6810
*	17	9.5660	1.978	0.9073	1.3642	1.3268	1.1623	1.7730	2.7047
*	18	9.5660	2.102	0.9275	1.3681	1.3162	1.1549	1.7484	2.6975
*	19	9.5660	2.225	0.9465	1.3724	1.3042	1.1474	1.7216	2.6796
*	20	9.5660	2.349	0.9651	1.3763	1.2933	1.1404	1.6973	2.6652
*	21	9.5692	2.472	0.9834	1.3832	1.2532	1.0633	1.6163	2.5037
*	22	9.5692	2.596	0.9980	1.4589	1.1246	-0.0706	1.3278	1.6360
*	23	9.5692	2.720	1.0085	1.5587	1.0936	-0.0579	1.4001	1.3507
*	24	9.5692	2.843	1.0162	1.6792	1.0720	-0.0490	1.8464	1.3997
*	25	9.5692	2.967	1.0462	1.8073	1.7764	-0.0444	0.6917	1.3993
*	26	9.5692	3.150	1.0462	1.9552	1.7083	-0.0442	0.5799	1.3989
*	27	9.5692	3.345	1.0462	1.0172	1.7129	-0.0463	0.5657	1.3987

APPENDIX

<i>i</i>	<i>x/l</i>	<i>h/l</i>	<i>P/PINF</i>	<i>T/TINF</i>	<i>U/UINF</i>	<i>V/VINF</i>	<i>GAMMA</i>	<i>PT/PTINF</i>
28	9.5692	.3534	1.0402	1.0376	.7451	-.0480	.5858	1.3987
29	9.5692	.3722	1.0402	1.0410	.7825	-.0491	.6135	1.3986
30	9.5692	.3911	1.0459	1.0369	.8239	-.0496	.6473	1.3987
31	9.5692	.4100	1.0452	1.0297	.8641	-.0496	.6811	1.3987
32	9.5692	.4289	1.0444	1.0220	.9001	-.0492	.7121	1.3987
33	9.5692	.4478	1.0436	1.0153	.9294	-.0484	.7376	1.3987
34	9.5692	.4667	1.0428	1.0107	.9488	-.0473	.7546	1.3987
35	9.5666	.4856	1.0377	1.0108	.9570	-.0335	.7621	1.4000
36	9.5666	.5045	1.0369	1.0104	.9579	-.0325	.7628	1.4000
37	9.5666	.5234	1.0362	1.0102	.9588	-.0315	.7636	1.4000
38	9.5666	.5422	1.0355	1.0100	.9596	-.0306	.7643	1.4000
39	9.5666	.5611	1.0348	1.0098	.9604	-.0299	.7649	1.4000
40	9.5666	.5800	1.0341	1.0096	.9612	-.0292	.7656	1.4000
41	9.5666	.5989	1.0335	1.0095	.9619	-.0285	.7663	1.4000
42	9.5666	.6178	1.0328	1.0095	.9627	-.0278	.7669	1.4000
43	9.5666	.6367	1.0322	1.0091	.9634	-.0272	.7676	1.4000
44	9.5666	.6556	1.0316	1.0089	.9641	-.0266	.7682	1.4000
45	9.5666	.6744	1.0310	1.0088	.9648	-.0261	.7688	1.4000
46	9.5666	.6933	1.0304	1.0086	.9655	-.0256	.7694	1.4000
47	9.5666	.7122	1.0298	1.0084	.9662	-.0251	.7699	1.4000
48	9.5666	.7311	1.0293	1.0083	.9668	-.0249	.7705	1.4000
49	9.5666	.7500	1.0287	1.0081	.9674	-.0242	.7711	1.4000

REFERENCES

1. Bergman, Dave: Effects of Engine Exhaust Flow on Boattail Drag. AIAA Paper 70-132, Jan. 1970.
2. Swanson, R. Charles, Jr.: Numerical Solutions of the Navier-Stokes Equations for Transonic Afterbody Flows. NASA TP-1784, 1980.
3. Diewert, G. S.: Numerical Simulation of Three-Dimensional Boattail Afterbody Flow Fields. AIAA-80-1347, July 1980.
4. Reubush, David E.; and Putnam, Lawrence E.: An Experimental and Analytical Investigation of the Effect on Isolated Boattail Drag of Varying Reynolds Number up to 130×10^6 . NASA TN D-8210, 1976.
5. Wilmoth, Richard G.: Computation of Transonic Boattail Flow With Separation. NASA TP-1070, 1977.
6. Putnam, Lawrence E.: DONBOL: A Computer Program for Predicting Axisymmetric Nozzle Afterbody Pressure Distributions and Drag at Subsonic Speeds. NASA TM-78779, 1979.
7. Reshotko, Eli; and Tucker, Maurice: Approximate Calculation of the Compressible Turbulent Boundary Layer With Heat Transfer and Arbitrary Pressure Gradient. NACA TN 4154, 1957.
8. Presz, Walter Michael, Jr.: Turbulent Boundary Layer Separation of Axisymmetric Afterbodies. Ph. D. Thesis, Univ. of Connecticut, 1974.
9. South, Jerry C., Jr.; and Jameson, Antony: Relaxation Solutions for Inviscid Axisymmetric Transonic Flow Over Blunt or Pointed Bodies. AIAA Computational Fluid Dynamics Conference, July 1973, pp. 8-17.
10. Abeyounis, William Kelly: Boundary-Layer Separation on Isolated Boattail Nozzles. NASA TP-1226, 1978.
11. Presz, Walter M., Jr.; King, Ronald W.; and Buteau, John D.: An Improved Analytical Model of the Separation Region on Boattail Nozzles at Subsonic Speeds. NASA CR-3028, 1978.
12. Wilmoth, R. G.; and Dash, S. M.: A Viscous-Inviscid Interaction Model of Jet Entrainment. Computation of Viscous-Inviscid Interactions, AGARD-CP-291, Feb. 1981, pp. 13-1 - 13-15.
13. Dash, Sanford M.; and Pergament, Harold S.: A Computational Model for the Prediction of Jet Entrainment in the Vicinity of Nozzle Boattails (The BOAT Code). NASA CR-3075, 1978.
14. Wilmoth, Richard G.: Viscous-Inviscid Calculations of Jet Entrainment Effects on the Subsonic Flow Over Nozzle Afterbodies. NASA TP-1626, 1980.
15. Dash, S. M.; and Thorpe, R. D.: A New Shock-Capturing/Shock-Fitting Computational Model for Analyzing Supersonic Inviscid Flows (The SCIPPY Code). Rep. No. 366, Aeronaut. Res. Assoc. Princeton, Inc., Nov. 1978.

16. Keller, James D.; and South, Jerry C., Jr.: RAXBOD: A Fortran Program for Inviscid Transonic Flow Over Axisymmetric Bodies. NASA TM X-72831, 1976.
17. Dash, Sanford M.; Pergament, Harold S.; and Thorpe, Roger D.: Computational Models for the Viscous/Inviscid Analysis of Jet Aircraft Exhaust Plumes. NASA CR-3289, 1980.
18. Abbott, Michael: Mach Disk in Underexpanded Exhaust Plumes. AIAA J., vol. 9, no. 3, March 1971, pp. 512-514.
19. User's Manual for the External Drag and Internal Nozzle Performance Deck (Deck XI) - Supersonic Flow Analysis (Applicable to Deck VI). PWA-3465, Suppl. F, Pt. I (Contract No. AF33(615)-3128), Pratt and Whitney Aircraft, Sept. 1, 1968.
20. Peters, C. E.; and Phares, W. J.: An Integral Turbulent Kinetic Energy Analysis of Free Shear Flows. Free Turbulent Shear Flows. Volume I - Conference Proceedings, NASA SP-321, 1973, pp. 577-624.
21. Reubush, David E.: Experimental Study of the Effectiveness of Cylindrical Plume Simulators for Predicting Jet-On Boattail Drag at Mach Numbers up to 1.30. NASA TN D-7795, 1974.
22. Abeyounis, William K.; and Putnam, Lawrence E.: Experimental and Theoretical Study of Flow Fields Surrounding Boattail Nozzles at Subsonic Speeds. NASA TP-1633, 1980.
23. Reubush, David E.; and Runckel, Jack F.: Effect of Fineness Ratio on the Boat-tail Drag of Circular-Arc Afterbodies Having Closure Ratios of 0.50 With Jet Exhaust at Mach Numbers up to 1.30. NASA TN D-7192, 1973.
24. Mason, Mary L.; and Putnam, Lawrence E.: Pitot Pressure Measurements in Flow Fields Behind Circular-Arc Nozzles With Exhaust Jets at Subsonic Free-Stream Mach Numbers. NASA TM-80169, 1979.
25. Cline, Michael C.; and Wilmoth, Richard G.: Computation of High Reynolds Number Internal/External Flows. AIAA-81-1194, June 1981.

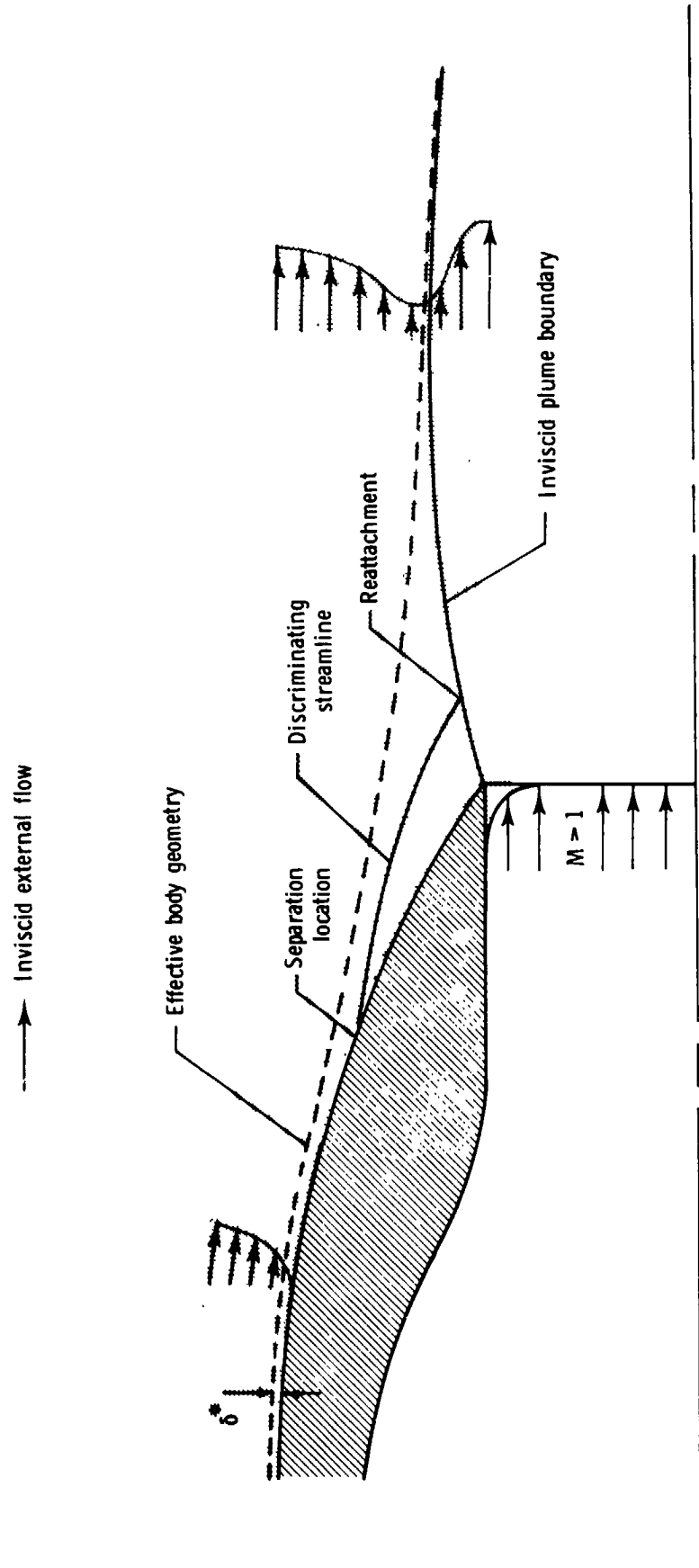


Figure 1.— Schematic of nozzle afterbody flow field.

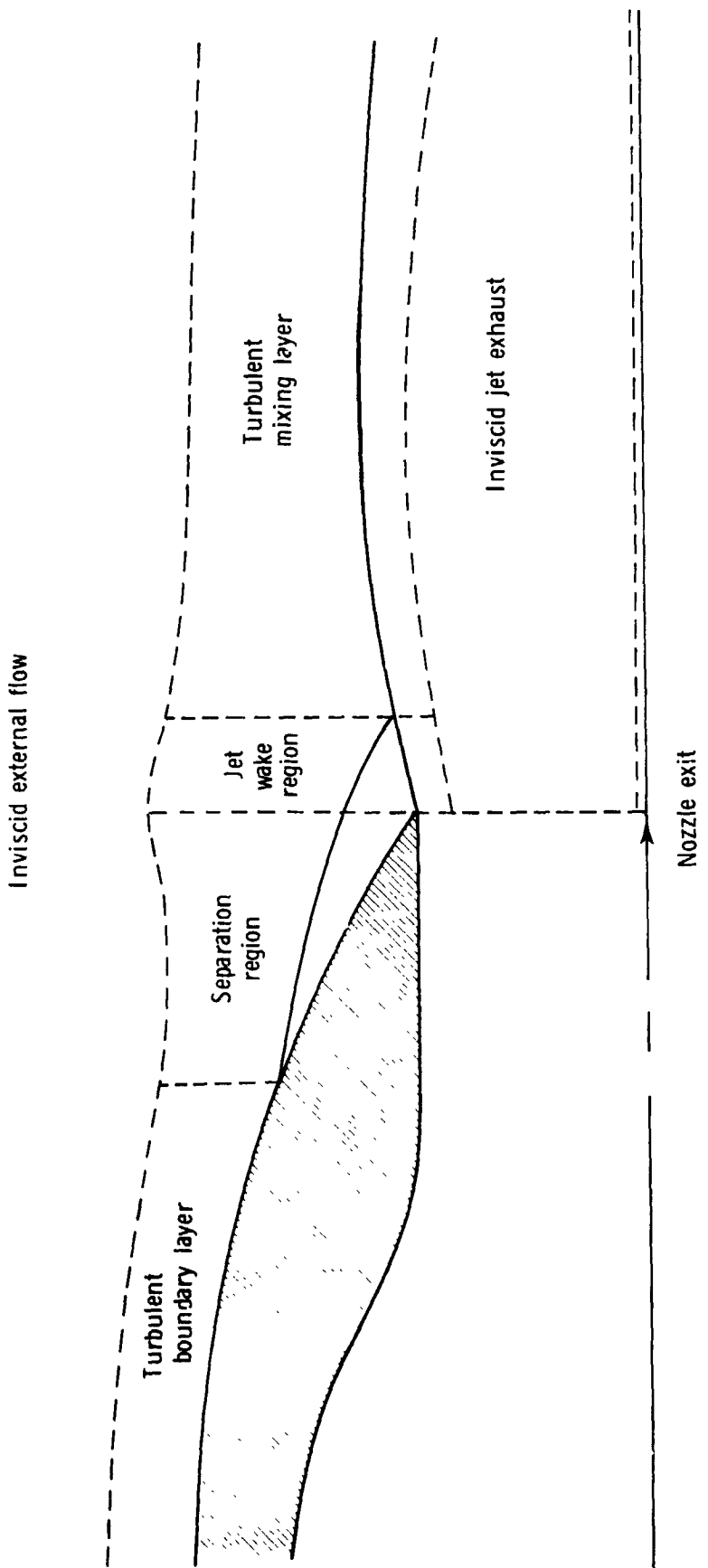


Figure 2.- Patched viscous-inviscid interaction model.

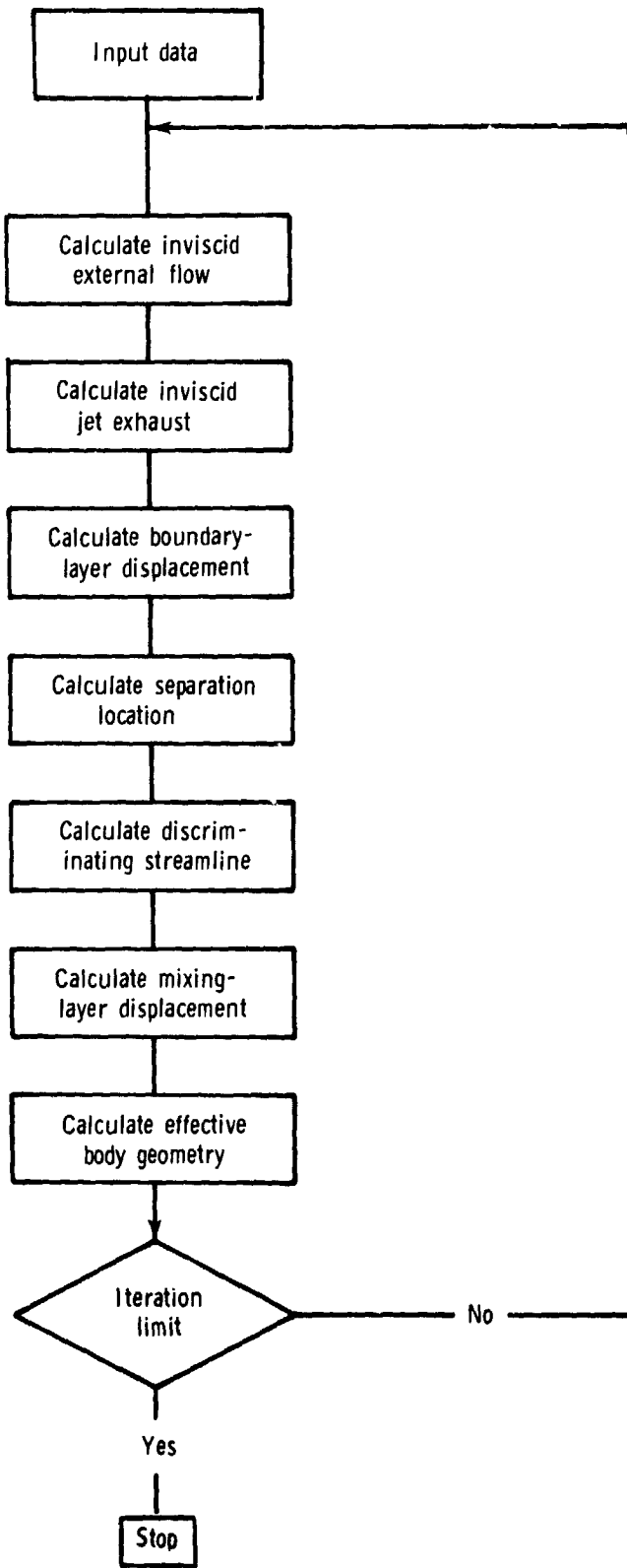


Figure 3.- Viscous-inviscid iteration scheme.

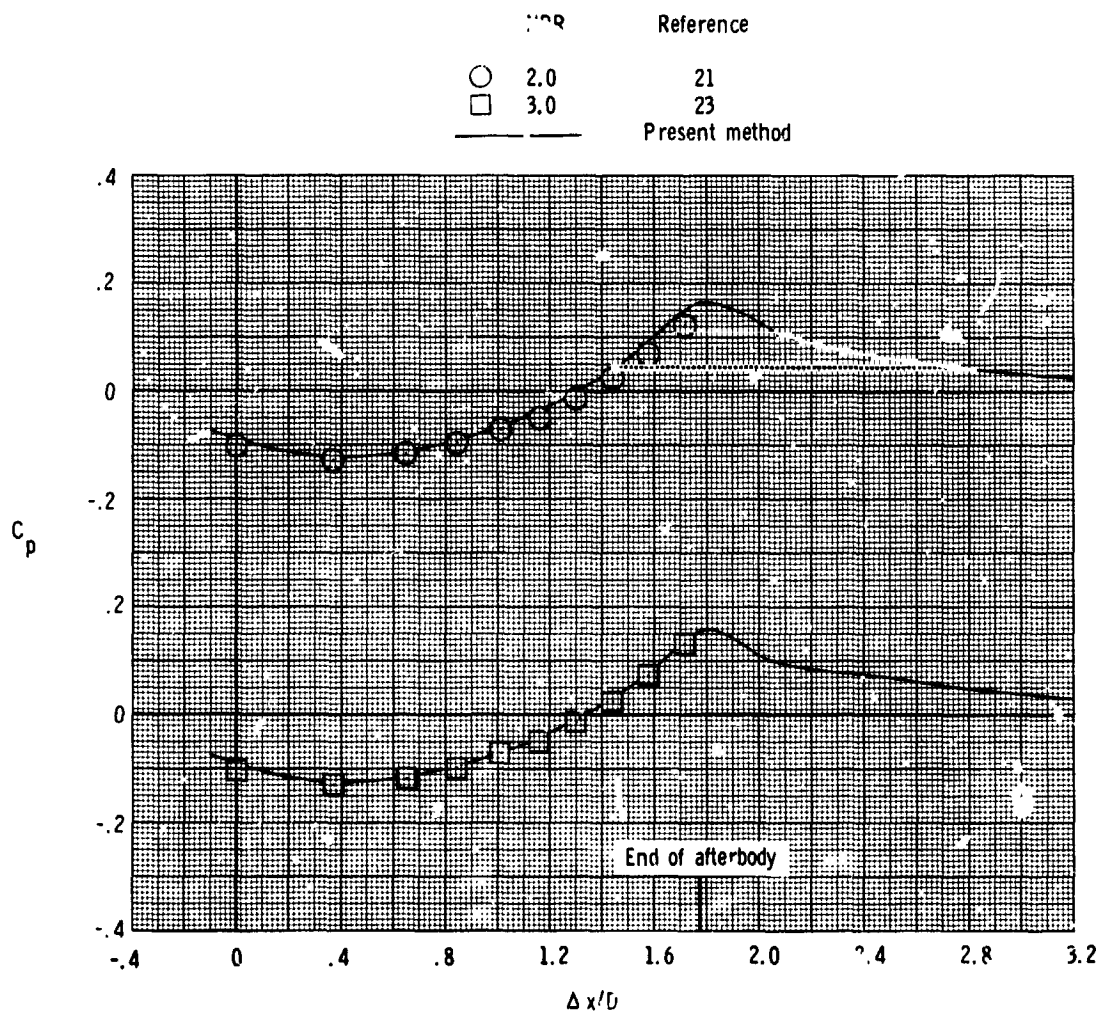
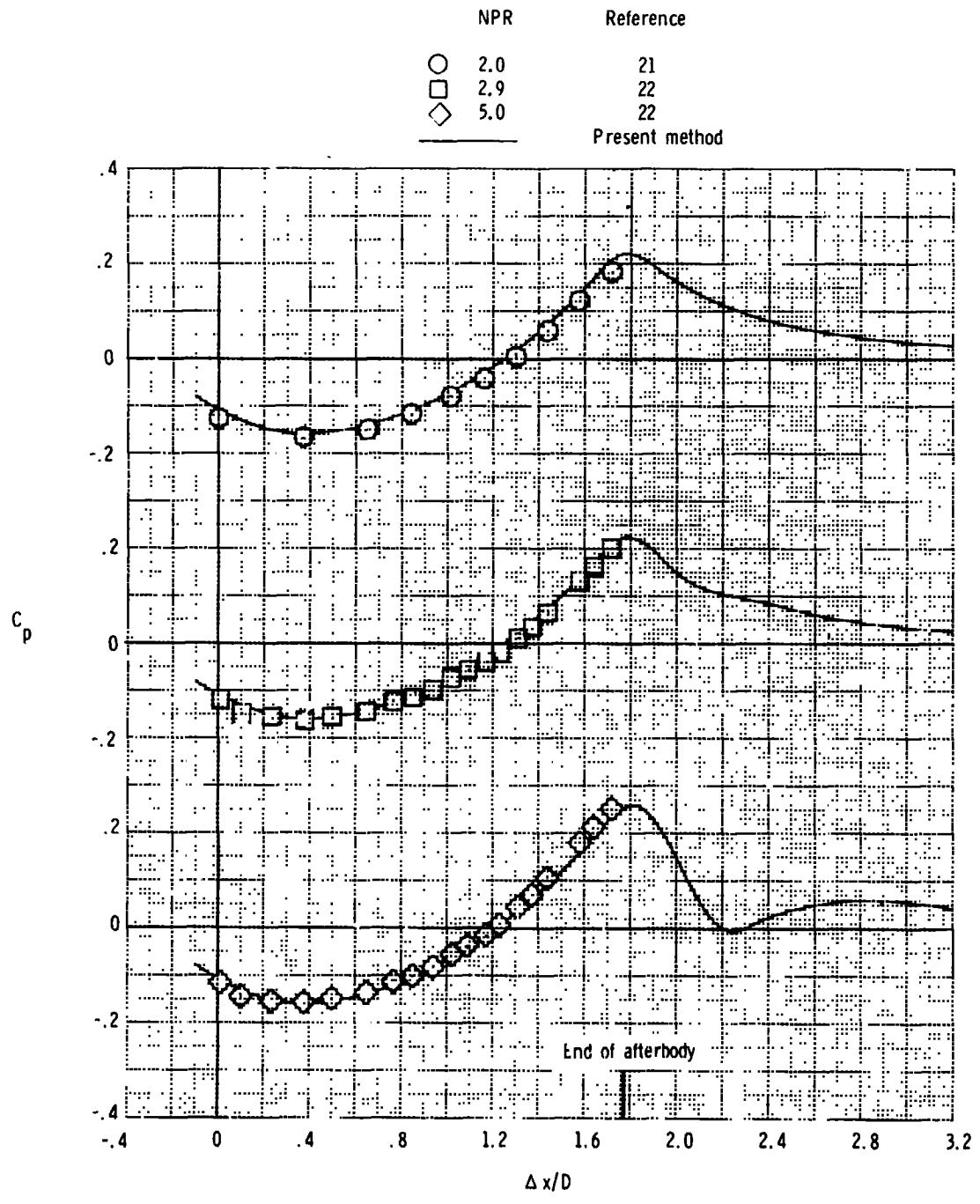
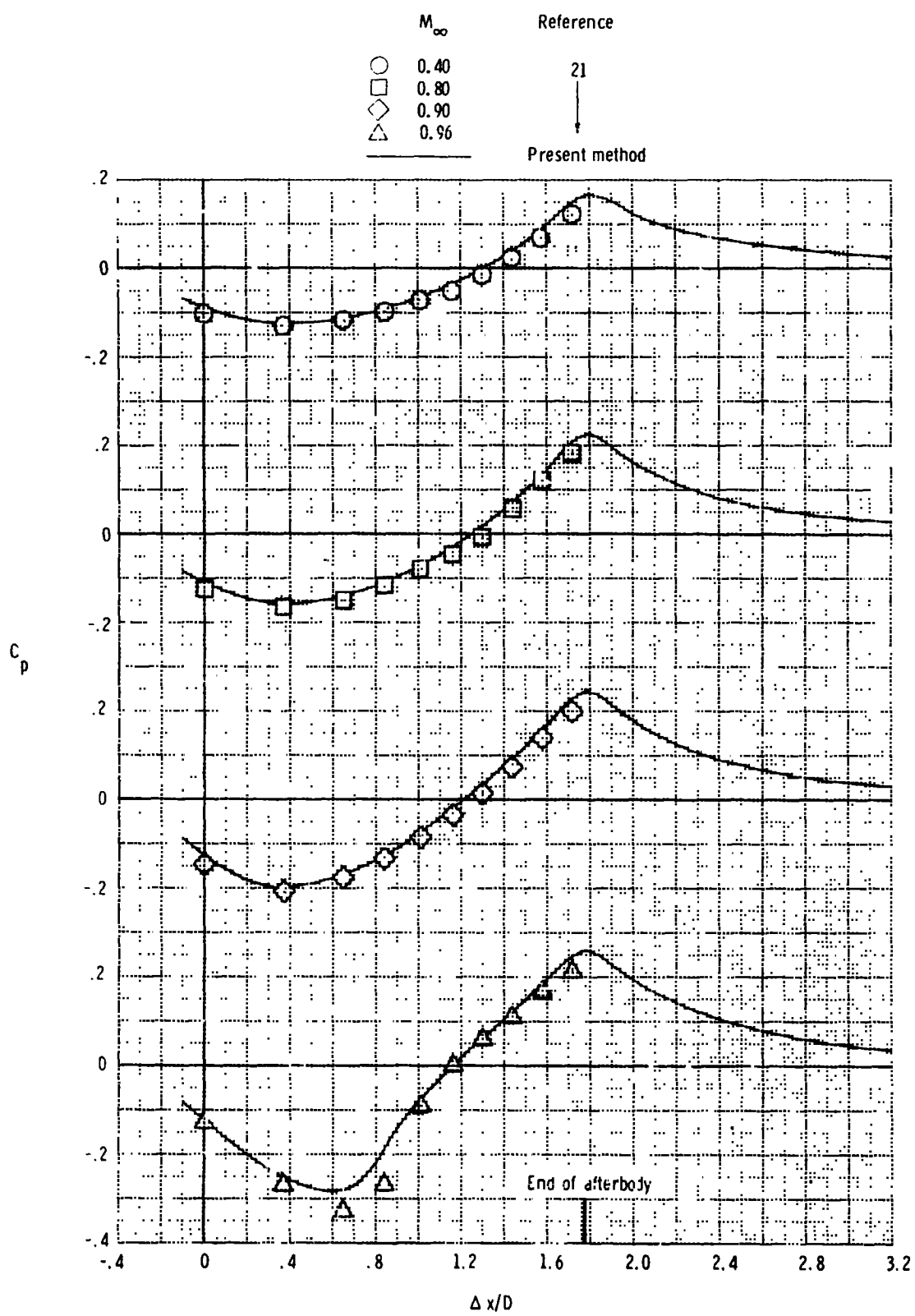


Figure 4.- Predicted and experimental afterbody pressures for attached flow on a circular-arc boattail nozzle with $l/D = 1.768$ and $D_b/D = 0.51$.
 $\Delta x = x - x_A$.



(b) Effect of NPR. $M_\infty = 0.8.$

Figure 4.- Continued.



(c) Effect of M_{∞} . NPR = 2.0.

Figure 4.- Concluded.

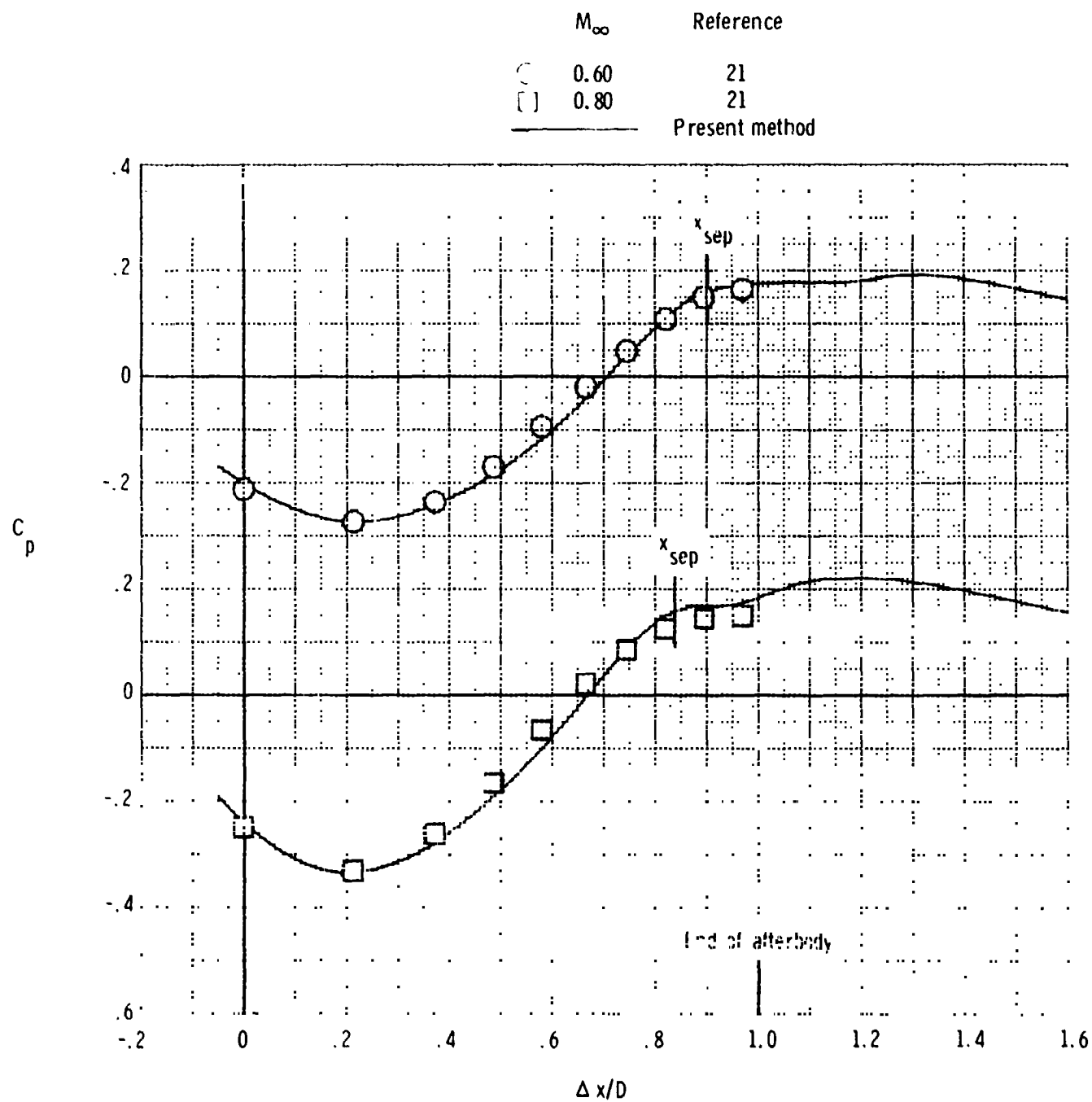
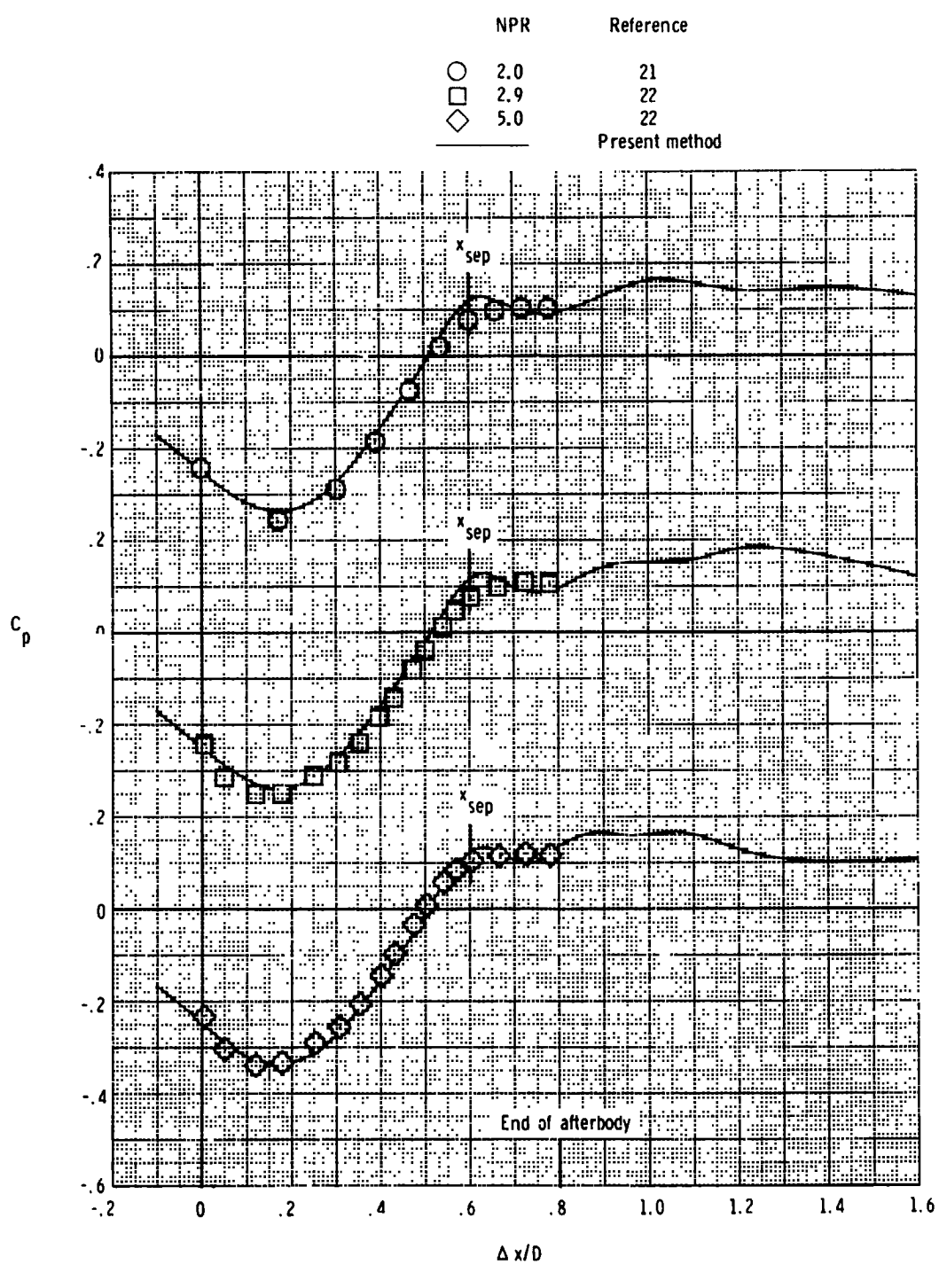
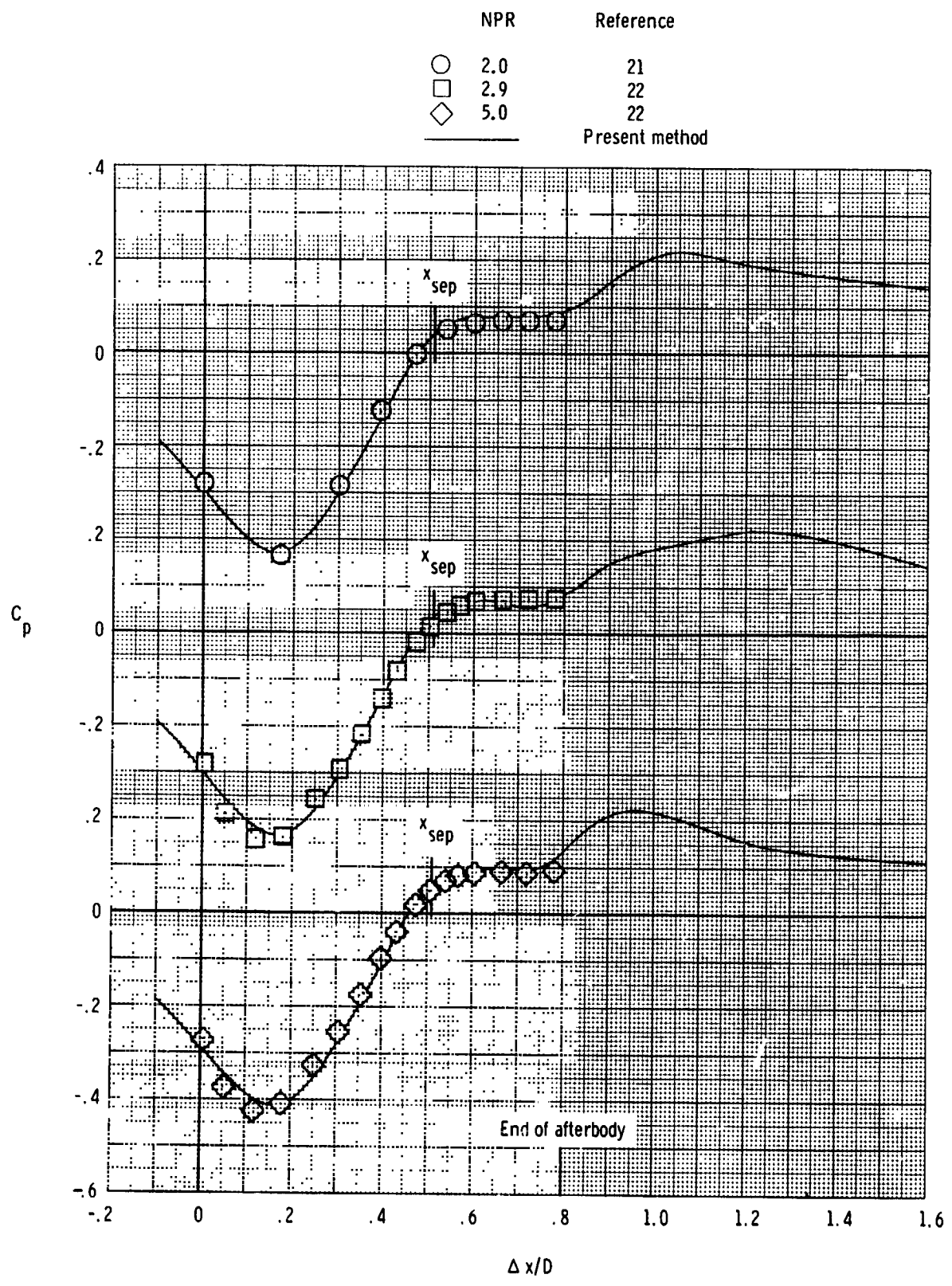


Figure 5.- Predicted and experimental afterbody pressures for separated flow on a circular-arc boattail nozzle with $1/D = 1.0$ and $D_b/D = 0.51$.
 $NPR = 2.0$. Experimental separation and extrapolated wake model used.
 $\Delta x = x - x_A$.



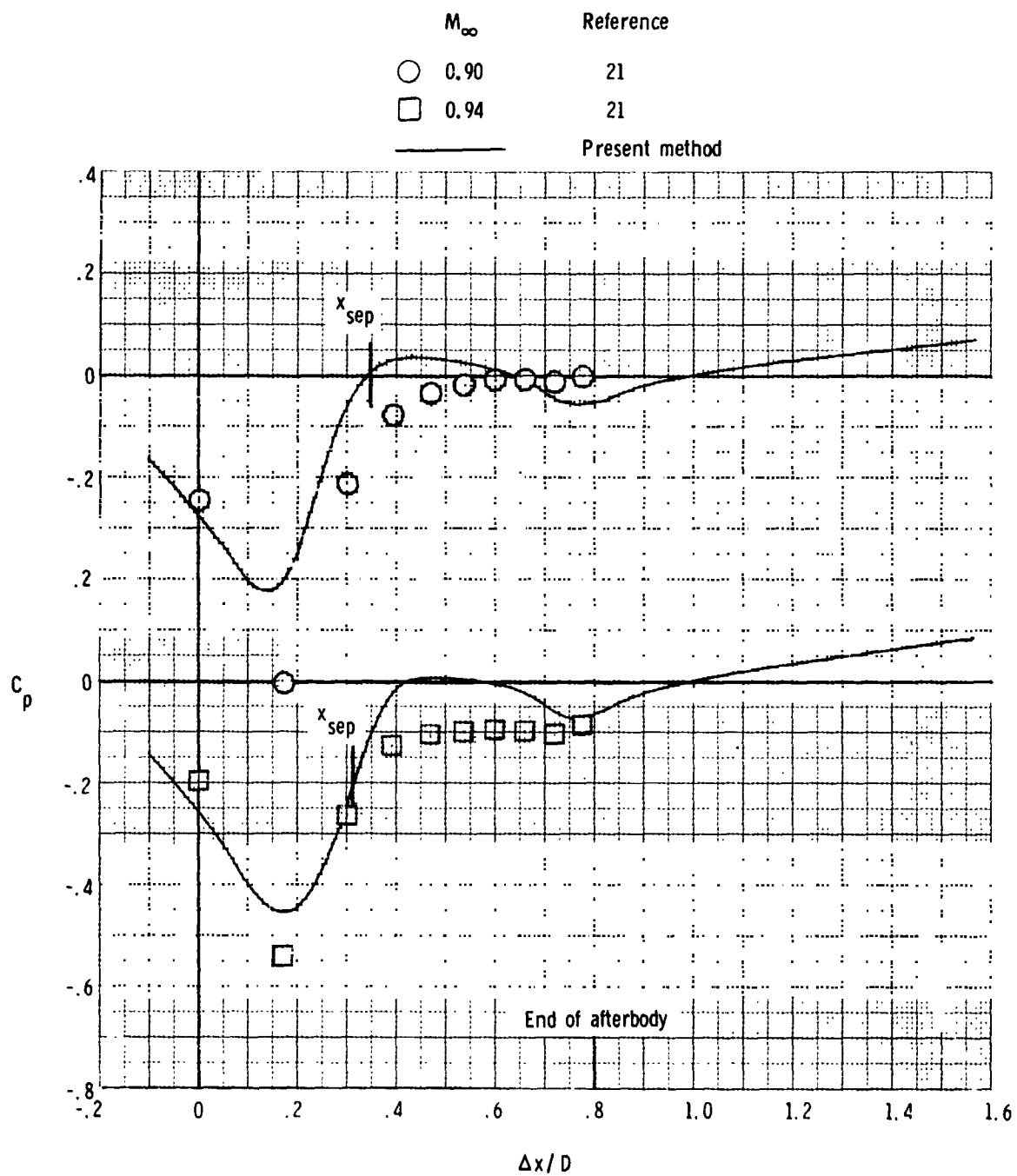
(a) $M_\infty = 0.6.$

Figure 6.- Predicted and experimental afterbody pressures for separated flow on a circular-arc boattail nozzle with $l/D = 0.8$ and $D_b/D = 0.51$. Experimental separation location and extrapolated wake model used.
 $\Delta x = x - x_A$.



(b) $M_\infty = 0.8.$

Figure 6.- Continued.



(c) $M_\infty = 0.9$ and 0.94 ; $NPR = 2.0$.

Figure 6.- Concluded.

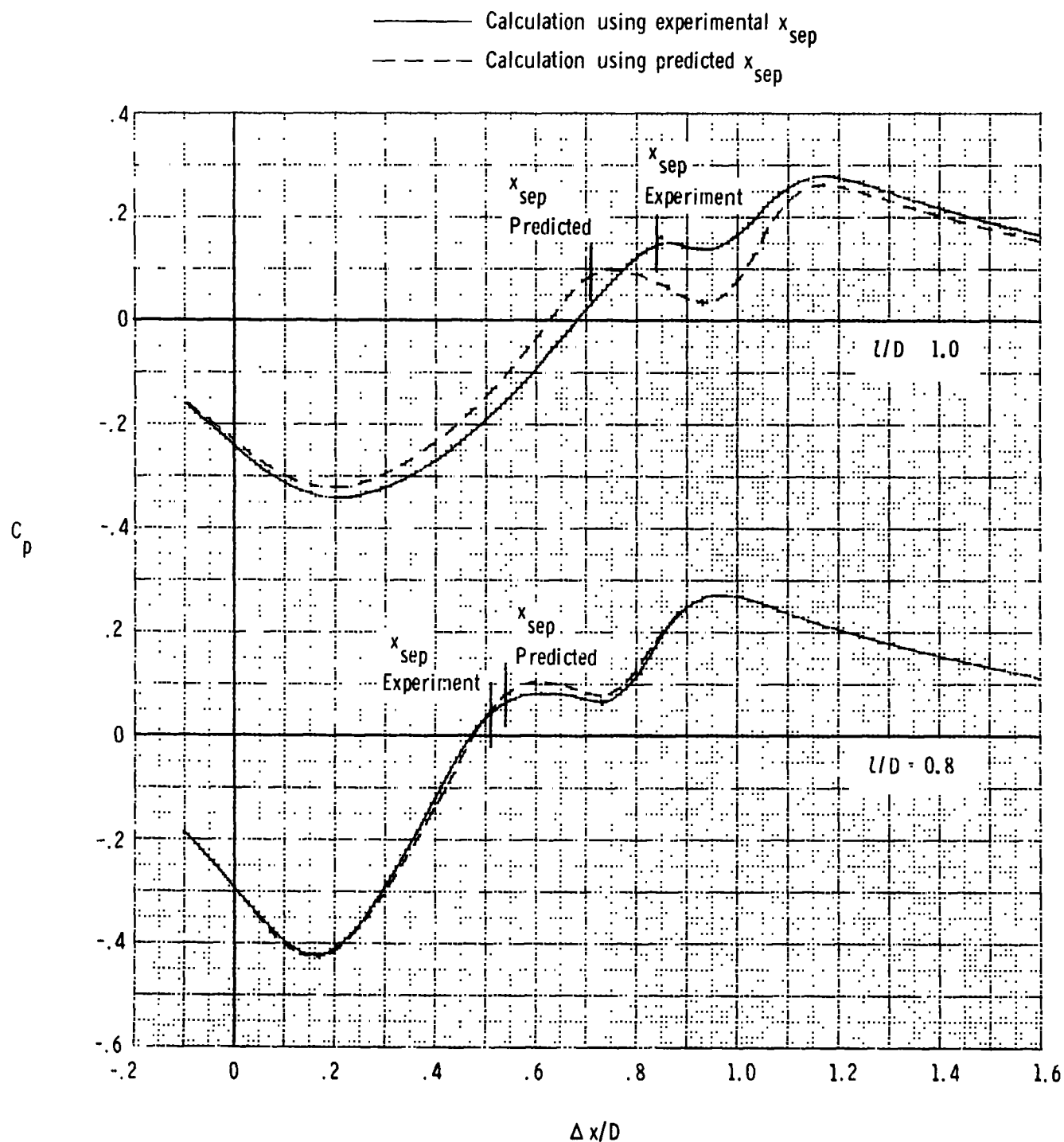


Figure 7.- Effect of separation location prediction on predicted afterbody pressures. Integral wake model used for both calculations. $M_\infty = 0.8$; $NPR = 2.0$; $\Delta x = x - x_A$.

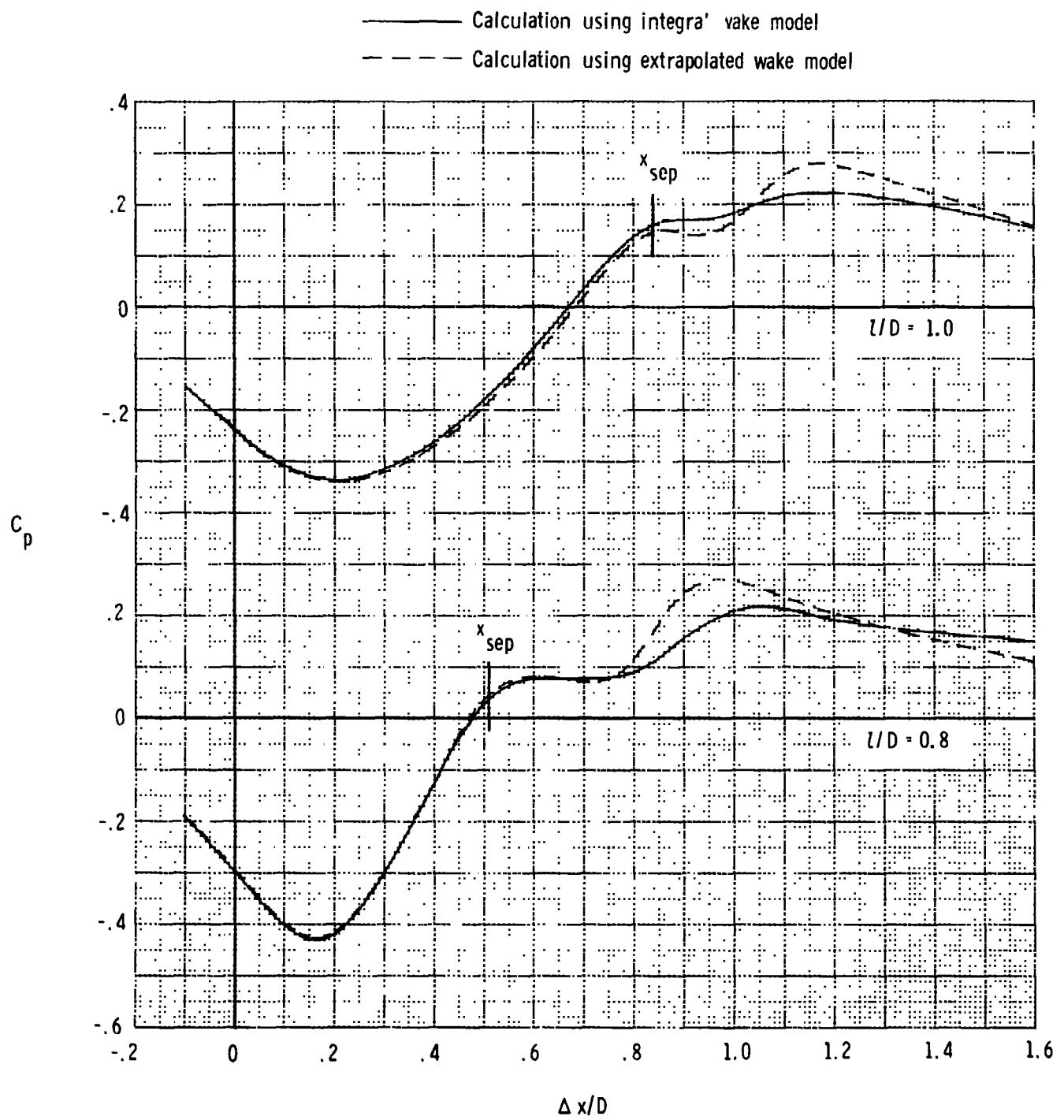


Figure 8.- Effect of jet wake model on predicted afterbody pressures.
 Experimental x_{sep} used for both calculations. $M_\infty = 0.8$;
 $NPR = 2.0$; $\Delta x = x - x_A$.

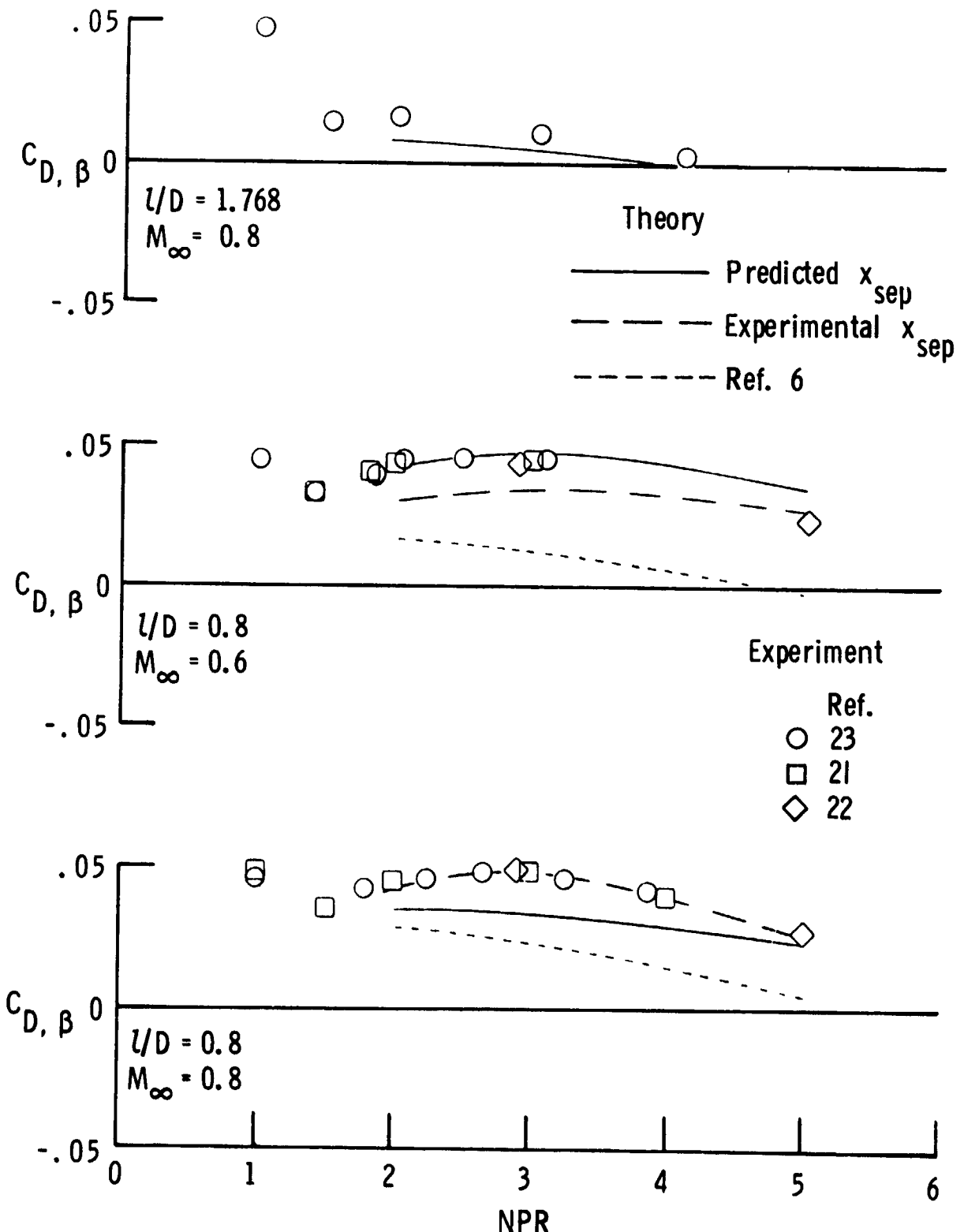
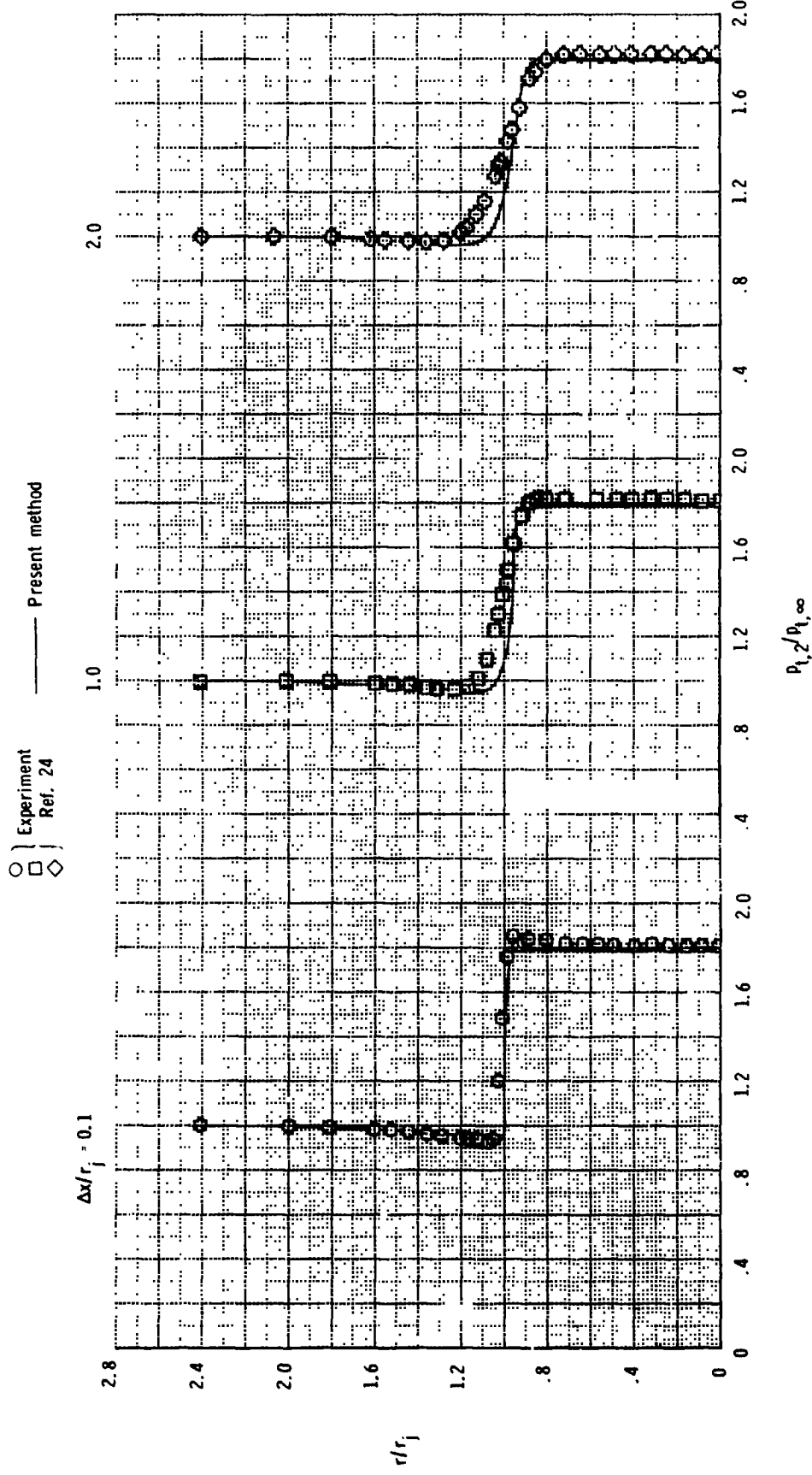
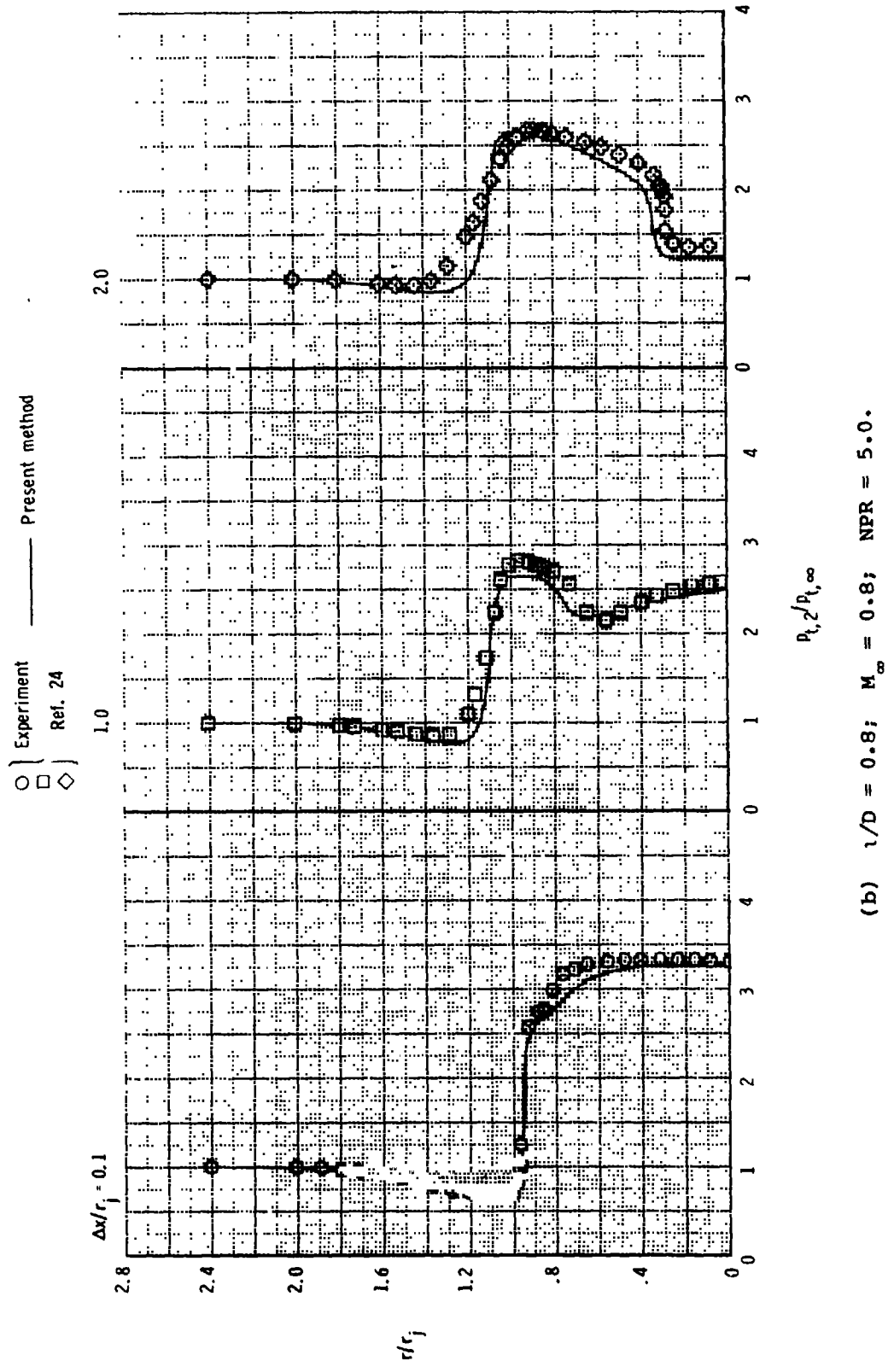


Figure 9.- Predicted and experimental afterbody pressure drag. Integral wake model used with predicted x_{sep} and extrapolated wake model used with experimental x_{sep} .



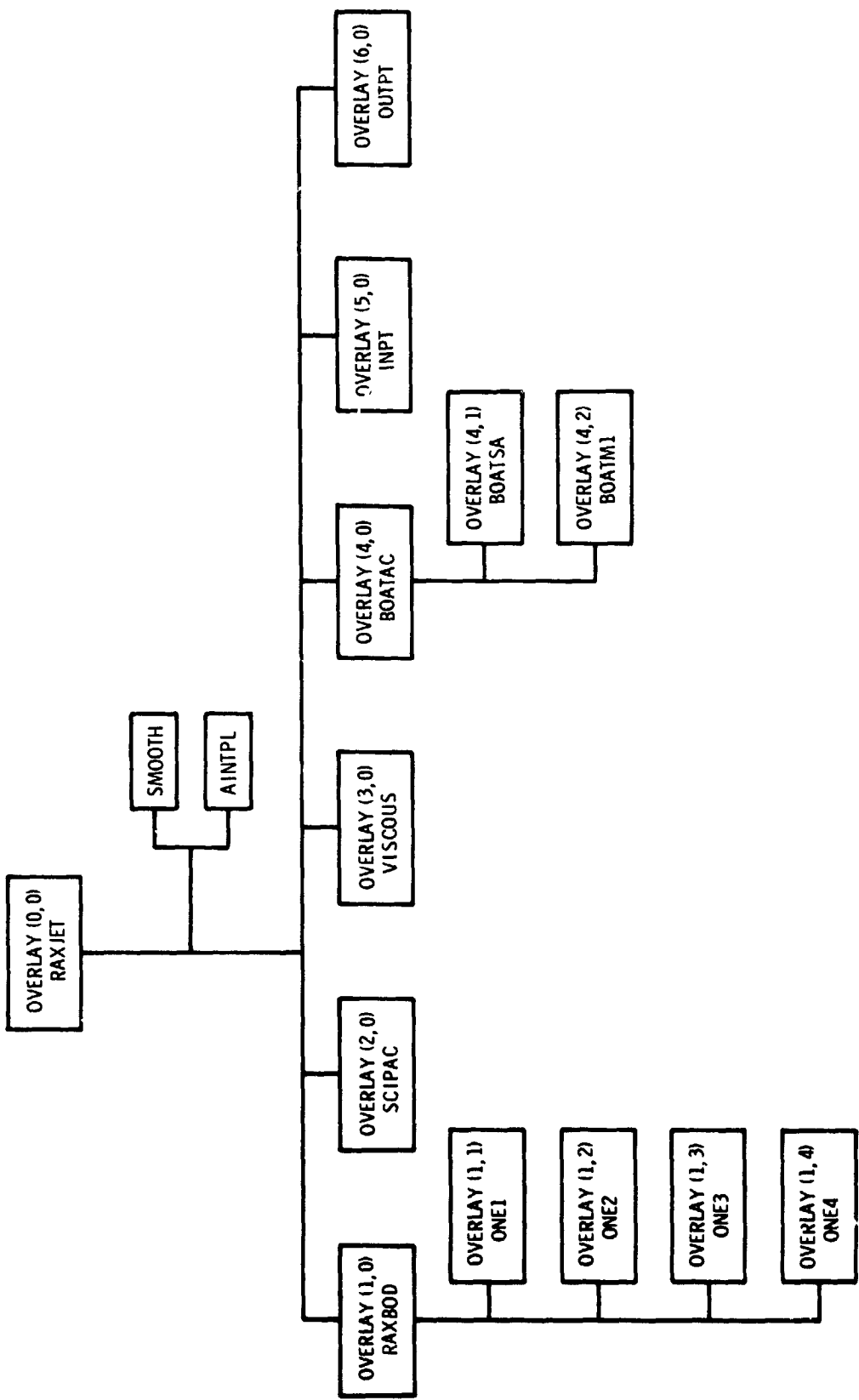
(a) $i/D = 1.768; M_\infty = 0.4; \text{NPR} = 2.0.$

Figure 10.— Predicted and experimental pitot pressure profiles across jet and mixing layer. $\lambda x = x - x_M$.



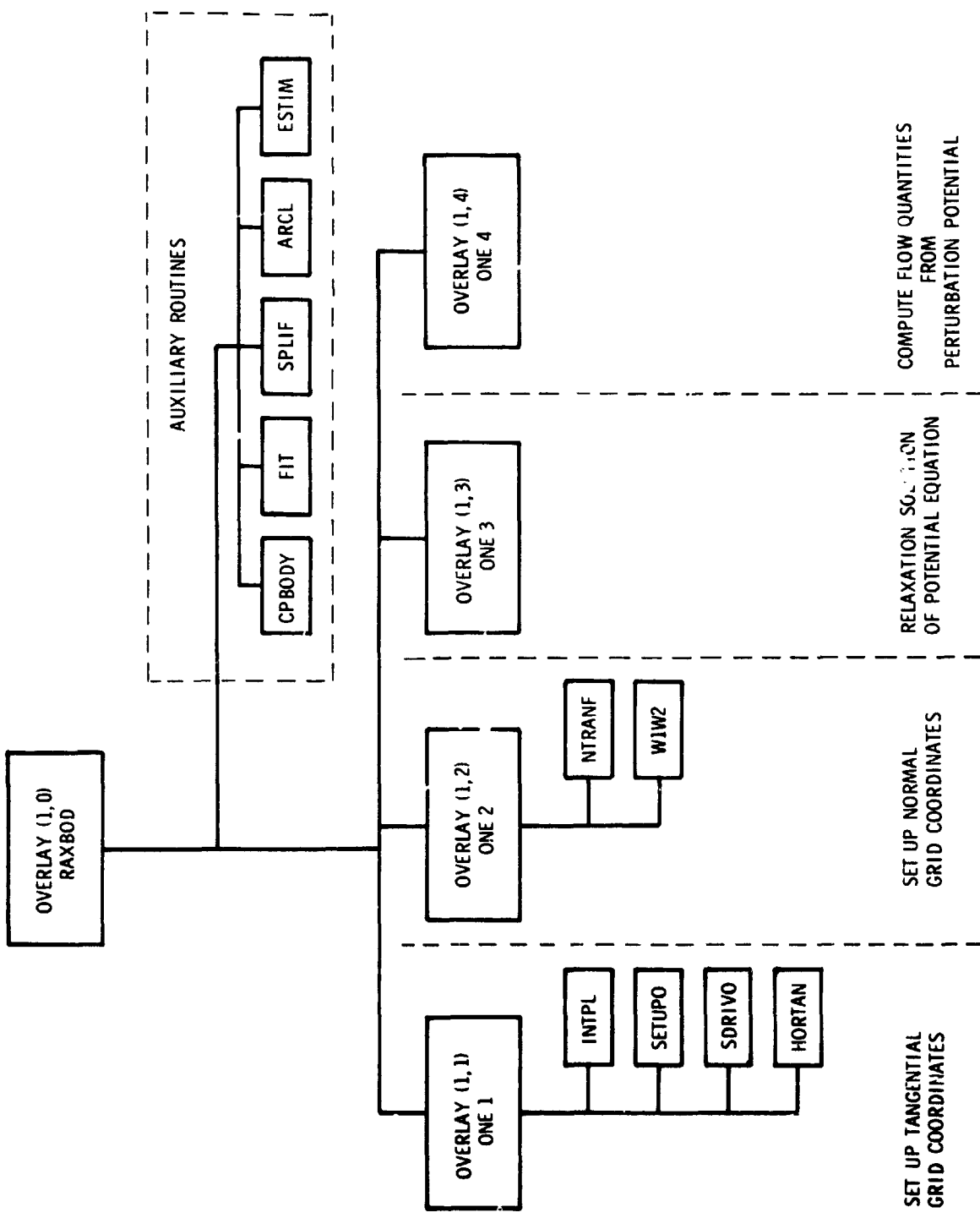
(b) $1/D = 0.8; M_\infty = 0.8; NPR = 5.0$.

Figure 10.- Concluded.



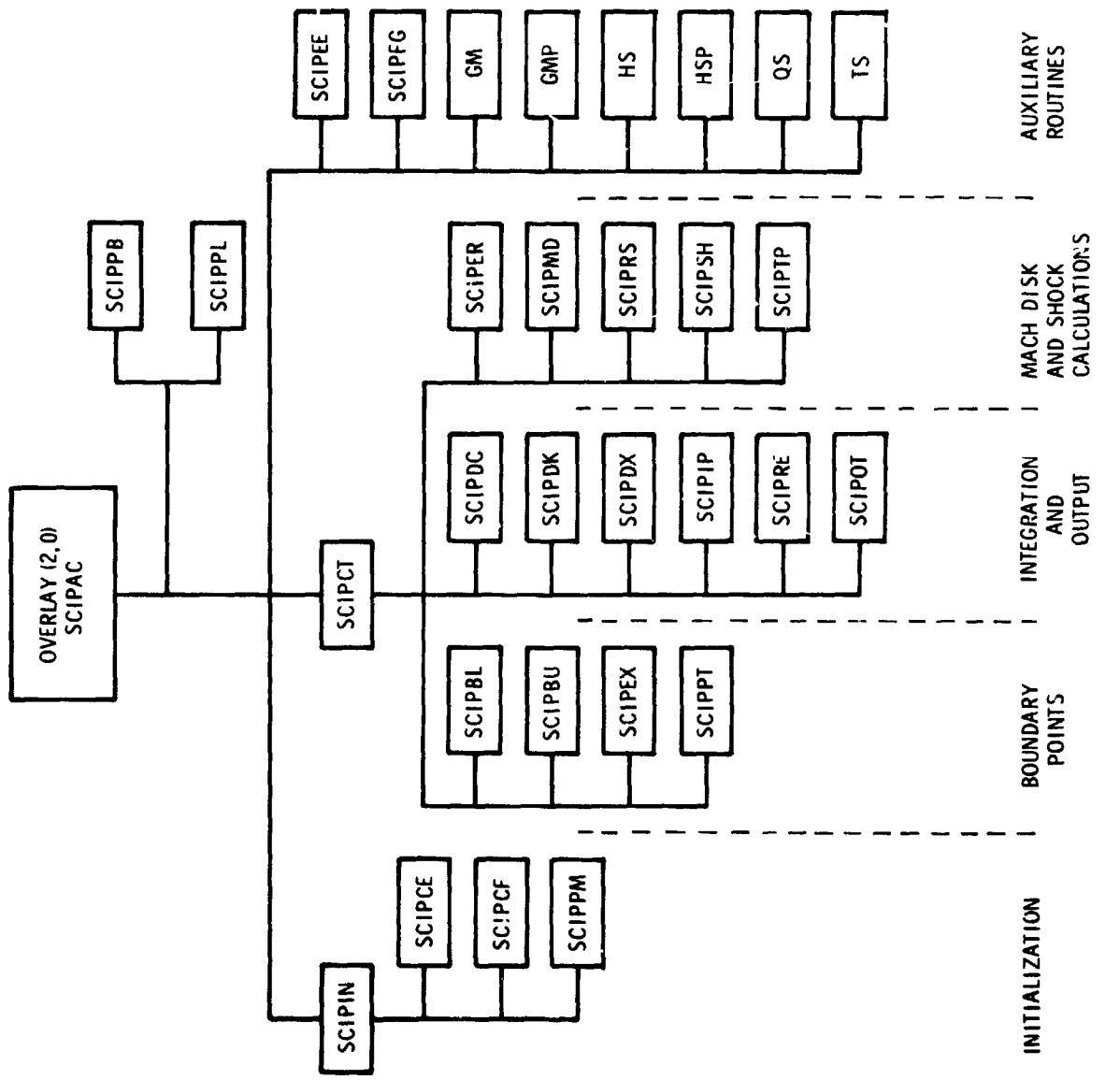
(a) Primary overlay chart.

Figure 11.- Organizational chart for program RAXJET.



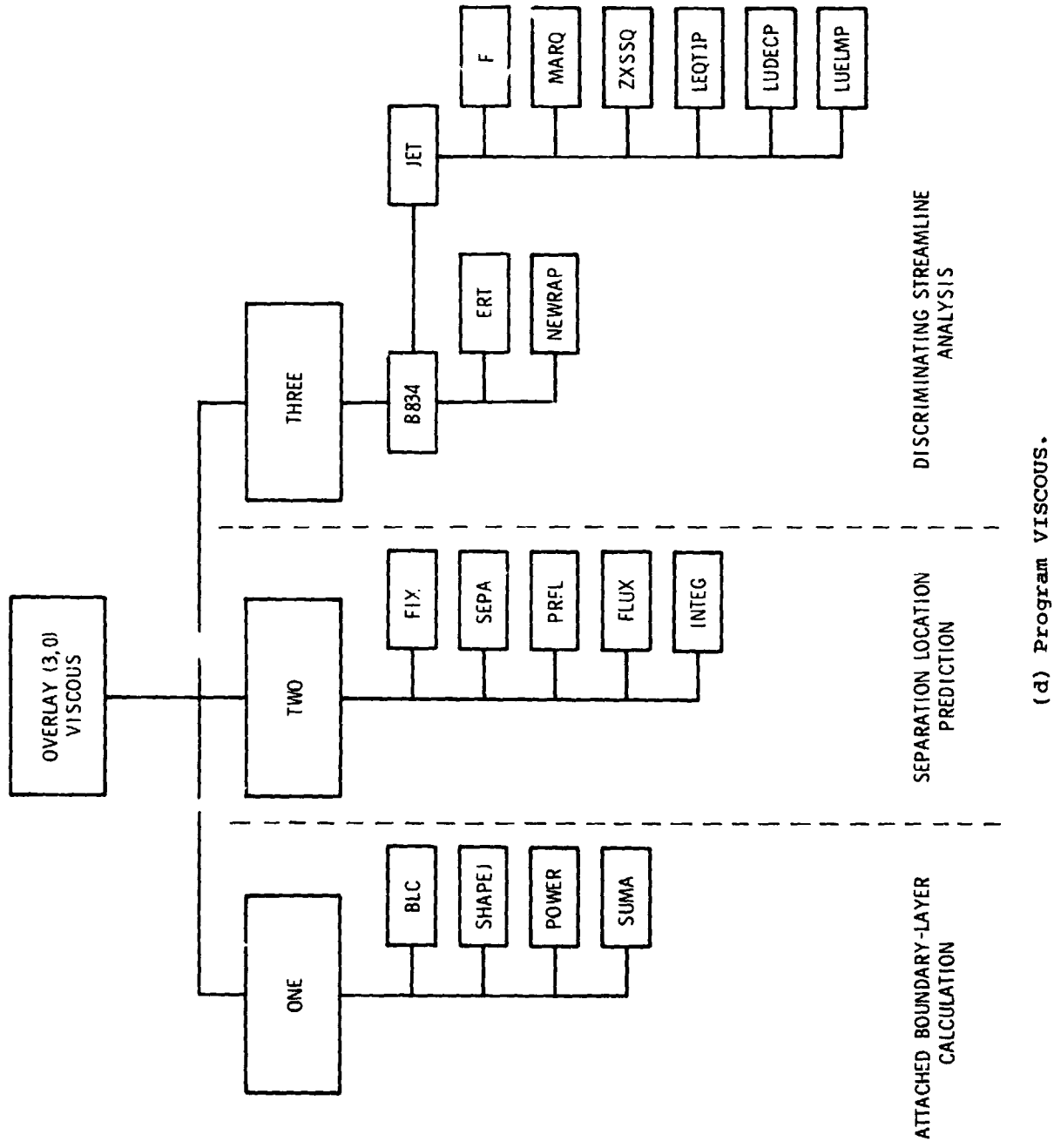
(b) Program RAXBOD.

Figure 11.- Continued.



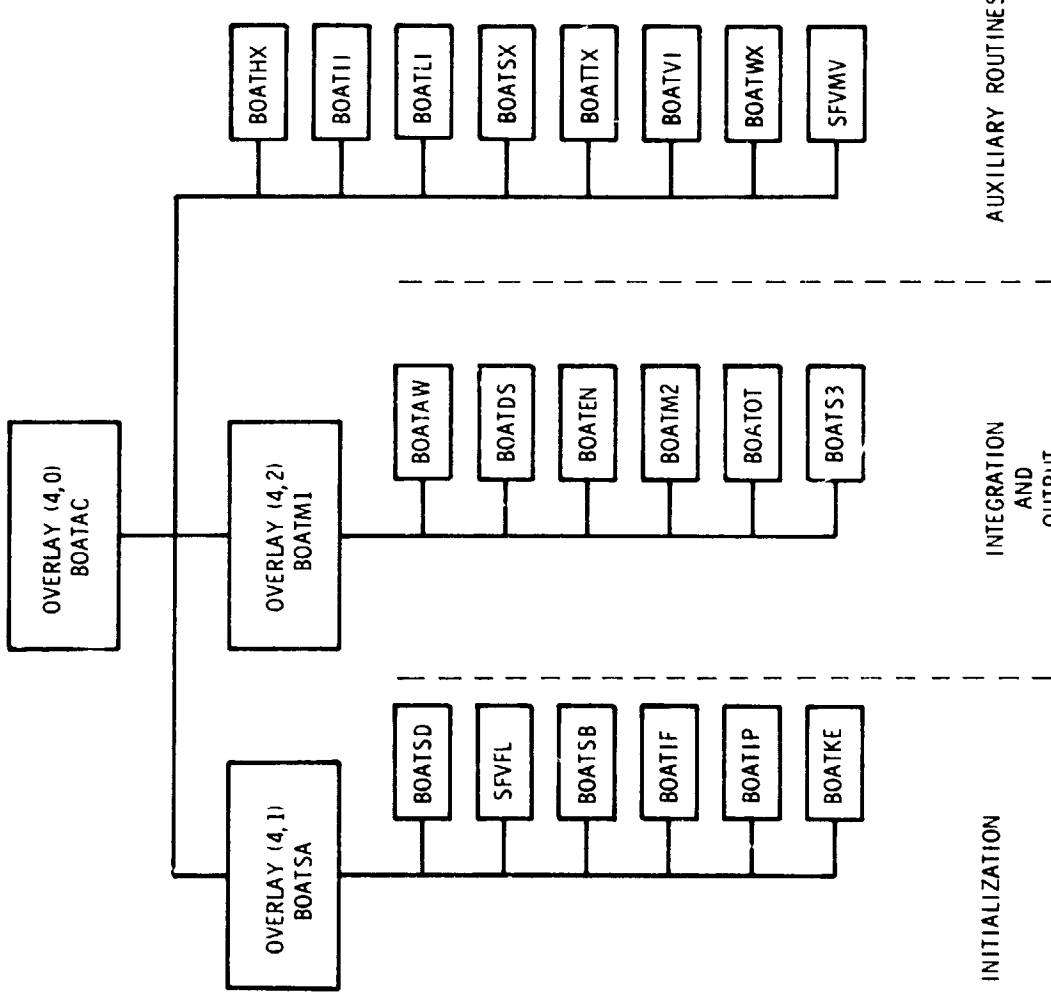
(c) Program SCIPAC.

Figure 11.- Continued.



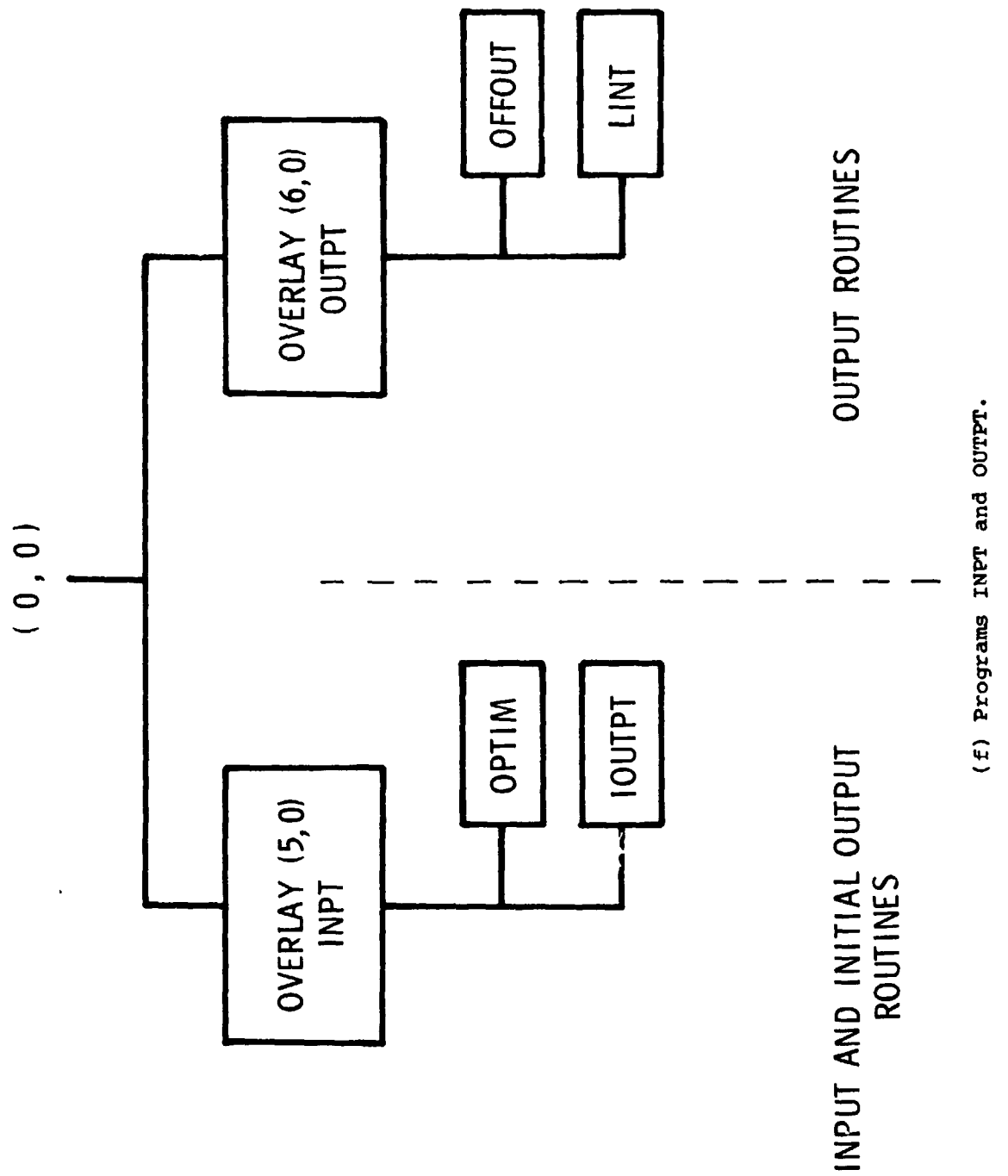
(d) Program VISCous.

Figure 11.- Continued.



(e) Program BOATAC.

Figure 11.- Continued.



(f) Programs INPT and OUTPT.

Figure 11.— Concluded.

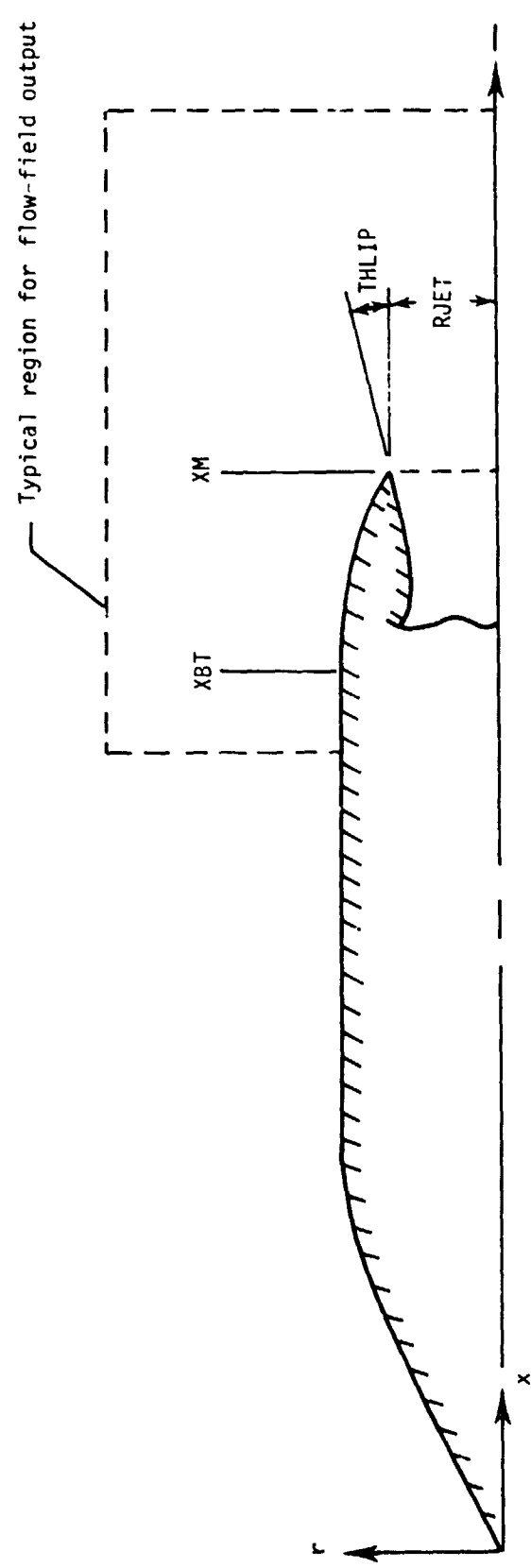


Figure 1 Definition of geometric input parameters.

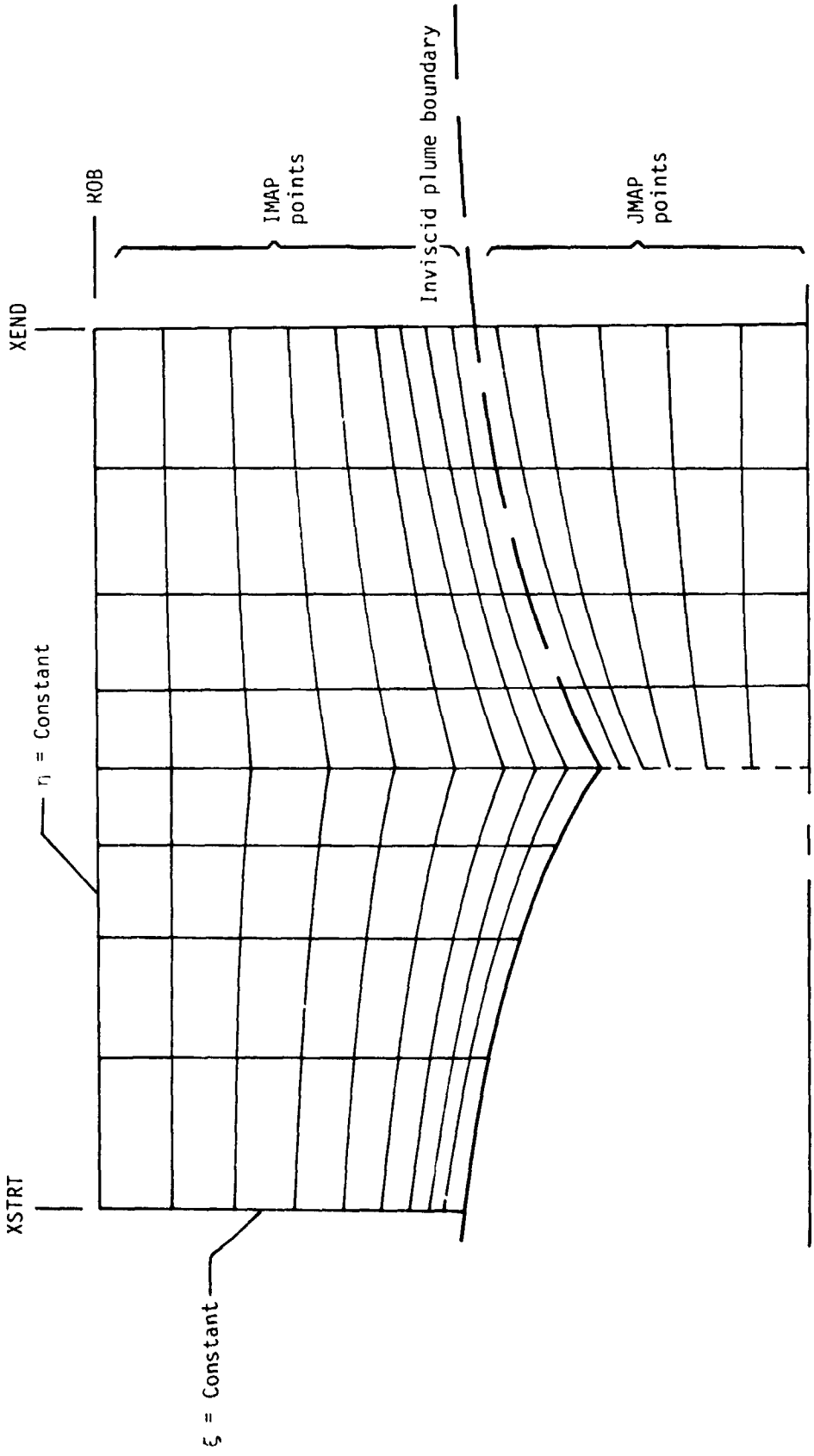


Figure 13.- Definition of flow-field output grid parameters.

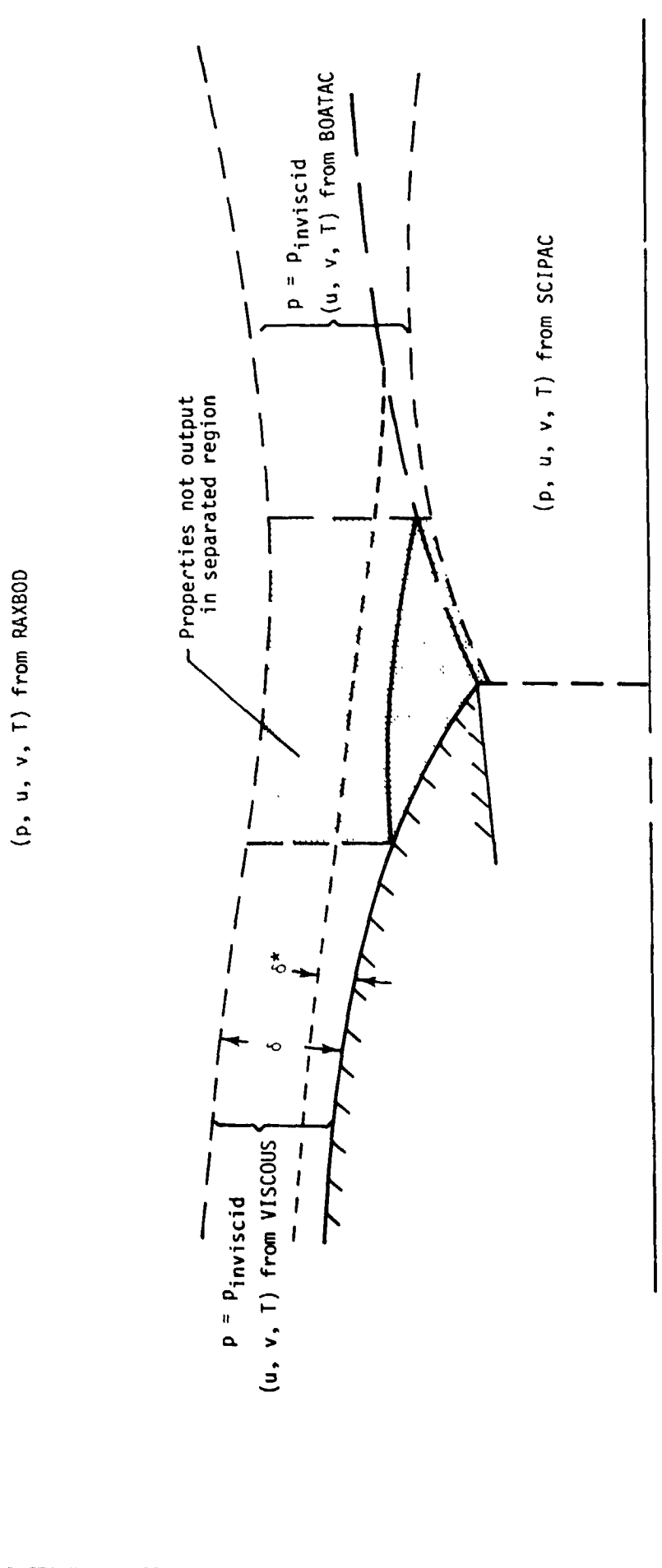


Figure 14.- Composite Flow-field properties.